



	Establishing a Two-Regime Plasma Jet for Interdisciplinary Studies of Plasma Treatment of Chronic Wounds and Fibrosis
Auteur: Author:	Juliette Letellier-Bao
Date:	2024
Type:	Mémoire ou thèse / Dissertation or Thesis
	Letellier-Bao, J. (2024). Establishing a Two-Regime Plasma Jet for Interdisciplinary Studies of Plasma Treatment of Chronic Wounds and Fibrosis [Mémoire de maîtrise, Polytechnique Montréal]. PolyPublie. https://publications.polymtl.ca/59160/

Document en libre accès dans PolyPublie Open Access document in PolyPublie

URL de PolyPublie: PolyPublie URL:	https://publications.polymtl.ca/59160/
Directeurs de recherche: Advisors:	Stephan Reuter, & Caroline Boudoux
Programme: Program:	Génie physique

POLYTECHNIQUE MONTRÉAL

affiliée à l'Université de Montréal

Establishing a two-regime plasma je	for interdisciplinary studies of plasma
treatment of chron	c wounds and fibrosis

JULIETTE LETELLIER-BAO

Département de génie physique

Mémoire présenté en vue de l'obtention du diplôme de Maîtrise ès sciences appliquées Génie physique

Août 2024

POLYTECHNIQUE MONTRÉAL

affiliée à l'Université de Montréal

Се	mémoii	re	intitulé	é	:

Establishing a two-regime plasma jet for interdisciplinary studies of plasma treatment of chronic wounds and fibrosis

présenté par Juliette LETELLIER-BAO

en vue de l'obtention du diplôme de *Maîtrise ès sciences appliquées* a été dûment accepté par le jury d'examen constitué de :

Denis SELETSKIY, président
Stephan REUTER, membre et directeur de recherche
Caroline BOUDOUX, membre et codirectrice de recherche
Véronique MOULIN, membre externe

ACKNOWLEDGEMENTS

A master thesis makes you grow as a student, and as a scientist. You owe it in part to yourself but mostly to the people who accompany you on the journey. The people who guide and inspire you. It means a lot to acknowledge these friends and colleagues that have made my master's possible and fun and worthwhile.

The biggest thank you to Stephan, my thesis director. I am so glad to have ended up in his lab. He has been the best mentor, never shy of seeing my potential and gently pushing me towards it. He always finds the time for his students and is present in the kindest ways. He is an incredible teacher and has taught me so much about science, about being a researcher evolving in different environments, about perseverance. Maybe most importantly, he taught me patience, and that science takes time but in the end it is worth every lost hair.

A big thank you to Caroline, my co-director. Caroline gave me my first conference experience, generously inviting me to tag along with her lab. It was an experience which I adored and it introduced me to the effervescent world of the international science communities. She has encouraged me to embrace a devotion to science, and to woman in science, through our chats and simply by being such an incredible model for us. Ce n'est que partie remise, je l'espère.

I huge thank you to all my colleagues. Jean-Baptiste, Laura, Sean, Julien T., Jean-Philip, Nathan and Julien B-D, without whom my Master's might have taken five years. I could always count on them for helping out with experiments, for solution-finding, for administrative muddles, for elaborate team-bonding activities and that was very important. I look forward to working with them some more.

I have worked several months in Anie Philip's lab and want to thank her for welcoming me and allowing me the resources to learn so so much cell biology lab work. I have met incredible researchers in this lab, that have taken me under their wings. A special thank you to Shikha and Amani who trained me on cell culture techniques and much more. They were teachers, and friends as well. It was a chance to meet such passionate woman who work hard at advancing science and it has very much inspired me. A big thank you as well to Kenneth, Varsha and Tenzin, who were always present for encouragements and to answer my constant questions.

Thank you to Mihaela, Derek, and Rahul for accompanying us in the security assessment procedures for installing our plasma device in the hospital lab. It took multiple months but in the end we did succeed in getting the necessary approvals, and now more biology can

happen.

I also want to thank all the collaborators on this project, who have shared their expertise, their equipment, their time. Sylvain and his students Philip and Dante who have organized that we could borrow their deuterium lamp and later their multipass cell, for spectroscopic experiments that gave me many results. Willem who gave me a much appreciated crash course on FTIR. Oussama who gave us access to his Vertex 80, and Mahmoud who helped out a lot during measurements. It was an intensive week, setting up gas bottles, optical equipment, and a bunch of plasma stuff, all just to take that one precious measurement at 3pm on a Friday before the lab next door caught fire. Frédéric, Trang and Esmat for planning Raman measurements with me before the microscope motor unfortunately broke down the day of the experiments. A thank you to Robert who was willing to exchange emails and emails on demystifying the hapi interface.

It takes many people to run a lab and we are lucky to have great technicians running this lab with us. A big thank you to Joël for being such a huge help in achieving all my experimental setups, for having a solution to everything and for making the magic happen. Thank you to Mikaël who looked through lenses, curved, aligning some barely visible light beams, for the good of my mental health.

And of course, because they make me who I am and are my main reason for love and joy, an infinite thank you to my family and friends. To my boyfriend who instills me with confidence, makes me laugh and fills me with love always, which are the best gifts. To my family who are my absolute rock, my much needed comfort haven and who endlessly support me in so many ways. To my friends who care for me and show me loopholes for all the funner ways of life.

RÉSUMÉ

Le plasma froid comme traitement médical a fait son entrée dans les hôpitaux en 2013 avec l'obtention de la certification «CE» (Conformité Européenne). Ses domaines d'application principaux sont l'oncologie et le traitement de plaies telles que les brûlures et les plaies chroniques. Avec le vieillissement de la population et la hausse du diabète et de l'obésité, le taux d'incidence des plaies chroniques est grandissant. Le présent mémoire porte sur la fibrose, un type de plaie chronique. La fibrose est une maladie qui se traduit par une phase inflammatoire persistante et une hyper-cicatrisation des tissues. Le plasma physique froid génère des espèces hautement réactives à basse température, permettant un traitement des tissus humains in vivo. Ces espèces exogènes, aussi produites naturellement par nos cellules, peuvent induire des réactions d'oxydoréduction locales dans les organismes biologiques en agissant comme des messagers secondaires dans de nombreux processus cellulaires. Ainsi, le traitement par plasma déclenche des réponses inflammatoires et influence la prolifération, la maturation et la différenciation des cellules. Ultimement, il peut favoriser la guérison et la cicatrisation des plaies.

Si nous parvenons à comprendre les mécanismes d'action des espèces réactives sur les processus cellulaires qui causent et maintiennent l'état chronique d'une plaie, et si nous arrivons à en contrôler le dosage pour inverser la pathologie, nous disposerons d'un outil prometteur. Le plasma froid permet de contrôler les concentrations et la composition des espèces réactives. L'objectif de la présente recherche est de développer un outil permettant de produire avec le plasma froid une composition contrôlée d'espèces réactives dans un contexte biologique de recherche fondamentale sur la médecine du plasma. Une approche simplifiée est proposée: développer un jet plasma produisant deux régimes d'espèces réactives opposés, soit un plasma produisant des espèces réactives d'oxygène et un plasma produisant des espèces réactives de nitrogène. L'hypothèse est que ces deux régimes engendrent des réponses cellulaires différentes.

D'abord, des diagnostiques optiques sont réalisés afin de caractériser la production d'espèces dans le plasma froid et de définir deux régimes opposés. Différentes techniques spectroscopiques ont servi à identifier et à quantifier les espèces réactives produites par différents régimes de plasma, question de choisir les deux régimes optimaux. Une fois les deux régimes définis, un montage est conçu pour pouvoir utiliser la source en double-modalité dans un laboratoire de recherche hospitalier. Une méthodologie est développée pour traiter des modèles biologiques de fibrose et pour étudier l'interaction de ces modèles avec les traitements à

l'aide de plasma. Des analyses d'activité métabolique et d'expression de protéines sont accomplies pour caractériser la réponse de cellules traitées au plasma. L'expression de protéines impliquées dans l'hyper-cicatrisation des tissus est modifiée par certaines doses de plasma, établissant une relation causale prometteuse pour la suite. D'autres tests devront être complétés pour comparer les effets biologiques des deux régimes de plasma sur des modèles de plus en plus complexes.

À terme, la cible est d'arriver à des modèles intégraux de tissus fibrotiques et de pouvoir prendre une approche théranostique pour le traitement de plaies au plasma froid. La solution envisagée est d'intégrer au dispositif plasma des techniques d'imagerie médicale. Ces techniques serviront à caractériser en temps réel l'état du tissue traité et d'adapter la réactivité du plasma afin d'optimiser le traitement. Le traitement au plasma augmente la coagulation des plaies. La tomographie en cohérence optique (OCT) peut observer la coagulation en réaction immédiate au traitement par plasma. L'imagerie hyperspectrale permet d'observer l'état d'oxygénation local du tissu qui réagit au traitement par plasma. L'imagerie peut être utilisée pour diagnostiquer les phases de cicatrisation d'une plaie et pour rendre compte en temps réel de l'effet du traitement. Cela permet d'établir un lien avec la caractérisation des espèces réactives dans le plasma et de définir lesquelles sont les plus bénéfiques à chaque phase de guérison. Une boucle de rétroaction avec la biophotonique est proposée comme travail futur à mener avec des modèles animaux ou des échantillons de tissus ex vivo.

ABSTRACT

Chronic wounds place a heavy burden on the Canadian healthcare system in terms of quality of life, as well as from a societal and economic perspective. A novel treatment for chronic wounds is cold atmospheric plasma. Non-equilibrium plasmas generate highly reactive species at low temperatures. This allows treatment of human tissue *in vivo* and can induce locally confined redox-chemistry in biological organisms, thus positively influencing cellular communication. Reactive oxygen and nitrogen species are known to play a vital role in cell signaling and modulate a range of mechanisms involved in all phases of wound healing—hemostasis, inflammation, vascular formation, proliferation, remodeling of scar tissue.

Plasma gives us a tool for controlling and modulating dosage of the redox species cocktail deposited on the wound. By better understanding the effect of reactive species on cells, we can tailor the plasma reactivity to supply an adapted redox-based treatment to the tissue. A special focus is put on fibrosis. Fibrosis is a form of disrupted wound healing where scar formation is hypertrophic due to excessive synthesis of extracellular matrix proteins e.g., collagen, fibronectin.

Reactive species have dual functions depending on their concentrations, the state of the tissue, the healing phase, etc. This is why a good characterisation of the plasma composition is essential. Diagnostic techniques are necessary for characterising redox species cocktail produced by the plasma. This work uses optical absorption and emission spectroscopy alongside Fourier transform infrared spectroscopy to measure a number of reactive oxygen and nitrogen species in the plasma effluent. Two opposing plasma regimes are established by modulation of plasma composition and electrical parameters. These regimes producing more oxygen oxides in one case, and more nitrogen oxides in the other, can be used to treat biological models and study the effects on specific healing processes, signaling pathways, cell functions, etc. The hypothesis is that both regimes might have dual or complementary effects on fibrosis. Reactive oxygen species are known to be pro-inflammatory by increasing the oxidative stress in the environment of the cells, and reactive nitrogen species have anti-inflammatory and angiogenesis effects. Establishing a dual-regime plasma source and designing a hospital compatible setup are the achieved objectives of this thesis.

Cell biology experiments are conducted, analyzing cell behavior as a response to modulated plasma treatment. Fibroblasts cells are chosen as the biological model since they play a key role in fibrosis and produce a range of proteins that can be used as biomarkers. Plasma dosage is adjusted with a metabolic activity assay and this dosage is applied to fibroblasts in order

to study changes in their expression of proteins. Two proteins are looked at: type I collagen and alpha smooth muscle actin. Biological results confirm that plasma can cause redox based changes in fibroblasts cells: stimulating them and modifying collagen gene expression. With this information, more tests should be done comparing biological effects of both established plasma regimes, studying other proteins, growth factors, cytokines and improving the model by adding more complexity.

Tailoring the plasma reactivity to biological needs, to reach a bio-chemical effect on imbalanced healing environment in tissue models will deepen our comprehension on the physiology of chronic wounds. The aim is to reveal links between disturbed wound healing and initiated plasma based redox response in the affected tissue based on a controlled and tailored exogenous redox trigger through plasma treatment. This will also pave the way to a personalized plasma treatment technology greatly benefiting the health sector. There are different strategies to taylor plasma reactivity. It can be done by evaluating tissue reaction to plasma treatment with traditional cell biology assays. It can also be done in real-time to obtain a feedback control loop. Biophotonics feedback signals are an explored solution. Imaging can be used to diagnose the healing phases and heterogeneous zones of a chronic wound, by highlighting structures and biomarkers specific to each. This will help identify which plasma species most benefits each healing phase, and adapt plasma to each zone's needs. Plasma treatment enhances wound coagulation and tissue oxygenation, as well as influencing gene expression of many proteins. Optical coherence tomography (OCT) provides in depth 3D structural imaging of tissues and can observe coagulation in immediate response to plasma treatment. Hyperspectral imaging (HSI) renders information about the biochemical composition of the tissue. It can observe local oxygenation status of tissues in response to plasma treatment. It can also collect fluorescent signals from local proteins such as collagen. Therefore, a feedback loop with biophotonics (OCT and HSI) imaging plasma sensitive biomarkers is proposed as future work to be conducted with more complex in vivo animal models or ex-vivo tissue samples. Now that dual-regime plasma setup is installed and approved by a hospital research laboratory, everything is in place to move forward with this project.

TABLE OF CONTENTS

ACKNO	OWLEDGEMENTS	ii
RÉSUM	1É	V
ABSTR	RACT	vii
TABLE	OF CONTENTS	ix
LIST O	F TABLES	X
LIST O	F FIGURES	xi
LIST O	F SYMBOLS AND ACRONYMS	xiv
LIST O	F APPENDICES	xvi
СНАРТ	TER 1 INTRODUCTION AND LITERATURE REVIEW	1
1.1	Literature Review	1
	1.1.1 Non-Thermal Plasma: Definitions and Applications	1
	1.1.2 Plasma Medicine	3
	1.1.3 Plasma-Tissue Interaction	5
	1.1.4 Redox Biology	5
	1.1.5 Plasma for (Chronic) Wound Healing	8
	1.1.6 Diagnostics: Plasma and its Biological Outcomes	21
1.2	Goals and Outline	24
СНАРТ		25
2.1	Plasma Diagnostics Methodology	25
	2.1.1 Emission and Absorption Spectroscopy	25
2.2	Plasma Source Design	29
2.3	Plasma Control	31
2.4	Establishing Plasma Regimes	32
СНАРТ	ΓER 3 Plasma Diagnostics: Experimental Setups and Results	39
3.1	Optical Absorption Spectroscopy: Measuring Ozone Densities	36
3.2	Optical Emission Spectroscopy: Plasma Plume Emission	44

3.3	Fourier Transform Infrared Spectroscopy: Plasma's Far Field	47
СНАРТ	TER 4 Plasma Treatment of Fibroblasts	52
4.1	Plasma Jet Setup in Biohood	52
	4.1.1 Dual-Regime Plasma Jet Installation at MUHC	54
4.2	Biological Model Used for Plasma Treatment	56
4.3	Metabolic Activity Assay	59
4.4	Western Blotting	60
4.5	ROS- vs RNS-Regime	63
4.6	Exploration of an Improved Fibrosis Model	64
СНАРТ	TER 5 CONCLUSION	65
5.1	Summary of Works	65
5.2	Limitations and Future Research	67
REFER	ENCES	68
APPEN	IDICES	78

LIST OF TABLES

Table 2.1	Nitrogen oxides vs oxygen oxides	33
Table 2.2	Voltage, current, temperature of plasma regimes	37
Table 3.1	Parameters used to retrieve cross sections	50

LIST OF FIGURES

Figure 1.1	Threshold levels of ROS and general biological effects [1]	7
Figure 1.2	Wound healing and fibrosis progression steps [2]	11
Figure 1.3	Drivers of fibrosis [3]	12
Figure 1.4	Neutrophils and macrophages use reactive species to damage and kill	
	pathogens by performing a respiratory burst [4]	13
Figure 1.5	Comparison in wound area for self-healing wound, control and plasma	
	treatments from day 0 to 14. Plasma treated wound is significantly	
	smaller on day 14 $[5]$	17
Figure 1.6	Wound contraction and wound reepithelialization increase after plasma	
	treatment compared to self-healing wound [6]	19
Figure 1.7	Migratory ability of various cell types modulated by plasma treatment [7]	20
Figure 1.8	OCT and HSI dual-modality 3D rendering of an epithelial wound (note	
	from article: $ER = epithelial regrowth$) [8]	23
Figure 2.1	Absorption cross sections of plasma-relevant species in the UV-spectral	
	range [9]	28
Figure 2.2	Schematics of plasma jet with key elements	29
Figure 2.3	Plasma jet feed gas and curtain gas flows, imaged with Schlieren pho-	
	tography a) imaged in free space b) imaged over well plate filled with	
	liquid	31
Figure 2.4	Switching plasma composition from ROS- to RNS-dominated chem-	
	istry [10]	34
Figure 2.5	Humidity calibration curve (room temperature water in the bubbler)	36
Figure 2.6	Plasma regimes' emission a) Ar-plasma b) ROS-plasma and c) RNS-	
	plasma	37
Figure 2.7	Thermocouple temperature measurements compared to other gas-temperature	ture
	measurements [11]	38
Figure 3.1	Schematics of UV-absorption spectroscopy setup	40
Figure 3.2	UV-absorption spectroscopy: raw measurements (left) and experimen-	
	tal and simulated absorption profiles (right)	41
Figure 3.3	Ozone densities in plasma far-field for different percentages of oxygen	
	admixtures	42
Figure 3.4	SNR of ozone density measurements	42
Figure 3.5	Ozone densities in function of different plasma compositions	43

Figure 3.6	SNR of ozone density measurements for the different plasma compositions	44
Figure 3.7	Schematics of OES setup	44
Figure 3.8	UV emission of RNS- and ROS-plasma (normalized to the max value	
	of RNS-plasma)	45
Figure 3.9	UV emission of argon-plasma (normalized to the max value of RNS-	
	plasma)	45
Figure 3.10	IR emission of normalized argon-plasma and RNS-, ROS-plasma (nor-	
	malized to the max value of ROS-plasma)	45
Figure 3.11	Schematics of FTIR setup	47
Figure 3.12	3D printed adapter plate for aligning multipass cell with Fourier trans-	
	form infrared (FTIR) spectrometer	48
Figure 3.13	FTIR signals of reactive nitrogen species (RNS)-plasma at $4 \mathrm{cm}^{-1}$ res-	
	olution	49
Figure 3.14	Absorption cross sections of relevant reactive species in the infrared	
	(IR) retrieved form HITRAN database	50
Figure 3.15	Fitting of molecule densities to FTIR absorbance signal of RNS-plasma	51
Figure 4.1	Plasma jet setup in laminar flow hood for cell culture treatments	52
Figure 4.2	Fiber fixed on CNC router aligned with plasma plume emission	53
Figure 4.3	Evolution in time of OH emission from plasma jet plume	54
Figure 4.4	Dual-regime plasma device setup	56
Figure 4.5	Plasma streak left by plasma on adherent cells (left) and no streak after	
	plasma treatment (right)	58
Figure 4.6	Metabolic activity of fibroblasts 24h after plasma treatment	59
Figure 4.7	Protein bands	62
Figure 4.8	Western blot results: quantification of type I collagen (coll 1) and alpha	
	smooth muscle actin (α sma) expression	62
Figure 4.9	3D fibrosis model—fibroblasts in spheroid formation	64

LIST OF SYMBOLS AND ACRONYMS

lphasma alpha smooth muscle actin CAP cold atmospheric plasma CNC computer numerical control

coll 1 collagen type I

DBD dielectric barrier discharge

DMEM dulbecco's modified eagle medium

ECM extracellular matrix
EGF epidermal growth factor

eV electron volt

FBS foetal bovine serum
FGF fibroblast growth factor

FN fibronectin

FTIR Fourier transform infrared HIF-1 hypoxia-inducible factor-1

HITRAN high-resolution transmission molecular absorption

HSI hyperspectral imaging

hTERT human telomerase reverse transcriptase

ICCD intensified charge-coupled device

IL-1 interleukin 1
IL-6 interleukin 6
IL-8 interleukin 8
ILs interleukins
IR infrared

MFC mass flow controller

MMPs matrix metalloproteinases

MRSA methicillin-resistant S. aureus

NF- κ B transcription factor nuclear factor- κ B

NO nitric oxide

NOS nitric oxide synthases
Nox NADPH oxidase

Nrf2 nuclear factor erythroid 2-related factor 2

OCT optical coherence tomography
OAS optical absorption spectroscopy

OES optical emission spectroscopy

PAM plasma activated media

p53 tumor suppressor protein p53 PDGF platelet-derived growth factor

ppm parts per million redox oxidation-reduction

sccm standard cubic centimeter per minute

SLA stereolithography

slm standard liter per minute
SNR signal to noise ratio
SOD superoxide dismutase

TGF β transforming growth factor beta TNF α tumor necrosis factor-alpha

UV ultraviolet

VEGF vascular endothelial growth factor

Gases and reactive species:

Ar argon

 $\begin{array}{c} {\rm CO} & {\rm carbon\ monoxide} \\ {\rm CO}_2 & {\rm carbon\ dioxide} \end{array}$

 H_2O water

 H_2O_2 hydrogen peroxide

 $\begin{array}{ccc} \text{He} & & \text{helium} \\ \text{HNO}_3\text{O}_2 & & \text{nitric acid} \\ \text{N}_2 & & \text{nitrogen} \\ \text{N}_2\text{O} & & \text{nitrous oxide} \end{array}$

 N_2O_5 dinitrogen pentoxide NO_2 nitrogen dioxide

 $\begin{array}{ccc} NO_2^- & & \text{nitrite} \\ NO_3^- & & \text{nitrate} \\ O_2 & & \text{oxygen} \\ O_2^- & & \text{superoxide} \\ ^1O_2 & & \text{singlet oxygen} \end{array}$

 O_3 ozone

OH hydroxyl radical ONOO peroxynitrite

RNS reactive nitrogen species

RONS reactive oxygen and nitrogen species

ROS reactive oxygen species

LIST OF APPENDICES

Appendix A	Security risks assessment and mitigation protocol	78
Appendix B	FTIR python code	87
Appendix C	Automated plasma treatment of 12-well plate	92

CHAPTER 1 INTRODUCTION AND LITERATURE REVIEW

Plasma medicine is a new field of research that started about 20 years ago and thus many questions on its fundamentals remain. The most promising fields of applications of plasma medicine are chronic wounds and cancer. Plasma is an exogenous source of reactive species which act as secondary messengers in many of our body's processes. If we can better understand these processes, where they go wrong in specific diseases, and how we could dose reactive species to remedy the pathology, a very powerful tool will be unlocked. Plasma represents a means for controlling reactive species concentration and composition in order to better understand cell signaling in different biological contexts—by treating tissues with known composition of plasma and characterizing the biological effects. Plasma can be both the research tool and the treatment device.

The aim of the present research is to develop a tool to do precisely that: Provide a controlled reactive species composition by plasma in a biological setting of fundamental research of plasma medicine. The focus is set on the disease of chronic wounds. Aging population, diabetes and obesity are important predispositions for chronic wounds. With all three on the rise, chronic wounds increasingly represent a social, economical and clinical challenge. Treatment costs are estimated to be 1-3% of total medical care expense in developed countries [12]. An efficient treatment to cure this disease will have a major impact on the quality of life.

It is in this context that this work is set and orients the objectives. We aim to develop diagnostic techniques for characterising plasma specie production for different plasma conditions. Thus, we gain means for controlling plasma reactivity and defining different plasma regimes. We also aim to develop a methodology and a plasma device setup in a hospital setting for treating biological fibrosis models and studying plasma regimes' interaction with such models. The objectives of the thesis are further detailed in section 1.2.

1.1 Literature Review

1.1.1 Non-Thermal Plasma: Definitions and Applications

Plasma is a state of matter immensely present in our environment. The sun, lightning, auroras are all plasma. By definition, plasma is a quasi-neutral, partially ionised gas, with equal amount of positively and negatively charge particles, who's particles have a collective response to external perturbations. To achieve plasma, a continuous supply of energy—

photo-ionization, heat, electricity— to the gas is needed. A dominant ionizing mechanism is electron impact, where high-energy electrons collide with atoms and molecules and transfer their energy to partially ionize the gas. The gas particles dissociate into ions and more electrons, thus creating reactive species, radicals, light emission, etc. Charged particles make plasma conductive with a current and often a magnetic field. Particles in plasma further interact with their environment such as ambient air, surfaces, liquids and create more byproducts [13].

When speaking of non-thermal, non-equilibrium plasma, the gas is ionized weakly enough so that the heavy species (ions, neutrals) remain near-room temperature, even if electrons are very hot. Heavy species remain below 40°C compared to electrons which reach temperatures equal to 1-2 electron volts (eV). One eV represents the energy an electron gains when the electrical potential is 1V [14]. This temperature disequilibrium enables the field of plasma medicine: Cold plasma can be applied to living tissues without harming it. Plasma in a clinical context is operated under atmospheric pressure conditions. The main interest for plasma medicine lies in the reactive oxygen and nitrogen species produced in the plasma: These reactive species play an essential role in the biological effects of non-thermal plasma [15,16]. Hereinafter, cold plasma, non-equilibrium plasma or non-thermal plasma, which are all synonyms, will be referred to simply as plasma.

The physicochemical characteristics of plasma depend on many parameters. The gas or gas mixture used to generate the plasma, the applied energy, the power source, the environment e.g., pressure, temperature. All these parameters can be controlled and adjusted depending on the application of the plasma source [13,15].

Plasma has many applications in biomedical fields. One main aspect of cold plasma is its antiseptic properties. Plasma is used to sterilize medical surfaces, equipment and implants: by inactivating bacteria, viruses and fungi [15]. In the same way it is also used in medicine to decontaminate tissues and prevent infection [17]. Another major application field for plasma in medicine is wound healing. This is the subject of the present research and more details will be given in the following chapters. A further topic of plasma research is cancer treatment, with currently several clinical trials using plasma in oncology [18]. Plasma can selectively kill cancer cells which makes it a targeted therapy. Furthermore, plasma has immuno-promoting effects, making it a promising candidate for immunotherapy [19].

1.1.2 Plasma Medicine

The first clinical trial in plasma medicine took place in 2010, studying antimicrobial effects of plasma for improving patients' chronic wounds [20]. Starting in 2013, gas plasmas devices were approved as medical device class IIa in Germany and Europe for treatment on chronic wounds, ulcers, and skin conditions involving some form of infection [19]. Nowadays, thousands of patients in dermatology are being treated with plasma with no notable side effects [19].

The main therapeutic component of plasma for medicine are the reactive species produced in this ionized gas. Plasma medicine is based on a controlled exogenous supply of reactive oxygen and nitrogen species (RONS) to treat pathological tissue conditions. Before it is possible to achieve precise plasma treatment, there are still many open questions left to answer. Plasma on the one hand is a complex ionized medium, electrically charged, containing many particles that will interact with their immediate environment. On the other hand, tissues are complex biological systems with many different cell types, cell organizations, etc. which will interact with and react to external triggers in various ways. Combining the two complex systems creates a reaction pathway network of potentiated complexity. New approaches need to be found to shed light into plasma-tissue interaction. Standardized plasma treatment should generate specific reactive species with a controlled concentration to treat in the right place and the right time a specific tissue or pathology [14]. One objective of this work is to provide such a controlled reactivity for precise plasma medical studies.

There are two main types of plasma devices used in medicine: the dielectric barrier discharge (DBD) and the plasma jet. In DBDs, plasma is created in a gap between two high-voltage electrodes isolated with a dielectric material. The discharge electrode configuration makes use of the treated tissue as ground electrode or integrates its own ground electrode. As for plasma jets, they are technically DBDs but have a different nomenclature because of their particular gas flow configuration, causing a plume-like plasma [14]. Plasma is created inside a tube-like structure, with both electrodes and the dielectric integrated in the device. These sources use dielectric between the electrodes to prohibit high current flows and stop the discharge from transitioning to an arc [14].

Working gases generating the plasma are typically noble gases argon (Ar) or helium (He). Ionization of these gases is achieved at lower energies, allowing lower plasma temperatures for interaction with tissues. When plasma interacts with air, or if oxygen, nitrogen are added in small concentrations to the working gas, the energy contained in the plasma will dissociate them and create medical-relevant reactive species like ozone (O_3) , oxygen (O_2) ,

oxygen (superoxide (O_2^-)), singlet oxygen $(^1O_2)$, hydrogen peroxide (H_2O_2) , nitric oxide (NO), peroxynitrate $(ONOO^-)$, hydroxyl radical (OH), etc.

The main plasma sources commercialized are: kINPen MED (Germany) an argon-plasma jet powered with radio frequencies, MicroPlasSter (U.K.) an argon-plasma jet powered with microwaves and PlasmaDerm (Germany) an ambient air-dielectric barrier discharge [13]. It has long been confirmed that plasma treatment is not cytotoxic for cells, that it is well tolerated by our bodies without any side effects, and most importantly that it can heal skin pathologies or at least improve their outcomes [21].

Plasma's main mechanisms of action are [13]:

- microorganisms inactivation;
- stimulation of tissue regeneration;
- cell apoptosis which can be selective to cancer cells.

The different effects of plasma on cells or tissues will depend on many things but especially on the dosage of the RONS being administered, influencing cellular redox-regulated processes [13].

Challenges in plasma medicine are manifold. The main ones, important for expanding the application of plasma devices in hospitals: standardization and defining plasma dosage. As this is the foundation for guaranteeing safety and effectiveness of plasma sources in treating any kind of disease [22].

The notion of dosage is most complicated because so many factors will impact. There still lacks a universal unit or measure defining plasma dosage. Is it the amount of reactive species diffusing in the interface? Is it the total energy deposited in the treated tissue? Plasma has a hormesis effect, meaning that biological effects are very sensible to dosage. Small dosages tend to be beneficial to cells but high dosages cause damage. This is why defining and controlling dosage is an important question: each study attempts to set definitions of their own. This work approaches dosage on two fronts. First, by characterizing plasma reactivity by measuring dominant plasma-produced species concentration and composition. Secondly, by controlling plasma treatment distance and exposure on a biological model. These considerations do not reflect all of the plasma's activity but it's a simplified solution to a complex problem.

Another challenge lies in plasma's interaction with wounds, especially chronic wounds which are very heterogeneous. Some zones of the wound might be infected and inflamed vs others

zones show features of fibrotic lesions, etc. This calls for an adapted plasma treatment depending on the zone of the wound and its specific needs. Chronic wounds can have different root causes like obesity, diabetes, deficient immune response, etc., which modify the wounds imbalances. The aim ultimately is to have an optimized healing response by adapting the plasma treatment to the specific tissue type, status, zone, etc. Varying plasma gas composition to produce specific species is a way to adapt the treatment, given we know which species are most beneficial for the context.

1.1.3 Plasma-Tissue Interaction

In predicting biological effects of plasma on tissues, we first need to gain insight on plasmatissue interaction.

As plasma interacts with soft matter, its electrical and chemical properties are being modified and vis-versa. The interaction encompasses exchange of electrons, collision cascades on the surface, bond breaking, diffusion and long-lasting effects (in time and space) beyond the interface [22]. Plasma power and temperature will be altered by the target tissue since it is a conductive substrate [23]. All of this ultimately impacts the reactive species being created, as well as their transport and diffusion to and into the tissue [23].

Reactive species, as the name hints, have high reactivity, which limits their diffusion in the tissue. When applying the plasma, reactive species have strong localised effects on the cells. This burst of reactive species also triggers systemic effects that last in time and can penetrate deeper into the tissues. Reactive species react with cell membranes or with intracellular components by diffusion inside the cell, and they activate cascades of cell signaling [22]. Reactive species cause oxidation–reduction occurrences in contact with biomolecules, leading to changes in proteins, DNA, lipids, proteins, fatty acids etc. [24]. Different reactive species have different reactivity and diffusion capabilities vis-à-vis a given tissue which contributes to the heterogeneous phenomena of the interaction [14,25]. Species like OH have high reactivity and will react close to their site of formation [25,26]. Other species, like O_2 –, can't diffuse so well and will have a more localized impact. Species like NO and H_2O_2 , that easily diffuse through membranes (in the range of 100μ m [19]), will have more impact on intracellular signaling [26,27].

1.1.4 Redox Biology

Since RONS are the dominant actors of the biological plasma effects, plasma medicine has been coined a field of applied redox biology. RONS are important signaling molecules pro-

duced and used by our bodies to regulate a wide variety of physiological functions. Processes regulated by signals delivered through changes in redox chemistry make up the field of redox biology. Redox is short for reduction-oxidation: Reactive species are acceptors and donors of electrons which contain energy. But how can RONS have such determining effects on cells and what are the mechanisms by which they can alter cell function? There are two mechanisms by which RONS initiate cellular signaling. The first is to modify structure and/or function of target proteins, by reducing/oxidizing them via thiol switches [28]. The second is to induce changes in the intracellular redox state [25]. This activates redox-sensible pathways and modulates chemical reactions in the cell. Cellular processes regulated by redox-signaling include gene activation, cell proliferation, migration and differentiation, metabolic activity, apoptosis, inflammation, etc. [29]. In wound healing, many signaling pathways are under redox control.

Our bodies have mechanisms to endogenously produce reactive species. For example, mitochondria reduces oxygen to O_2^- as a by-product of the electron transport chain. O_2^- can be converted to H_2O_2 by mitochondrial superoxide dismutase. In the Fenton chain, H_2O_2 becomes OH [25]. Phagocytic cells also produce reactive species as a defense against pathogens. Nitric oxide is produced from metabolism of amino acid L-arginine, a process catalyzed by nitric oxide synthases (NOS) enzymes [25].

The balance of oxidation-reduction in the tissue allow cells to carry out physiological objectives. Short bursts of oxidants are necessary when a break in hemostasis occurs, and to repair damage. But alterations from baseline levels lasting in time can cause oxidative stress, causing irreversible oxidative modification and damage to cellular macromolecules present in our bodies e.g., lipids, DNA and proteins [28,30]. Oxidative stress is the cause of many pathological conditions e.g., cardiovascular disease, diabetes, autoimmune disorders, osteoarthritis, cancer, reproductive disorders, neurodegenerative disorders and chronic inflammation [7,14,25,26,31–33]. This is why maintaining or returning to a balance in the amount of redox species—oxidants—and the amount of antioxidants is essential.

The body has defense mechanisms against oxidative stress. Antioxidants are a system of proteins who's role is to balance oxidative potential, permitting RONS to perform their biological functions without causing damage [14]. Antioxidants achieve this by donating their electrons, thus preventing oxidants from capturing electrons from other biomolecules [34].

Dose-response: redox state refers to oxidative eustress (positive form of stress) and oxidative distress and this is dependent on low or high levels of oxidants in tissues. Oxidative eustress has beneficial or stimulatory effects, but oxidative distress is rather inhibitory or toxic for cells [19, 25, 35]. If we look at this from a wound healing point of view, oxidative eustress tends to promote proliferation, migration, angiogenesis thus contributing to the healing. One study from Van Huizen and al. further argues that in the oxidative eustress range there are sub-thresholds. The first threshold of reactive species promotes healing and the second threshold promotes wound closure and tissue regeneration in different time points (Figure 1.1) [1]. While oxidative distress activates pathways that induce senescence, apoptosis, or necrosis [36]. The biological role of RONS is always paradoxical since redox is needed for cellular homeostasis but can also be a factor for diseases. But this boundary between oxidative eustress and distress is not so clear.

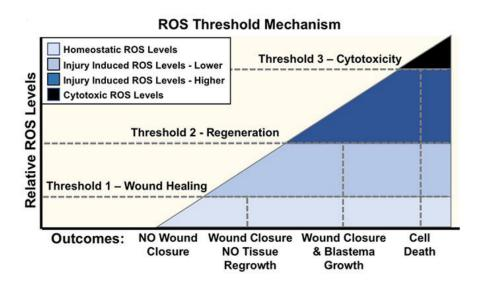


Figure 1.1 Threshold levels of ROS and general biological effects [1]

Many studies support the idea of RONS having an hormesis effect on cell response. One article by Szili and al. varied dosage of RONS by varying the flow of plasma and the exposure time, both increasing RONS concentration. The results showed that cells better tolerate a low dose of RONS over longer exposures vs a high dose delivered quickly, even if the final concentration of reactive species is the same [35]. This is interesting because it adds a time frame to dosage: It is not just about how many RONS are delivered but also about how much/time.

1.1.5 Plasma for (Chronic) Wound Healing

Plasma supplies an exogenous source of reactive species to the wound, modifying the redox state and influencing it's healing. Wound healing involves many actors such as endothelial cells, immune cells, fibroblasts and keratinocytes. These cells use cytokines and growth factors to communicate. Plasma's reactive species act as messengers via autocrine cell communication (within an individual cell) or via paracrine cell communication (among other cells in proximity). This is how plasma treatment can penetrate into the tissue and have a long term effect. Reactive species are both wound-healing molecules and capable of producing other such molecules. These molecules in turn activate intracellular signaling pathways that will influence cellular functions e.g., cell migration, cell proliferation, extracellular matrix (ECM) remodeling, angiogenesis, as well as cytokines and growth factors expression [7].

Phases of Healing

Wound healing is a multi-step process encompassing: hemostasis, inflammation, proliferation (new tissue formation), and tissue remodeling.

When skin damage occurs, there is a localized hemorrhage. The body reacts to cease the bleeding by creating a plug, a process called hemostasis. Platelets in the blood aggregate and attach to the damaged site to build a blood clot composed of fibrin, fibronectin and other extracellular matrix (ECM) proteins [37,38]. The ECM is a network of macromolecules linked together to form a structurally stable environment for cells. It is highly dynamic, acting as a reservoir of bioactive molecules, giving mechanical strength to tissues and allowing cell proliferation, adhesion, migration, etc. [39]. The fibrin network that forms during hemostasis acts as a provisional matrix for cells to migrate in [38,40]. Platelets release chemotactic factors to attract leukocytes (neutrophils, macrophages) and growth factors to initiate the subsequent phases of healing. These include pro-inflammatory factors such as interleukins (ILs), tumor necrosis factor-alpha (TNF α) and pro-proliferation factors such as platelet-derived growth factor (PDGF) and transforming growth factor beta (TGF- β) [38,40].

TGF- β is a key cytokine for wound healing processes, as well as deregulated healing. It will be referenced often in the sections to come. It is one of the main triggers to fibrosis. TGF- β is sensible to redox states, linking it to plasma treatments. Since TGF- β influences cell differentiation, protein expression, etc., it presumes detectable biomarkers that will change under plasma treatment. This also motivates the choice of fibrosis tissue pathology as the focus of this research. Any mentions of TGF- β 's role in the wound healing processes, could also imply plasma's potential in influencing these processes.

Once the bleeding is controlled, the inflammation phase begins to prevent infection of the wound. This phase involves immune cells. Blood vessels dilate and become more permeable, increasing the flow of cells coming into the wound [38,41]. The first cells that reach the wound bed are neutrophils. They come to engulf and kill foreign particles, and pathogenic organisms and also secrete cytokines to recruit macrophages, T-cells and more neutrophils. Macrophages come shortly after to kill what is left of contaminant, to scavenge tissue debris and engulf the spent neutrophils still on site [37,38,40,41]. Macrophages are pivotal in the transition between inflammation and tissue repair as they are the main cells that launch the proliferation phase by releasing chemotactic factors, cytokines and growth factors, mostly anti-inflammatory, to resolve the inflammation process e.g., epidermal growth factor (EGF), fibroblast growth factor (FGF), Vascular endothelial growth factor (VEGF), TGF- β , ILs [14, 38, 40].

The proliferation phase overlaps the inflammatory response with it's main objective being to close the wound. Proliferation phase includes fibroplasia, reepithelialization and angiogenesis [37, 38, 40]. Cytokines and growth factors, secreted by platelets, and immune cells, promote migration and proliferation of epithelial cells, fibroblasts and keratinocytes, which are the main cells implicated in the proliferation phase. Growth factors furthermore promote angiogenesis [14]. As fibroblasts populate a lesion, they produce collagen, proteoglycans and glycosaminoglycans to start fibroplasia, building a granulation tissue and bridging the wound gap for dermal reconstruction. There is formation of an ECM [37, 38, 40]. The predominant type of collagen in this new connective tissue matrix is type III collagen. Reepithelialization happens simultaneously with the migration and proliferation of epithelial cells and keratinocytes, from the wound edges [38, 41]. Angiogenisis is essential so that blood vessels can carry oxygen and nutrients to the cells in the newly formed tissue [14, 37, 38, 40, 41]. Cytokines, such as TGF- β , push differentiation of fibroblasts to myofibroblast which are the cells responsible for wound contraction [37, 38, 40]. Together, fibroblasts and myofibroblasts orchestrate the closing of the wound and synthesize the new dermis [41].

Wound contraction is essential for increasing the stiffness of the scar tissue and restoring tensile strength of the skin. It starts in the proliferation phase and when it reaches its peak, the remodeling phases has begun (2-3 weeks after injury) [42]. In the remodeling phase, the granulation tissue start reorganizing itself into a mature dermis—it is replaced mostly by a collagenous scar of type I collagen [37, 38, 42]. This phase serves to restore function and aesthetics to the tissue. There is an ECM turnover where simultaneously the new collagen is synthesized and the old collagen is lysed: This action is carried out by matrix metalloproteinases (MMPs) [38, 40, 41]. MMPs can be expressed by all mentioned cells [43]. Finally, ECM-producing cells go through apoptosis and are replaced by mature fibroblasts that preserve the tissue's structure [37, 41, 42].

Chronic Wounds

Wound healing depends on numerous actions carried out by a fragile balance between signaling molecules, cell response, and a inter-play between healing phases. If the balance is disrupted, if the phases fail to properly succeed each other, the wound can become chronic. It gets stuck in a given state and starts secreting too much of one thing and not enough of another. In a way the new state of the wound hijacks the healing program and uses it to over-heal itself. Another important aspect of wound healing is impaired vasculator formation. Without appropriate supply of blood to the new tissue: The cells don't have enough oxygen to go through a normal wound repair [44]. There are many causes for failure of normal healing, such as infection, malnutrition, age, diabetes, pressure necrosis, etc. [45]. Chronic wounds are always infected, and colonized with pathogens which the body has insufficient defense against [46]. Non-healing wounds also have in common chronic and excessive inflammation, dysregulation of important cytokines and MMPs activity, excessive levels of reactive oxygen species, decreased oxygenation, along with deficient and altered cell function [12, 45].

Fibrosis can be attributed to a deficient immune response, deficient ECM-producing cells responses, resulting in fibrotic lesions. A key motivation for the present work is future application of plasma against fibrosis. Tissue fibrosis accompanies numerous diseases and is a prominent cause of death and morbidity in the developed world, making up about 45%of deaths [3]. The excessive deposition of connective tissue that characterises fibrosis affects the biomechanical properties of organs, impairs its structure and function, eventually leading to its failure [42]. Figure 1.2 illustrates fibrosis' progression. Fibrosis arises when ECM producing cells such as fibroblasts, myofibroblasts become increasingly active, and numerous. Usually, this starts with a persistent inflammation response. Pro-inflammatory cytokines have a primordial role in regulating scar formation through their interactions with the ECM and the signaling pathways that regulate it's development [47]. When inflammation fails to resolve, macrophages accumulate in the wound bed and instead of resolving the inflammation, their production of pro-inflammatory signaling increases and persists. Cytokines including TGF- β and interleukin 6 (IL-6) recruit and augment the proliferation of fibroblasts. Abnormal amounts of collagen accumulate, with excessive deposition of ECM proteins [37, 38, 41, 44]. In parallel, uncontrolled differentiation of fibroblasts, driven mainly by TGF- β , leads to enduring myofibroblastic populations. Myofibroblasts are big players in fibrosis. They produce incessant amounts of ECM and fibrotic markers, and more specifically they produce α sma protein—a contractile protein—which causes pervasive contraction of the matrix [43,47]. The tissue overgrowth from the excessive matrix deposition causes hardening and increases stiffness, also exacerbating the contraction signals. ECM contraction favors

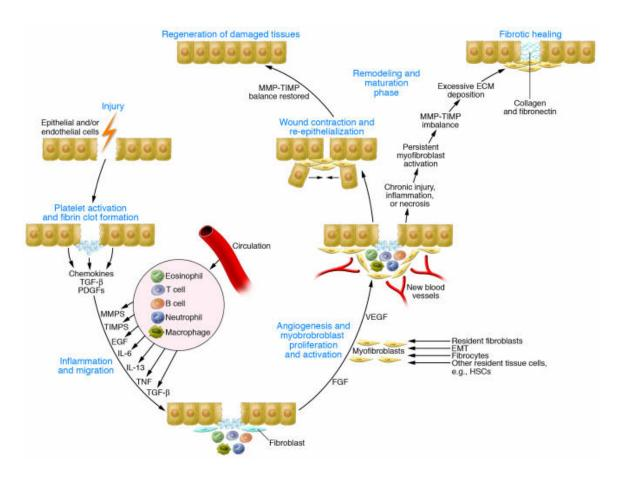


Figure 1.2 Wound healing and fibrosis progression steps [2]

even more collagen production, expression of α sma and favors release of TGF- β . All these mechanisms fuel a positive feedback for fibrosis [3,43]. Many cytokines and growth factors are involved in triggering and maintaining fibrosis. They are mostly the same messengers that drive the proliferation in wound healing phase but have become self-regulated and are present in excessive amount.

TGF- β is a key inducer of fibrosis [7,38,47]. TGF- β signaling in fibrogenesis is characterized by strong activation of fibrotic genes and fibroblasts proliferation, migration and differentiation. TGF- β is a multifunctional cytokine that regulates cell growth, differentiation, and biosynthesis of ECM proteins. It is a very important mediator for resolution of inflammation in acute wounds, essential to engage the proliferation phase. But in a chronic wound, it pushes proliferation to the extreme and over-healing starts to occur. It is an exaggerated response to normal tissue repair processes and signals [44]. TGF- β is also know to downregulate MMPs in fibrotic tissues. MMPs are essential in the remodeling phase for enzymatic degrading of collagens, and other ECM proteins, and in assuring a balanced ECM composition. A wound environment lacking MMPs have impaired cellular functions like angiogenesis and matrix remodeling [7,47]. In the fibrotic tissue, their is reduced capillary density since ECM proteins take up all the space. This leads to oxygen depletion in the tissue [48]. Hypoxia activates hypoxia-inducible factor-1 (HIF-1) signaling pathways, triggering a number of profibrotic genes. Macrophage-secreted growth factors like VEGF, FGF, TGF- β can also be induced by hypoxia [49], adding to the already high amounts of TGF- β that are driving fibrosis. Figure 1.3 presents a summary of fibrosis drivers.

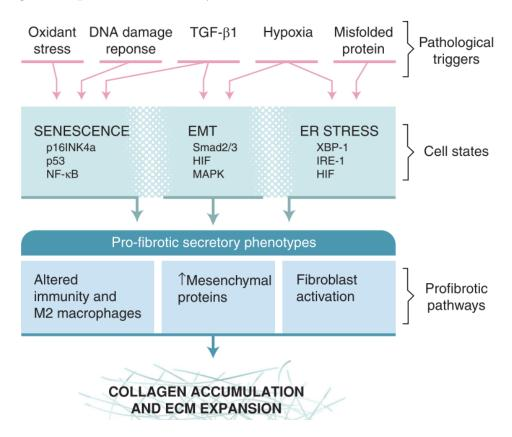


Figure 1.3 Drivers of fibrosis [3]

ROS and RNS Regulate all Phases of the Healing

All the majors cells involved in orchestrating wound healing—platelets, macrophages, fibroblasts, endothelial cells and keratinocytes—use reactive species as secondary messenger for regulating a number of functions [34]. The following paragraphs highlight the heavy lifting done by reactive species to regulate wound healing.

Reactive species play a key role in the innate immune system response and the inflammatory phase. During host defense, phagocytic neutrophils and macrophages engulf and destroy pathogens and contaminants by releasing bursts of radicals and reactive species in lethal levels [13,37,50]. To achieve this, phagocytic cells perform a respiratory burst by consuming O_2 in large quantities and reducing it to either O_2^- or H_2O_2 (Figure 1.4). These cells can also secrete reactive species, such as H_2O_2 , into the extracellular space, to extend their antibacterial effect throughout the tissue [14,34].

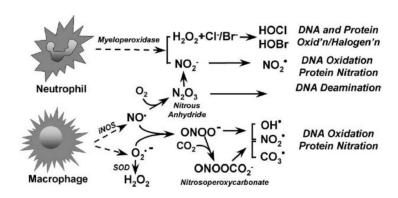


Figure 1.4 Neutrophils and macrophages use reactive species to damage and kill pathogens by performing a respiratory burst [4]

Reactive species also act as chemo-attractants and recruit more immune cells to participate in the defense against pathogens [12,32]. Further, reactive species are messengers for stimulating the release of growth factors e.g., PDGF, VEGF, etc. [14,51].

In the proliferation phase, redox signaling also conducts many processes. Reactive species, by promoting the release of growth factors such as FGF, increase proliferation and migration of vascular endothelial cells, keratinocytes and fibroblasts, facilitating vascular remodelling, reepithelialization and ECM / scar formation respectively. Reactive species are also critical regulators of angiogenesis. They modulate VEGF signaling which is a key proangiogenic growth factor: Reactive species can induce transcription of HIF-1 which up-regulates VEGF and VEGF receptors on endothelial cells [26]. H_2O_2 can stimulate VEGF expression by macrophages, keratinocytes, and fibroblasts [51]. NO is also a very strong messenger for vasculator events. During inflammation, NO can increase vessel dilatation and vascular permeability to ensure more immune cells enter the wound site to resolve the inflammation quicker [14,34,41,50]

Reactive species, specially reactive oxygen species (ROS), are huge mediators of TGF- β [34, 50–52]. Oxidation can activate latent TGF- β [3]. Through this relation between ROS and TGF- β , ROS have much control fibroblast function, over ECM synthesis and contraction. Reactive species are also responsible for ECM release of TGF- β [51].

If we consider reactive species in the context of fibrosis, many mechanisms upregulated by

ROS would favor a fibrotic behavior of the tissue. Still, facts support the idea of plasma as a therapy for fibrosis. Specific reactive species play important individual roles which could help counter fibrosis. Nitric oxide (NO) seems to be key in this explanation. NO bioavailability in chronic wounds is usually scarce [51], and plasma can be a source for a burst of NO in the tissue. NO is known to be a scavenger for ROS and an antioxidant e.g., neutralises O_2^- . This can prove to be usefully in fibrosis where redox levels are elevated [34, 51]. NO can also have anti-inflammatory effects. When it reaches its physiological concentration, a negative feedback loop occurs and pro-inflammatory proteins expression is reduced [53]. NO can also inhibit the activation of the transcription factor nuclear factor- κ B (NF- κ B). NF- κ B inhibition causes down-regulation of the expression of pro-inflammatory genes. [27]. Other key actions of NO are enumerated: regulates angiogenesis, regulates granulation tissue through inhibition of cytokines such as TGF- β . NO promotes apoptosis during scar remodeling as well as keratinocyte proliferation for accelerated reepithelialization [53]. NO can also alleviate oxidative damage by indirect inhibition of lipid oxidation reactions [51].

Low levels of RONS are essential in stimulating effective wound healing, excessive RONS cause cellular damage and impaired wound repair. But as described earlier, it remains more nuanced than this. Dosage isn't the only important factor. Redox signaling controls both pro-inflammatory feedback loops to kill off pathogens and anti-inflammatory feedback loops to avoid an exacerbated harmful inflammation phase and kick-start proliferation [14, 50]. Reactive species carry a huge paradox in their actions in wound healing. A quote from Graves in his article "The emerging role of reactive oxygen and nitrogen species in redox biology and some implications for plasma applications to medicine and biology' [14] illustrates this paradox well:

"in some ways the most important issue with inflammation is the need to terminate it fairly quickly since the non-specific anti-infective actions—mostly release of RONS—can be very damaging to the host"

It is not yet possible to single out a specific reactive specie and tell of its isolated role in the healing process. This is why it is hard to dose plasma to optimise its effects: we still seek to define what species and in which quantities are needed for a given pathology or status of the wound. The redox signaling pathways are much entwined, and reactive species have a fine-tuning regulatory role. It is still unclear all the parameters of this tuning. The body has its ways of balancing the redox levels. In the case when it fails, plasma could be of help. For this we need tools too take over the control board—to be able to have specific and tailored actions. The tricky part is that so many processes are at play—inflammation, cell proliferation, cell differentiation, vascular formation, etc.—which are activated or inhibited by common signals

and impact each other. Also, many signaling pathways and messenger molecules have dual functions depending on the healing phase, the concentrations of reactive species, etc. Plasma is a tool for delivering know concentrations and compositions of ROS/RNS by modulation of gas composition, power, etc. and disentangling some of the mechanisms behind the biological consequences of redox-signaling [24].

Plasma Sources Treating Wounds: Experimental Studies

Many experimental studies, in vitro and in vivo, support plasma's role in accelerating and improving wound healing—acute and chronic. In parallel, redox theory can account for why we are observing these outcomes: in part due to antisepsis effect, but more importantly due to direct influence on the inflammatory response and on stimulation of tissue regeneration [21, 22]. Despite studies using different plasma sources, gases, cells, biological contexts, etc., the majority agree that plasma treatment on tissue in a dose-dependent manner will reduce inflammation, influence migration, proliferation and differentiation of cells, modulate angiogenisis and impact the final outcome of the wound.

Healthy tissues vs pathological tissues won't always react in the same way to plasma treatment. A very insightful study reinforces this idea that different cells react in varying manners to plasma [54]. Tis study used plasma to treat scratch assays of normal fibroblasts (NFs) and keloid fibroblasts (KFs). KFs are a fibrotic phenotype of fibroblasts producing more collagen and keloid scaring (fibrotic tissue). Results showed that plasma induced coll 1 expression in NFs but reduced it in KFs. Similar results where observed for cell migration. TGF- β content was also reduced in KFs, and stayed the same in NFs following plasma treatment. Plasma showed opposite effects depending on cell phenotype: It stimulated healthy cells and had anti-fibrotic effects on deregulated cells. The plasma source used in this study was a DBD plasma with nitrogen (N₂) as carrier gas with 13% argon admixture. These results suggest that a plasma rich in RNS might be more beneficial to chronic wounds [54].

Few studies compared biological effects of different plasma compositions. One study compared a plasma source with Ar feed gas vs Ar + 5% air admixture feed gas. Plasma sources are used to treat mice biopsy punches. Both accelerated wound healing, and increased expression of cytokines IL-6 and TGF- β compared to control. But the argon-plasma with added air had a more significant impact [55]. This study tells us that added admixture to plasma feed gas yields a wider variety of reactive species and this can optimize treatment outcomes. Argon-plasma with added air will yield more nitric oxide, but it will still produce a lot of O₃. This plasma regime admittedly produces a bigger variety of reactive species but it does not maximize dominance of nitrogen oxides vs oxygen oxides and vis-versa. The

work of this thesis proposes rather to establish opposing plasma regimes that may lead to different biological outcomes and may help to decipher specific reactive specie's role in cell biochemical-mechanisms.

The following paragraphs detail the main experimental biological effects studied in wound models following plasma therapy. It is important to note that plasma dosage is tuned to achieve the results observed in these studies. Plasma treatment times, distances, etc. are optimized to get stimulating outcomes.

Plasma is anti-bacterial and shortens inflammatory response for wounds. All experimental studies confirm that plasma inactivates a great range of microorganisms, with a broad killing spectrum. Plasma is able to remove hard-wearing biofilms [21,46]. Plasma achieves this with the bursts of exogenous reactive species that kill pathogens. Pathogens haven't developed resistance against plasma—this could be due to the complex and multi-component nature of plasma which includes physical and chemical fronts of actions [46]. A major consequence of this antiseptic property of plasma is a shortened inflammatory response. Reduced contaminant loads allows the body to reduce inflammatory cell infiltration in the later stages of wound healing and temper the inflammatory response so it does not needlessly go on. This in turn efficiently promotes wound closure and tissue repair, and ultimately shortens healing time [12,56].

In vivo tests on animal models prove this time after time. Infected sheep and rabbit wounds treated with plasma showed no inflammation, no sign of infection—swelling, oozing—compared to control groups [42,57]. Histological analyses of wounds showed more immune cells migrating into control groups, indicative of a bigger inflammatory response [57,58]. The hypothesis is that plasma anticipates the inflammation phase by its early activation, recruiting inflammatory cells and inducing cytokine expression. This limits inflammation in the later phases [42]. Studies done on non-diabetic and diabetic rats showed more acute inflammation in both groups treated by plasma compared to self-healing group [48,58]. A similar study on diabetic mice vs healthy mice showed that the inflammation phase of plasma treated wounds was shorter in the diabetic group compared to control. Plasma can attenuate inflammation, especially in an pathological context.

Plasma accelerates and improves reepithelialization, and ECM formation. In all wound model studies, reepithelialization was quicker. Infected mice wound models showed improved reepithelialization in plasma treated groups compared to control groups which had persistent infection and immune cell infiltration [12]. Rabbit scalp defect infected with

methicillin-resistant S. aureus (MRSA) showed similar results: Severe infection obstructed the healing and the formation of healthy granulation tissue. Staining of collagen marker showed disordered hyperplasia in the self-healing group, which disrupted reepithelialization of the wound, compared to plasma treated group which displayed normal granulation tissue formation, covering the whole wound area, without excessive scar tissue formation [57]. Diabetic rat and mice wounds treated with plasma had increased keratinocyte migration and proliferation, increased epidermal layer formation and ultimately a greater percentage of reepithelialization [36, 48, 58]. One hypothesis is that plasma treatment induced TGF- β expression which enhanced keratinocyte activity, and promoted reepithelialization in general [12,48]. Further experiments are done on acute wound models. Studies compared plasma treated rat wounds to self-healing wounds. Results showed markedly reduced wound area in plasma groups as a result of increased migration and proliferation of cells [5,6]. Reduced wound area and quicker wound closure is demonstrated after plasma treatment in Figure 1.5.

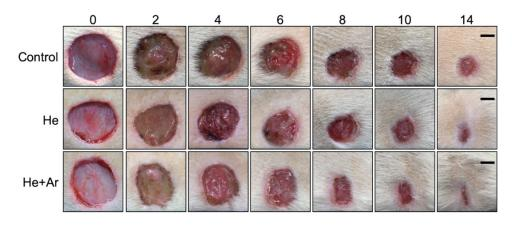


Figure 1.5 Comparison in wound area for self-healing wound, control and plasma treatments from day 0 to 14. Plasma treated wound is significantly smaller on day 14 [5]

Plasma has a large influence on gene expression. By regulating genes, plasma can have diversified impact on cell functions. This regulation of genes depends on many factors. In acute wound context, plasma generally up-regulates gene expression, stimulating cell function. Plasma activation or inhibition of genes is time-dependent. A study done on an infected rabbit wound showed expression levels of TGF- β , and VEGF after plasma treatment were significantly lower than in the control group, in the first week of wounding. This observation is attributed to the early control of inflammation by plasma. During the second week of healing, FGF, EGF, TGF- β , and VEGF are most expressed in the plasma treatment group since this corresponds to the proliferation phase where all these cytokines

are needed for wound closer [57]. Another research was done regarding MMPs expression in infected mice wounds. Plasma treatment promoted MMPs expression in the early stages of healing and than restored its expression to basal levels in the later stages. Many studies show plasma impact on collagen expression. In a treated mice model, mRNA expression levels of collagens were significantly increased compared with control group [24]. In another study, infected mice treated wounds showed significantly more collagen deposition than the control group which had insufficient collagen deposition probably due to the lasting inflammation [12]. Anti-fibrotic effects of plasma also depend on modulation of genes. In a study done with diabetic mice, plasma decreased TGF- β expression. Reduction in TGF- β cytokine limited the inflammatory response [58].

Plasma promotes vascularization which leads to increased nutrient intake by cells, tissue oxygenation and counteracts hypoxia which is a driver for chronic wounds. Vascularization accelerates granulation tissue growth, reepithelialization and reduces scar formation. An increase in levels of VEGF in plasma treated groups of various animal models promoted angiogenisis in granulation tissue [38,42,58]. Synthesis of FGF which is another promoter of angiogenesis can also be increased with plasma [21]. Many studies observe improved microcirculation after plasma treatment of chronic wounds [6,53], increased tissue oxygenation in superficial and deeper skin layers [24], and increased new blood vessels in diabetic or infected wounds [36,58].

Another mechanism by which plasma helps wounds heal is contraction. The most important maker for wound contraction is α sma. This protein is expressed in stress fibers. It gives cells contractile properties which is essential to close the wound. A study done on mice wounds demonstrated higher α sma expression levels in plasma treated group [24]. Direct observation of contraction is also observed. Plasma treated rat and sheep wounds showed increased contraction compared to control group. This contributed to more efficient and faster wound closer [5,6,42] (Figure 1.6)

The paradox of plasma. Cells, cytokines, growth factors and all the underlying mechanisms involved in the acceleration of wound healing are also responsible for provoking progression of fibrosis. Plasma has been shown experimentally to accelerate wound healing by acting on many signaling pathways, and paradoxically has been shown to combat chronic wounds via the same pathways. Redox signaling pathways have a huge overlap in their role in wound healing and pathological wounds.

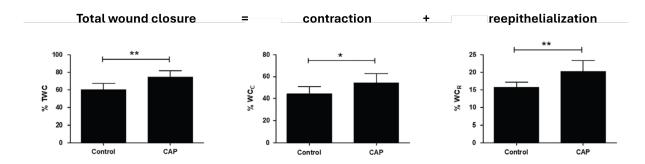


Figure 1.6 Wound contraction and wound reepithelialization increase after plasma treatment compared to self-healing wound [6]

A study from Arndt and al. attempts to shed some light on this paradox. studies have tried to demystify how plasma can impact healing in a positive way and by pressing all the same buttons can also be anti-fibrotic. This study from Arndt and al. [7] gives insight on these questions. By using comparison between fibrotic and healthy models and testing for effects of plasma via various fibrosis-related pathways and mechanisms. In vitro cells used as healthy models are a) human epidermal keratinocytes (hEK), and b) human normal fibroblasts (hNF). Fibrotic models used c) activated fibroblasts (hAF) which are hNF activated with TGF- β , and d) fibroblasts isolated from the skin of patients with localized scleroderma a form of fibrosis (hLSF). hLSF naturally have elevated levels of TGF- β . The study also used an mice model with a healthy wound vs a scleroderma wound induced using bleomycin (BLM). Many results stand out in this study. Migration assay achieved with spheroid cell models for all fibroblast cell types is done since fibrosis implies elevated migratory ability of fibroblasts. Plasma treatment vs control showed hNF have increased migratory ability informing us on plasma's ability to accelerate healing in an acute context. As for hAF and hLSF, migration was reduced after plasma treatment compared to control, hinting plasma can also have an anti-fibrotic effect in a pathological context (Figure 1.7).

These results are the perfect example of how plasma outcomes can be opposite to the expected outcomes simply by changing the cells under treatment. Pro-fibrotic genes are investigated cultured fibroblasts treated with plasma and co-cultured fibroblasts with plasma treated-keratinocytes. Collagen type 1 and alpha smooth muscle actin are both increased after plasma treatment for hNF. As for hAF and hLSF, their expression of these proteins remains unchanged. The hypothesis is that if pro-fibrotic genes are already over-expressed in hAF and hLSF, plasma doesn't further induce them nor act as a fibrotic activator. As for co-culture model, coll 1 and α sma are once again induced in hNF and not affected in hAF and hLSF. This shows the paracrine effect of plasma, since keratinocytes are capable of sending cell-

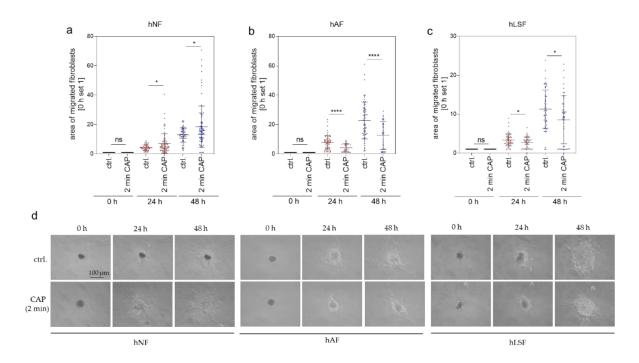


Figure 1.7 Migratory ability of various cell types modulated by plasma treatment [7]

to-cell signal to fibroblasts after being triggered by plasma [7]. Pro-inflammatory cytokines IL-6 and TNF α are investigated in co-culture model since they are usually over-expressed in fibrotic lesions. Both are induced in hNF after plasma treatment, and no effect is observed in hAF. Surprisingly, they are reduced in hLSF. This showcases a potential anti-inflammatory effect of plasma in chronic wounds [7,59]. Plasma treatments also induced expression of MMPs in hAF and hLSF. MMPs were negatively regulated in these cell cultures because of over-expression of TGF- β . MMPs are is usually down-regulated in fibrosis which impairs the wound's ability to degrade and remodel the granulation tissue leading to hypertrophic scar formation. Here plasma showcases it's ability to reverse fibrotic behavior of cells. Fibroblast cultures are also screened for myofibroblast differentiation. Control hAF and hLSF cultures had a lot of stress fibers and differentiated fibroblasts. After plasma treatment, stress fibers are reduced. This once again proves the ability of plasma to reverse fibrotic cell phenotype. Finally, a mice wound model with BLM-induced fibrosis is treated with plasma. Comparison to control showed a reduction in dermal thickness in the fibrotic wound treated with plasma. The number of myofibroblasts and macrophages was decreased in plasma treated group: Demonstrating anti-fibrotic and anti-inflammatory effects of plasma [7]. This study is a glimpse at an explanation for the paradox of plasma. Part of the answer lies in the biological context of the tissue which causes cells to react very differently to plasma.

1.1.6 Diagnostics: Plasma and its Biological Outcomes

Tailoring Plasma with a Feedback Loop

The interest for integrating plasma devices in a feedback-control loop is to be able to continuously monitor in real-time, and *in situ*, the varying plasma and target tissue features during treatment. By doing so, we can adapt plasma parameters to the needs of the tissue to optimise the therapeutic objectives. The 'black box' plasma and the 'black box' tissue can thus be partly demystified. This feedback loop would also ensure more stable and constant plasma treatment conditions.

Defining Reactivity of the Plasma

Plasma monitoring can be done through species concentration and composition measurements. Plasma reactivity is a crucial part of how plasma interacts with biological tissues and is the essence of the present research. One of the major questions in plasma medicine is 'how to correlate specific plasma-generated RONS mixtures to a given biological response?'. This question is precisely why it is important to have accurate and precise diagnostics of reactive species being produced in the plasma. Only this way can we control reactive species concentration and composition and begin to understand specific roles of RONS in tissue redox processes. Defining dominant species in the plasma and being able to relate this to affected biological functions is fundamental plasma medicine research. Measurements on reactive species in the plasma are achieved with complementary optical spectroscopy techniques: optical Absorption spectroscopy (OAS), optical emission spectroscopy (OES), and Fourier transform infrared (FTIR) spectroscopy. These techniques' methodology will be presented in detail in chapter 2, as well as associated results in chapter 3.

Monitoring Biological Responses

Tissues treated with plasma will respond with various changes. Biomarkers can be precisely measured through biological experiments, reflecting these changes in tissue biochemistry and relating them to plasma treatment. Such markers include protein expression, cytokine secretion, cell metabolism, etc. Biology experiments are well adapted to cell cultures and tissue samples. Chapter 3 presents the biology assays this work used to evaluate plasma outcomes on cells.

However, all of these assays are post-treatment analyses, and cannot be integrated in treatment feedback systems in a plasma device. To complete the feedback loop, real-time moni-

toring is needed. Spectral signals from treated tissues can yield spectral features, embodying biomarkers. This is our proposed method for real-time tissue monitoring, which is not used in this work but is proposed as a suitable technique for follow-up animal and clinical studies. The method is detailed in the next section of this chapter.

This work focuses on fibrosis. This choice of tissue pathology is strategic for collecting efficient feedback signals since the features will change drastically between healthy and fibrotic tissues. Many cytokines and proteins become overexpressed in fibrosis and hypertophic scars vary greatly from normal healthy dermis. This chronic wound model has high potential to be spectrally distinct before and after plasma treatment, thus giving good feedback for modulating plasma.

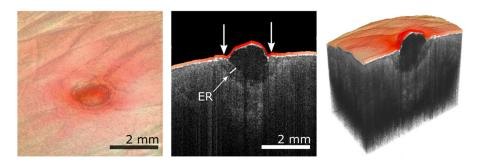
Dual-Modality: Optical Coherence Tomography and Hyperspectral Imaging

A combined optical coherence tomography (OCT) and hyperspectral imaging (HSI) system could be used in parallel to plasma treatment of wounds to give feedback in real-time on plasma effects. These imaging techniques are adapted for *in vivo* tissue monitoring. They offer complementary information, thus should be used together in a single imaging system. OCT images tissues in 3D (with a penetration depth of a few millimeters) and gives information on tissue structure, morphology but not so much on biochemical or molecular composition. HSI renders 2D information on biomolecular status of the tissue [8].

OCT measures back-scattered light and uses sources in the near-IR in order to penetrate deeper in the tissues—IR wavelengths are larger than bio-particles thus there is less interaction (scattering, absorbance) between the light and tissue matter [8]. The first step of wound healing, during the hemostasis phase, is blood coagulation where vessels have been damaged and a blood clot forms to cease the blood loss. OCT can measure changes in blood-scattering coefficient or refractive index [60]. It can quantify the attenuation coefficient (μ) which comes from both scattering (μ_s) and absorption (μ_a) of the light in the tissue— $\mu = \mu_s + \mu_a$. This attenuation property can be used for characterizing local changes in blood's optical properties when coagulation occurs [60]. Since plasma is known to induce coagulation in the wounds, OCT could be used to monitor this phenomena. OCT also allows for monitoring epithelial regrowth underneath the wound. Plasma is known to increase and accelerate reepithelialization of a wound, as seen in detail in prior sections. If we can measure this real-time and fine-tune plasma parameters e.g., the gas composition to optimize the effect, then we have unlocked personalized plasma medicine.

As for HSI, biological absorbers show most spectral variations in the visible range [8]. Such bioabsorbers are hemoglobin, melanin, other proteins like collagen and elastin. Contrast

agents can be autofluorescent like collagens, or exogenous fluorescent markers can be injected to the imaged site [61]. Some researches have already explored tissue oxygenation and perfusion in animal wound models with HSI following plasma treatment [29,62]. Surface oxygen saturation and tissue hemoglobin distribution, and other microcirculatory parameters in the wound zone can be quantified using visible light. A more oxygenated, vascularized tissue will absorb further light and this is detected with HSI. Successful experiments on animal models showed differences between plasma-treated and control wounds microcirculatory features. HSI measured oxygen saturation to be greater in plasma treated wounds. The same trend was observed for hemoglobin concentration. This reveals higher blood vessel outgrowth after plasma-treated in vivo [62]. The visible spectral window can also be adjusted to measure collagen fluorescence (from 426–490 nm). Measurements of collagen has a lot of potential for monitoring plasma biological effects on tissues. Collagen is strongly involved in wound reconstruction: it is essential to have sufficient collagen to assure new dermis structure and strength but too much collagen will lead to fibrotic tissue. Sensitive techniques to measure collagen content will be useful. HSI can also be used to capture true-color of the skin which can enable measurements of inflammation in the superficial layer surrounding the wound [8]. Such a system combining both imaging modalities has been developed in Pr. Caroline Boudoux's lab using a double-clad fiber coupler as is demonstrated on Figure 1.8. OCT



images overlaid with inflammation status extracted from hyper-spectral imaging gives struc-

tural and biochemical portrait of an epithelial wound. [8,61].

Figure 1.8 OCT and HSI dual-modality 3D rendering of an epithelial wound (note from article: ER = epithelial regrowth) [8]

The motivation for this proposition of integrating imaging modalities to a plasma device is to be able to get insightful feedback from treated biological model once these start to become more complex. Ex vivo tissue samples, in vivo animal wound models, and eventually clinical wounds of patients need technologies that will yield instant feedback of several features in one capture. This is a major advantage of using spectral feedback for plasma adaptation.

1.2 Goals and Outline

Plasma medicine has made great progress since the early 2000s. Many studies, and clinical trials have demonstrated without a doubt that plasma can accelerate wound healing and most impressively turn a chronic wounds into an acute one. Certified plasma devices are being used in hospitals to treat patients. Even if plasma as a field of redox biology is now better understood, there lacks understanding on the specific role of reactive species in the wound healing processes. Such knowledge could lead to better, more precise, or novel plasma therapy options. This research proposes to address some of these questions: By shifting plasma reactivity and the composition of reactive species distributed to a biological sample, plasma can be a precision tool for redox-research and therapy. Plasma characterization is essential to be able to identify and quantify the species. With these assets in hand, a compact plasma jet setup is required in a hospital environment: Setting the the stage for experiments that plan to reveal interactions between a fibrosis model and plasma-based redox changes.

The following objectives set out to achieve what is mentioned above and to start answering some of these challenges in the field of plasma medicine for wound healing:

- 1. Characterization of plasma source reactivity with optical diagnostic tools;
- 2. Establishment of dual-regime plasma setup compatible in a hospital environment;
- 3. Plasma treatment procedure with a biological fibrosis model and investigation of plasma's effects on cell activity and function.

Chapter 2 presents the methodologies for spectroscopic monitoring of plasma reactivity as well as the plasma source used for the thesis and the parameters that can be tweaked to modulate plasma reactivity. Chapter 3 focuses on optical diagnostics used to establish and validate both plasma regimes. Chapter 4 addresses the biological experiments performed with the plasma source to gain insight on plasma's role in wound healing and to set the basis for a plasma treatment protocol.

At length, chapter 5 summarizes the work completed in this thesis and discusses the improvements and future work that can be done on the subject of tailored plasma treatment of chronic wounds.

CHAPTER 2 Plasma Characterization

Characterizing plasma species composition is one of the key objectives of this work. Tuning plasma parameters and entry gases can shift plasma reactivity, producing distinct dominant reactive species in the effluent. These species interacting with biological models trigger specific cell signaling pathways that yield different biological outcomes in a tissue. Characterizing plasma and controlling its reactivity allows us to link biological outcomes to specific species and gain more insight about wound healing and eventually make plasma treatments most efficient. Plasma can also be characterized other ways than by produced species: it generates heat that can be measured, it comprises charged particles thus has electrical parameters, it is visually different from one regime to the other, etc. This chapter will present the methodology for characterizing molecule densities and species present in the plasma effluent. It will also present the plasma device and some of its key parameters. Established plasma regimes will be introduced and characterized but results supporting the choice of both regimes will be detailed in chapter 3.

2.1 Plasma Diagnostics Methodology

2.1.1 Emission and Absorption Spectroscopy

Particles can absorb and emit energy. Energy transitions of particles correspond to specific wavelengths which is how we can identify particles' emission and absorption lines. The light absorption or emission gives us spectral signatures, which are used to identify atoms, molecules, ions, and, in some cases, quantify them. Atoms have electronic transitions, where electrons go from one energy level to another. Molecules also have vibrational and rotational transitions ($E_{electronic transition} < E_{vibrational transition} < E_{rotational transition}$).

Plasma naturally emits light which can be measured with optical emission spectroscopy (OES). Particles in the plasma are excited by free electron collisions, causing spontaneous emissions with radiative decay (downward transitions). The emission line intensity is relative to the particle density in the excited state. Emission spectroscopy is not well suited for particle density measurements, but it is a very easy tool to use for particle species identification in the plasma. The light emitted is also sensitive to plasma parameters (species temperature, impurities, etc.) and emission spectra can give insights into plasma processes [63]. The light plasma emits in the visible originates from its atoms' and molecules' electronic transitions. Since different atoms and molecules emit specific wavelengths, the composition of plasma

feed gas will modify the plasma plume's color [63].

Particle density measurements are easier done with optical Absorption spectroscopy (OAS). OAS requires an independent light source to cross the sample and to be detected on the other side. The light detected is lower than the incident light, as particles in the sample will absorb the photons and excite to a higher level (upward transitions). Difference in intensity is relative to particle density in the ground state [63]. This is the main advantage of OAS: Absolute densities can be measured with a calibration-free optical setup [9].

Plasma spectroscopy is a fundamental diagnostic tool for plasma physics [63]. The ideal spectral range used for plasma spectroscopy reaches from 200nm to 1μ m, encompassing the ultraviolet (UV), the visible light (VIS) and the infrared (IR). In this range, the air is still transparent, eliminating the need for vacuumed light path. Quartz windows are also transparent over 200nm, allowing measurement of UV light. At the other end of the spectral range, above 1μ m, the thermal background noise becomes strong and diminishes greatly the signal to noise ratio (SNR) [63]. Spectral features from electronic transitions of plasma species are typically observed in the vacuum-UV to near-IR region. Ro-vibrational transitions are usually observed in the mid-IR spectral region [9]

When performing OES, and OAS, lineshapes of the spectral profiles will be modified by experimental conditions (pressure, temperature, magnetic field, etc.) and spectroscopic properties. Factors like natural broadening, collisional broadening, Doppler broadening, instrumental broadening, and more, will contribute to the observed spectral profiles of particles. These phenomenons can also be exploited to extract more information from the spectra, like temperature, electron temperature, particle velocity [63].

Absorption spectroscopy can be used to trivially measure ground state densities.

If spectral properties are known, the absolute density is determined by a single equation: Beer–Lambert's law. Spectral properties are available in the National Institute of Standards and Technology (NIST) atomic spectra database [?] e.g., absorption cross section $(\sigma(\lambda))$ which describes electron impact excitation process probability.

Electronic transitions require more energy. This is why ground state density measurements are usually happening in the UV—UV radiations have higher frequencies and more energy [9]. When performing OAS, the light source chosen for a given sample should maximize the particles absorption. The absorbance spectrum is a function of frequency. It is based on the ratio of incident light and transmitted light. From the absorbance spectrum the density can be calculated with the Beer–Lambert law:

$$I(\lambda) = I_o(\lambda) \ e^{\sigma(\lambda) \cdot N \cdot l}$$
$$Absorbance(\lambda) = ln(I_0(\lambda) \ / \ I(\lambda)) = \sigma(\lambda) \cdot N \cdot l$$

 $I_o(\lambda)$ is the incident light crossing the plasma sample, $I(\lambda)$ is the transmitted light detected after the absorption zone, $\sigma(\lambda)$ is the absorption cross section of the specific particle measured, l is the absorption length and finally N is the uniform density of the particle in the line-of-sight. The absorption of radiation, with a certain frequency f, occurs as the particle transitions from one energy level E_k to a higher energy E_j with this energy difference corresponding to the photon energy of the radiation. The equation for the photon energy is presented below, where h is the the Planck constant.

$$E_j - E_k = h \cdot f$$

A few things might be considered in order to enhance sensitivity of the setup for increasing the detection limit. Especially since when dealing with plasma species measurements, where concentrations can be very low. Sensitivity of the measurement is quantified with the SNR. The absorbance signal refers to the change in intensity of the incident light crossing the gas sample and the noise is the standard deviation of the baseline signal. Looking at the absorbance equation, two variables can be optimized to increase sensitivity: the path length l, and the choice of the radiation for maximizing the cross section. A particle will absorb a range of wavelengths which are equal to its energy transitions (rotational, vibrational, electronic). The absorption cross section, which illustrates the particle's interaction with each wavelength, will span over many orders of magnitude. Many species produced in plasma have very high absorption cross sections in the UV, several orders higher than in the IR (Figure 2.1).

Choosing a radiation where cross section is maximum will yield more sensitive absorption signals [9]. As for longer path lengths, a greater radiation traveling distance means more particles absorbing the radiation thus resulting in a signal of greater magnitude. The disadvantage of this technique is that when using an absorption cell, the measured densities are spatially averaged, not space-resolved densities. Nor are the measurements time-resolved since the cell fills up over time. This means that, in absorption cell measurements, short-lived species densities cannot be determined. The second possibility to increase detection limit is by minimizing the noise. Noise originates from many sources e.g., electrical, optical, etc. One simple way of reducing white noise, which is random, is by averaging the signal [9].

Fourier Transform Infrared Spectroscopy

Fourier transform infrared spectroscopy (FTIR) is an IR absorption spectroscopy technique. In the Mid-IR, a variety of heteronuclear molecules exhibit vibrational and rotational energy

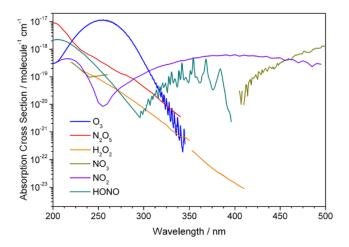


Figure 2.1 Absorption cross sections of plasma-relevant species in the UV-spectral range [9]

transitions. FTIR spectroscopy has the advantage of measuring absorption spectra of many species in parallel, simultaneously collecting information over a wide spectral range and allowing identification and quantification of individual species (even if sometimes peaks can overlap) [9]. The collected information quantifies the amount of light absorbed by a sample at each frequency. Because the absorption cross sections of particles in the IR are orders of magnitude lower than e.g., in the UV-spectral region, this yields lower sensitivity of FTIR spectroscopy compared to UV-absorption spectroscopy. To compensate, gas samples can be analysed in optical multipass cells, which significantly increase the path length. In the case of plasma measurements, this means that species are being monitored in the far-field of the device.

In a FTIR, a Michelson interferometer is used in the optical light path. The interferometer has a beam splitter, a moving and a fixed mirror. The light beam is split, reflected by both mirrors and recombined to produce interference light which then enters the sample. As the mirror moves, the phase difference between the split beams changes and light exits with various combinations of frequencies of IR light which will be absorbed by the sample. The raw signal detected at the end of the optical path is called an interferogram—the amount of light absorbed as a function of the moving mirror's position with position zero corresponding to the maximum intensity (since both mirrors reflect perfectly in-phase beams). This signal is then mathematically Fourier transformed to a light intensity as a function of frequency spectra which can be interpreted [61].

Absorption signals obtained with FTIR spectroscopy are not easily transformed to density values. Added components in the optical path, such as the interferometer, modify the signal

and need to be mathematically accounted for in the calculation of densities—e.g., spectral convolution with instrumental functions [9]. This is why simulations, fitted to the experimental signals, are a better option. Simulations can be achieved using **high-resolution** transmission molecular absorption (HITRAN) database that gives access to spectroscopic parameters of molecules. Parameters such as the line strength of molecules, the pressure broadening coefficients, etc. which are needed for fitting routines. Molecules available in this database are many of the species produced in plasma such as O_2 , O_2 , O_3 , O_4 , etc.

2.2 Plasma Source Design

The plasma source used for all experiments was a plasma jet designed in-lab by master's student Jean-Baptiste Billeau [64]. For this thesis, implementations of the jet have been constructed. The body of the jet is printed in a formlabs stereolithography (SLA) printer with high temp resin which is heat resistant up to 200 °C. Heat resistance is important because the electrodes transmit a lot of heat under the high voltages. This type of printer uses a UV laser to photopolymerize and cure the resin layer by layer into a 3D object which allows for high precision printing and more durable materials. See Figure 2.2 for simplified schematics of the jet.

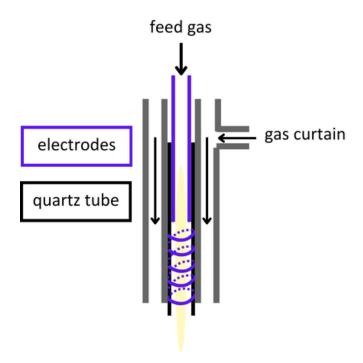


Figure 2.2 Schematics of plasma jet with key elements

The core of the plasma jet consists of two electrodes separated by a dielectric: a quartz tube. The first electrode connected to the ground is in the shape of a helix and surrounds the quarts tube—guiding the plasma towards the tip of the tube. The second electrode, a small copper tube inserted inside the quartz tube, is connected to the high voltage of the PVM500 power supply. The high voltage applied across the electrodes ignites the feed gas which flows through the quartz tube. The plasma plume exits the tip of the quartz tube, called the jet nozzle. This plume is a glow discharge at atmospheric pressure. Feed gas fed into the jet is argon with molecular admixtures up to 2%. Gas bottles are connected to the plasma jet via Teflor tubes as they better prevent humidity compared to other plastic materials. Humidity control is important because in significantly alters plasma reactivity [65]. The gas flows are controlled with mass flow controllers (MFC) (MKS Instruments). If more than one gas in used for the feed gas, a mixing gas chamber assures homogeneous mixture of all ingredients. A curtain gas is available, by adding a gas flow to the side entry designated for it. The curtain gas exits near the jet nozzle in a cylindrical fashion. This way it surrounds the plasma plume and protects it from interacting with ambient air species. This allows better control of the plasma reactivity.

Schlieren measurements are performed, the plasma configured with a curtain gas, to get a better understanding of the gas flows and how they are interacting with treated liquid surfaces. Schlieren imaging is based on the principle that parameters such as flow rate, pressure, temperature, etc. affect refractive index of medias. This change in refractive index of transparent media can be captured using Schlieren photography. The setup is devised and described in detail in [11]. Components are placed in a z-shape configuration using two mirrors. A collimated laser at 532 nm is turned into a point light source with an iris and collimated again with an aspherical parabolic mirror. The plasma plume is placed in the lightpath of this collimated beam—where changes in reflective indexes will be detected. A second aspherical parabolic mirror refocuses the light on a razor blade. The light is then detected with a camera rendering an image of flows. The reason we can see the flow phenomena is that changes in the refractive index caused will bend the light that interacts with it. Bent rays will be displaced when they are refocused at the focal point. By adding a sharp edge that blocks a part of the focused light, right near the center, we are creating a spatial filter in the Fourier domain, optically rejecting part of the light that's been deflected. The brightness of the image is proportional to the refractive changes' magnitude. Figure 2.3 shows plasma flows for two case scenarios. These schlieren images show linearity of the flows exiting the plasma jet. The curtain gas can be seen to enclose the plume in image a) with the jet in free space. In image b), the jet is placed 1cm over a well plate filled with water to mimic plasma treatment of cells. We can see a certain turbulence has settled in but the feed gas still shows

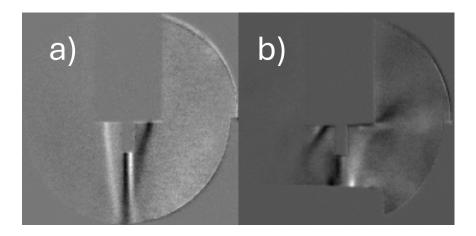


Figure 2.3 Plasma jet feed gas and curtain gas flows, imaged with Schlieren photography a) imaged in free space b) imaged over well plate filled with liquid

nice linearity and we trust the curtain gas still efficiently protects plasma from interacting with ambient air. These results allow to confidently state the impact of the gas curtain on the final plasma composition which is important if we are to control the plasma reactivity and create varying plasma compositions.

Some minor modifications are made to the plasma jet design, to facilitate fabrication and usage. The first modification was done on the jet body's internal electrode circuits. Sharp edges are replaced with curves so that threading of the copper wire (ground electrode) inside the jet is made easier. Plasma jet is often used with a computer numerical control (CNC) router so it's position may be precisely manipulated and automated (especially useful when treating cell cultures see chapter 3). Therefore, the outside diameter of the jet is modified to securely fit the socket of the CNC router. The last modification was to decrease the risk of impurities infiltrating the feed gas. Gas connections have tubes of a certain diameter, and a smaller diameter tube is fitted to the plasma jet's entry. Prior to modification, a shrink tube was used to connect the tubes, which is not a good seal. Swagelok connections are added instead of a shrink tube, to ensure sealing. Connections for the gas curtain are also modified for better sealing. The seal is confirmed with soap bubbles test, indicating that no gas leak is present.

2.3 Plasma Control

Plasma source parameters are manifold:

gas flow

- voltage, current
- duty cycle
- frequency

It is complex to control the non-linear behavior of plasma, and its biological effects, as there are many interlinked parameters. Many parameters need to be tweaked back and forth with not so obvious boundary conditions. Some conditions are well defined such as plasma gas temperature, plume length, species concentration, etc.

One of the main parameters of plasma control is voltage, since it is the voltage that drives the ignition of the neutral feed gas. Voltage will significantly modify the amount of energy deposited in the plasma and on the treated surfaces. Voltage and current go hand in hand, defining the power in the plasma. A balance is needed in the amount of power applied to the jet. We want high power to produce enough reactive species to optimize biological response, but not too much power making the plume temperature and current exceed living tissue tolerances. Other parameters can be tuned for modifying deposited energy, such as the electric duty cycle. Duty cycle, interestingly, is linearly correlated with plasma temperature, making it as useful parameter for adjusting plasma to biological experiments. Plasma jet voltage and duty cycle were previously fine-tuned to biological needs. 20% power and 40% duty cycle were identified as good parameters for high reactivity and secure temperature of the plasma. These parameters were established for an Ar-plasma. Another tunable parameter is the gas flow. High gas flows tend to make the plasma cooler, but too high may dry out cell cultures or create pressure on the cells and damage them. If the gas flow in the plasma jet is too high, this also leaves less time for particles to interact with electrons and be ionized. Common gas flow ranges used for plasma jets are between 0.5-5standard liter per minute (slm) [5–7, 12, 35, 42, 48, 55]. For Ar-plasma, a flow of 2slm is used. When adding admixtures, higher gas flows can be used to increase gas plume length and reduce temperatures since higher powers are needed to ignite the mixture. When changing the feed gas composition, plasma power needs to be adjusted.

2.4 Establishing Plasma Regimes

Plasma composition is the key parameter of plasma reactivity control. Plasma composition comprises feed gas and curtain gas. Gas compositions are the best way to modify which reactive species are dominant in the plasma and start establishing different plasma chemistry. In this work, two distinct plasma regimes are defined to study differences in biological responses. In literature, many instances underline ROS as having a window of action leaning

towards increased proliferation, pro-inflammation, and RNS (especially NO) leaning more towards anti-inflammatory effects, angiogenisis, etc. The aim is a nitrogen oxides-dominated plasma vs a oxygen oxides-dominated plasma.

Table 2.1 Nitrogen oxides vs oxygen oxides

RNS	ROS
nitric oxide (NO)	ozone (O_3)
ONOO-	hydrogen peroxide (H_2O_2)
nitrogen dioxide (NO_2)	superoxide (O_2^-)
nitrite (NO_2^-)	singlet oxygen $(^{1}O_{2})$
nitrate (NO_3^-)	hydroxyl radical (OH)

The complexity in comparing varying plasma chemistries is that altering feed gas composition also modifies plasma characteristics such as electron density, electric field, amounts of metastables, etc. which also have an impact on the observed biological effects [66]. This makes it harder to compare different plasma regimes solely on the difference in reactive species concentration. One difficulty that arose while trying to establish both regimes was that O₂ admixture in plasma feed gas, vs N₂ admixture, need much more power to yield a stable plume. In other words, more energy is needed to ignite this plasma composition. There are two reasons for this: a) oxygen (opposed to nitrogen) is an electronegative gas, meaning that oxygen and atomic oxygen easily become negative ions in the plasma thus capturing electrons and reducing the total electron density. This makes it harder to achieve breakdown concentrations of electrons; b) nitrogen metastables exchange energy with argon, creating an additional channel of energy deposition which can create ions. For reliable comparison between two plasma regimes, similar plume lengths could be important, but difficult to achieve because of this phenomena. It also made it harder to collect emission spectra from ROS-plasma: For a given applied energy, the plasma plume was barely coming out of the nozzle. So when defining both regimes, the question that arose was 'how can we establish common parameters between different plasma regimes?'. In the end, the same electrical parameters (power, duty cycle) are used to have common denominators for comparison between both regimes. The electrical parameters are chosen to optimize the length of the plume when adding O_2 admixture, while still keeping plume temperatures below 40°C. Ideally, we could have had a more reliable and comparable measurement like total electron density or energy inside the plasma, but this requires sophisticated techniques to be developed in our lab.

Finding plasma opposing regimes with a nitrogen oxides chemistry vs an oxygen oxides chemistry is achieved by modifying feed gas admixtures and curtain gases.

Small molecular admixtures in the feed gas will generate more abundant reactive species in the plasma, and can also allow to tilt chemistry in the wanted direction. Curtain gas shields the surroundings of the visible plasma plume and is used to further control the environment of the plasma and influence it's reactivity to favor some RONS mixtures over others.

To achieve both regimes, we first based experiments on an article by Schmidt-Bleker and al. 'How to produce an NOx- instead of Ox-based chemistry with a cold atmospheric plasma jet' [10]. In applying the theory of this article, we looked to simplify experimental components to adapt the solution to a hospital setting. This is an important aspect of the objectives of this work. The study used an Ar-plasma jet with different mixing ratios of O_2 , and N_2 in the feed gas for a sum of 1% admixture. The study also looks into humidifying the feed gas which generates more H_2O_2 in the plasma, and also gives another knob to shift composition. A N_2 curtain is also used to achieve nitrogen oxides-dominated regime. Figure 2.4 illustrates the switch from one regime to the other. Ozone is used as a measure of the oxygen oxides-dominated plasma and nitric oxide as a measure of nitrogen oxides-dominated plasma.

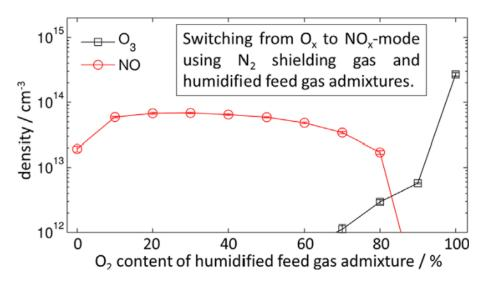


Figure 2.4 Switching plasma composition from ROS- to RNS-dominated chemistry [10]

Reaction pathways are investigated to understand plasma reactivity when composition is modified [10]. Ar-plasma with or without admixtures and humidity, operated in ambient air, produces more ROS. O_3 is primarily produced by the reaction between O_2 , atomic oxygen and metastable molecules. Metastable molecules like $N_2(A)$ carry a lot of energy and are highly efficient is dissociating O_2 molecule. Atomic oxygen is also created by O_2 impact with electrons. To summarize, as long as their is O_2 in the plasma, their will a be dominant O_3 production

electrons or metastables +
$$O_2 \rightarrow 2O$$
 + products
 $O + O_2 + M \rightarrow O_3 + M$

One strategy to favor a RNS-plasma is to eliminate traces of O_2 . By using an Ar-plasma, shielded with a N_2 curtain, this can reduce production of O_3 . Curtain gas is essential to shift reactivity towards nitrogen species.

Water can also help decrease production of O_3 . By adding humidity in the feed gas, dissociated water molecules can react with atomic oxygen.

$$O + HO_2 \rightarrow OH + O_2$$

 $O + OH \rightarrow H + O_2$

As for NO, it is mainly generated through equations:

$$N + OH \rightarrow NO + H$$

 $N_2^* + O \rightarrow +NO + N$

Another parameter explored for control of plasma reactivity is humidified feed gas. For achieving this, a portion of the Ar is diverted through a water (H₂O) bubbler and mixed back into the dry feed gas, introducing more or less molecules of water into the plasma. To much water could be detrimental to RONS production as water molecules added in thousands of parts per million (ppm) cause only water related by-products in the plasma [10].

When using the bubbler, the amount of evaporated water molecules is proportional to the gas flow entering the bubbler. A calibration curve is needed to relate gas flows to water concentrations introduced in the plasma. This curve is obtained by measuring initial and final masses of water in the bubbler under many gas flows, for constant amounts of time. Plasma feed gas flows are in the order of 1slm. To get humidity values under 1000 ppm, the fraction of total gas flow entering the bubbler needs to be in the order of standard cubic centimeter per minute (sccm). The calibration curve is presented in Figure 2.5. 320ppm was the targeted water content, since this is the amount of humidity used in the cited article [10]. Based on calibration curve, 320ppm equals to a 45sccm flow of Ar in the bubbler. Concentrations of humidity in the plasma feed gas are not confirmed experimentally.

Given all this, a variation of gas compositions are tested to find opposing regimes. Since the final setup needs to be installed in a very confined laboratory space, a special focus is put on minimizing the amount of bottles needed. Explanations on the measurements that helped

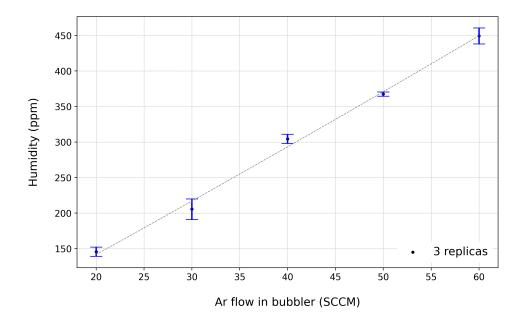


Figure 2.5 Humidity calibration curve (room temperature water in the bubbler)

decide and confirm the regimes are detailed in chapter 3. Ar-plasma was always the starting point. Different admixtures never exceed 1% (higher percentages make the plasma hard to ignite). O_2 , N_2 , and air are used as admixtures. Humidity was both added and not added. Air curtain vs N_2 curtain are compared. Electrical parameters are tuned to identify common voltage and duty cycle settings for both regimes and still have comparable plume length, gas temperatures, etc.

RNS-regime is achieved with 1% N₂ admixture in Ar feed gas flow of 3slm with N₂ gas curtain at 5slm flow vs ROS-regime achieved with 1% O₂ admixture in Ar feed gas of 3slm flow. Conclusions regarding this choice are detailed in chapter 3.

Voltage, current and temperature measurements are performed to characterise these regimes, also in comparison to base Ar-regime currently used for biological experiments. Pictures are taken of the three plasma reactivities, showing different emission colors (Figure 2.7). Voltage is measured by connecting an oscilloscope to the ground and to the PVM high voltage exit. Current is calculated by adding a 20hm resistance and measuring the voltage drop of the equivalent circuit with an oscilloscope connected to the ground of the plasma. The current measurement represents the plasma current, which is not equivalent to the current going through a conductive surface when treated with the plasma. Temperature measurements are taken with an electrically insulated (using a heat shrink tube) thermocouple. All temperatures, measured at treatment distances, are in the safety range of cell tolerance: approx. equal to 40° C. The uncertainty on the temperature values are $\pm 0.3\% + 1^{\circ}$ C. The tempera-

ture measurement technique is compared to other techniques and proves to be reliable, as demonstrated in Figure 2.7 [11].

Results are presented in the table below, for all three regimes.

Table 2.2 Voltage, current, temperature of plasma regimes

Plasma regime	PVM parameters	Temperature at	Voltage (kV)	Current (mA)	
		distance from nozzle			
		(°C)		I=V/2ohm	
Ar-plasma	20% voltage,	10mm: 42	2.33	58.25	
	40% duty cycle				
ROS-plasma	40% voltage,	10mm: 42.1	4.26	85.71	
	20% duty cycle	15mm: 40.2			
RNS-plasma	40% voltage,	10mm: 43.3	3.61	92.86	
	20% duty cycle	15mm: 41.1			

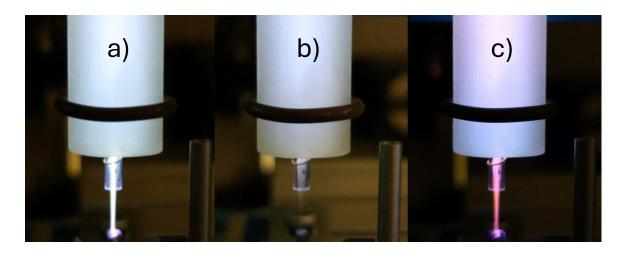


Figure 2.6 Plasma regimes' emission a) Ar-plasma b) ROS-plasma and c) RNS-plasma

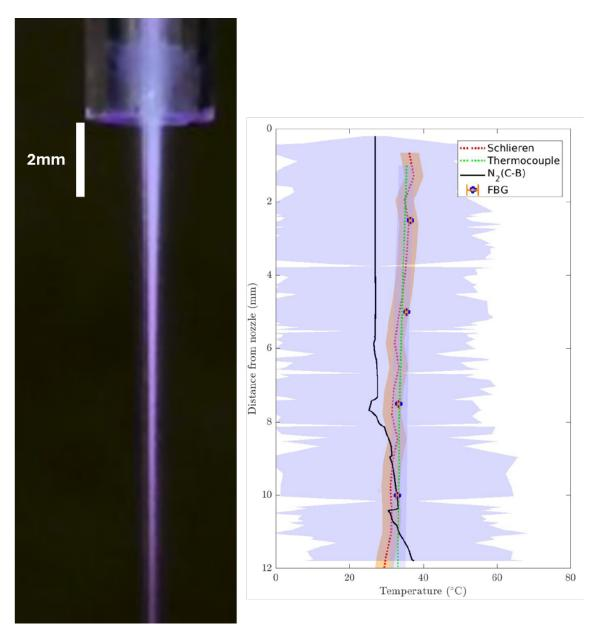


Figure 2.7 Thermocouple temperature measurements compared to other gas-temperature measurements [11]

CHAPTER 3 Plasma Diagnostics: Experimental Setups and Results

The aim of all the techniques presented in this chapter is to have complementary diagnostic tools which allow characterization of reactive species being produced in the effluent of the plasma jet. Species space- and time-resolved measurements are desirable but not a prerequisite since what is being established is which reactivity of the plasma is being favored: Are we producing more nitrogen oxides or oxygen oxides? Since plasma treatments last several minutes, it is relevant to look at species that are present in equilibrium on long time scales. Some diagnostic tools presented are specific to only one specie and others allow measurements of several species in parallel.

The results presented are used to base the choice of a ROS-plasma and of a RNS-plasma on concrete spectral diagnostics of plasma composition. As presented in the literature review, few studies have compared biological effects of differential plasma compositions. To achieve a tool for this was the motivation of the thesis.

3.1 Optical Absorption Spectroscopy: Measuring Ozone Densities

UV-absorption spectroscopy is the first diagnostics used for ozone density measurements. It is with this technique that RNS vs ROS-regimes are established. O_3 is a good marker for pointing out an oxygen oxides-rich plasma, and the absence of O_3 is a good indicator that nitrogen oxides production is being favored. Ozone is abundant in non-thermal plasma operated in air and has a long lifetime in ambient conditions, which makes it an ideal candidate for absorption spectroscopy. The optical setup used for carrying out absorption measurements of ozone is shown on Figure 3.1.

 O_3 has a high absorption cross-section centered at 254nm, in the Hartley band [67]. The light source used for UV-absorption setup is a deuterium lamp DH2000-DUV-Vis-NIR with a broadband spectrum 180-1000nm (OceanOptics, USA), which has a high intensity peak in the UV-spectral range around 254nm. This lamp's emission is also very stable (0.01% / h @ 254nm) This is important for sensitivity of the setup since absorption signals are obtained from the difference between transmitted radiation I (plasma ignited) and incident radiation I_0 (empty cell): The difference needs to come from absorbing molecules, not from variations in the lamp's intensity. The plasma sample is accumulated in a measurement cell with a length of 10cm. This path length is sufficient to measure O_3 densities in the range of $10^{14} - 10^{16}$. Plasma is continuously injected inside the glass cell and an outlet for exhaust is present to

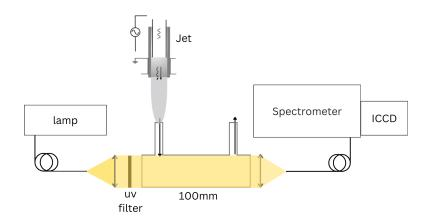


Figure 3.1 Schematics of UV-absorption spectroscopy setup

avoid accumulation of gases. Solarization-resistant fibers (Thorlabs, USA), transparent in the UV, are used to create a point source of light and to collect the focused light on either end of the optical path. UV fused silica plano-convex lenses (Thorlabs, USA) are used to collimate the radiation through the absorption cell and to focus it back to the detector. Placed before the glass cell, is a UV bandpass filter (Edmund optics, USA) centered at 254nm. SpectraPro 500i spectrometer (Acton Research, USA) measures the transmitted light. It is equipped with a PI-MAX 2 intensified charge-coupled device (ICCD) camera (Princeton Instruments, USA). The camera can multiply incident photons and yield a higher signal (better SNR) for low radiation intensities.

Absorption profile is obtained with the lamp signal (plasma-off) and the plasma-on signal:

Absorbance =
$$ln(I_0 / I) = ln(lamp signal / plasma-on signal)$$

Absolute densities are calculated from the absorption profile. The densities are a line-of-sight average. The assumption is made that ozone concentration is constant across the absorption path length—based on the relatively high gas flows and the long half-life of ozone (several minutes to hours [68]). The densities are calculated with Beer's law with the ozone absorption cross section at 254nm $\sigma(\lambda = 254nm)$ which is 1.14e-17 cm² [69] and the path length l = 10cm:

$$N = A(\lambda = 254nm) / \sigma(\lambda = 254nm) \cdot l$$

The right graph of Figure 3.2 shows an example measurement of ozone absorbance obtained experimentally, superposed to the simulated absorbance calculated with cross section, path length and determined density. Both overlap, showing that determined density fits theory. The experimental signal is filtered by a bandpass filter centered around 254nm. The red

dotted line shows the intensity data point used to calculate densities from absorption measurements at 254nm. The left graph of Figure 3.2 plots lamp signal (or background signal) alongside plasma-on signal with plasma-produced ozone particles absorbing part of the radiation.

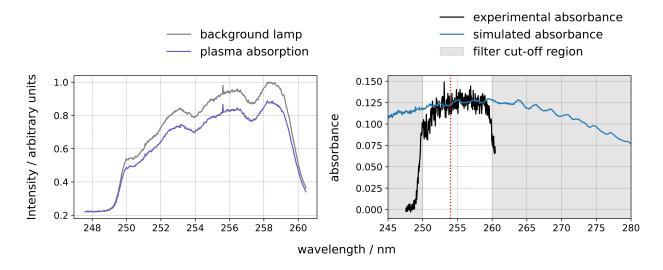


Figure 3.2 UV-absorption spectroscopy: raw measurements (left) and experimental and simulated absorption profiles (right)

Ozone density measurements are first done with an argon-plasma (2slm flow) with a range of O_2 admixtures from 0% to 2% (Figure 3.3). This test was performed to confirm measured densities are coherent with literature and that the setup is reliable. First, we see the expected trend: as we add more O_2 in the feed gas, more O_3 is produced since we have more molecules being dissociated by the electrons in the plasma. Second, the measured and calculated densities are in the same concentration range $(10^{12} - 10^{16} \text{molecules/cm}^3)$ as other similar plasma experimental conditions [9]. At high O_2 admixtures, the O_3 densities enter a plateau since there is not enough energy in the system anymore to dissociate O_2 efficiently and yield more O_3 . Signal to noise ratios are also plotted to get an idea of setup sensitivity (Figure 3.4). Above 0.4% O_2 admixture in the argon feed gas, measured densities of ozone have a mean SNR of 20dB, which is an acceptable signal quality. Below this, the SNR drops significantly, indicating measured densities could be anything lower than $1x10^{15}$ molecules/cm³. This stands as the lower detection limit of the setup.

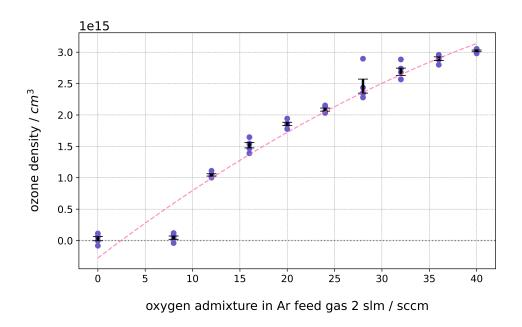


Figure 3.3 Ozone densities in plasma far-field for different percentages of oxygen admixtures

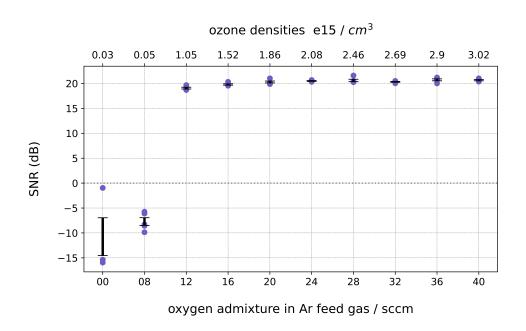


Figure 3.4 SNR of ozone density measurements

With the setup being validated, the objective in this section is to choose two opposing regimes—one with high O₃ production and the other with minimal (ideally zero) O₃ production. Figure 3.5 shows the tested plasma compositions and the produced ozone densities. All admixtures equal 1% of total Ar feed gas which is set at 3slm. Gas curtain is systematically added at a flow of 5slm—it is either air or nitrogen. Dry scenarios are compared to humid ones. Humidified feed gas is achieved by diverting 45sccm of the main argon flow into a bubbler before being mixed back in the feed gas in the gas chamber (where admixtures are also mixed into the feed gas). All dry measurements are taken first, then the humid measurements are taken to make sure residual water doesn't falsify results.

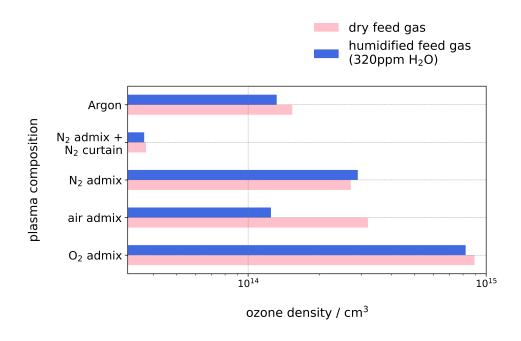


Figure 3.5 Ozone densities in function of different plasma compositions

Argon-plasma is used as the default plasma regime. We can see in Figure 3.5 that this regime still yields a high amount of O_3 , originating from the plasma's interaction with oxygen in air. Adding N_2 in the feed gas of this default regime, without eliminating the O_2 , generates more O_3 and oxygen oxides since N_2 metastable acts as an other oxygen dissociator. If O_2 is eliminated, by adding an N_2 curtain that shields the plasma plume, then O_3 production drops significantly. Air admixture was also tested, yielding ozone densities similar to N_2 admixture. The regime which generates the most ozone is argon with O_2 admixture. Comparing dry to humid feed gas yields inconclusive results. According to the aim of finding the most compact setup possible, eliminating the air bubbler and one mass flow is preferable. All further experiments are done with dry feed gas.

Figure 3.6 compares SNR values of each regime to measured ozone densities to define the lower detection limit of the setup with these new values. The red square points out the density value measured with an SNR lower than 20dB: The lower detection limit is approximately 0.5×10^{14} molecules/cm³. Looking back on the results presented in Figure 3.3, this would mean ozone densities for less than 0.4% O₂ admix in the feed gas are below 0.5×10^{14} molecules/cm³.

	argon air admix		O ₂ admix		N ₂ admix		N ₂ admix + N ₂ curtain			
	SNR	O_3 density	SNR (dB)	O ₃ density	SNR(dB)	O ₃ density	SNR (dB)	O_3 density	SNR	O ₃ density
	(dB)	(e14/cm ³)	SINK (UD)	(e14/cm ³)	SINK (UD)	(e14/cm ³)	SINK (UD)	(e14/cm ³)	(dB)	(e14/cm ³)
dry feed gas	22.65	1.32	24.01	1.25	32.45	8.20	33.69	2.89	14.11	0.37
humidified feed gas (320ppm H ₂ O)	29.87	1.53	35.13	3.19	31.83	8.94	35.66	2.70	17.22	0.37

Figure 3.6 SNR of ozone density measurements for the different plasma compositions

According to the thesis' aim of finding minimally complex setups of two plasma reactivities, two potential opposing regimes have been identified: argon-plasma with 1% N₂ admixture and N₂ curtain vs argon plasma with 1% O₂ admixture in ambient air, which are hereinafter referred to as RNS-plasma and ROS-plasma respectively.

3.2 Optical Emission Spectroscopy: Plasma Plume Emission

The optical emission spectroscopy (OES) setup uses a lens to focus plasma emission inside the SpectraPro 500i spectrometer (Acton Research, USA) slit, as shown in Figure 3.7.

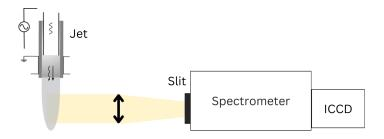


Figure 3.7 Schematics of OES setup

Ar-plasma, ROS- and RNS-plasma are ignited and spectra obtained for each regime are presented on Figure 3.8, Figure 3.9, and Figure 3.10.

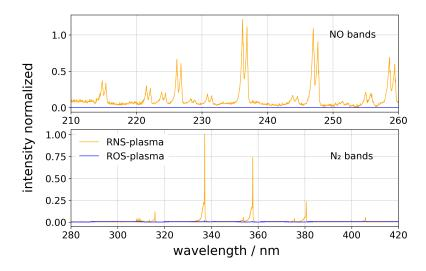


Figure 3.8 UV emission of RNS- and ROS-plasma (normalized to the max value of RNS-plasma)

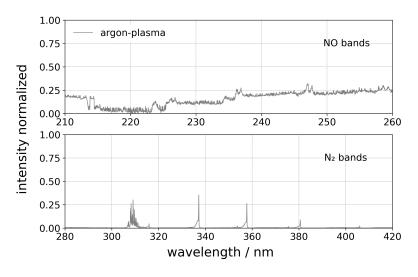


Figure 3.9 UV emission of argon-plasma (normalized to the max value of RNS-plasma)

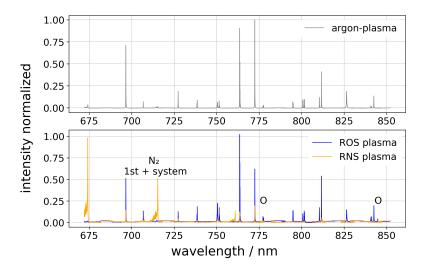


Figure 3.10 IR emission of normalized argon-plasma and RNS-, ROS-plasma (normalized to the max value of ROS-plasma)

These spectra inform us on which species are present in the respective plasma regimes. Lines from emission spectra are identified either through the NIST database or through literature.

ROS-plasma emission spectrum between 300 and 400nm contains very faint N_2 lines, barely visible compared to the high intensity emission lines in the RNS-plasma (Figure 3.8 top). These emission bands are part of the second positive system of N_2 [63]. As for argon-plasma, there are some N_2 lines visible, from interaction between Ar plasma plume with ambient air (Figure 3.8 bottom). These emissions come from N_2 molecule vibrations—after being excited by electrons or Ar metastables they spontaneously decay while emitting light with line intensities proportional to the population in the higher energy states [70]. ROS-plasma does not excite N_2 molecules, only the O_2 molecules admixed in the argon.

RNS-plasma shows clear NO emission lines in the UV between 210 and 260nm, corresponding to the NO γ system [71]. The presence of nitric oxide in the RNS-plasma supports the hypothesis that nitrogen oxides are being produced in this regime and the plasma reactivity is successfully shifted. Argon-plasma also has NO emission lines but these are very low in intensity (Figure 3.8 bottom). ROS-plasma's emission is flat in this spectral range: No nitric oxide is being produced. By adding oxygen to the feed gas, the energy of the plasma is being steered to other chemistry—when there is O_2 in the mix at ambient temperature, the reactivity of the plasma will tend towards producing O_2 oxides, this is why we do not observe NO in this regime.

Atomic oxygen is another emitting atom from which we can conclude on plasma reactivity. In argon-plasma and in ROS-plasma, there is emission at 777nm from atomic oxygen. We do not see this emission line in the RNS-plasma. This confirms that the N₂ curtain is efficient in blocking interaction between the plasma effluent and the ambient air—compared to the argon-plasma where interaction with air produced some atomic oxygen.

Hydroxyl radical (OH) is indicative of humidity content. No OH emission is observed at 309nm [72] in the RNS- and ROS-plasma, but in the argon-plasma there seems to be a high intensity line for OH. With admixtures in the feed gas, a smaller electron density is available to react with water molecules, and dissociate them into OH. This is the reason a higher OH intensity line is visible in the argon-plasma.

We can set argon-plasma to be an example of a 'in-between', more general plasma, since it is producing a bit of everything, even if oxygen oxides are favored. These results demonstrate that by modulating the plasma entry gases we can optimize output composition to have more precise plasma regimes.

3.3 Fourier Transform Infrared Spectroscopy: Plasma's Far Field

FTIR spectroscopy is used to identify and quantify RONS produced in the plasma's far field. Absorption measurements are taken with FTIR spectrometer Vertex 80v (Bruker Corporation, USA). The spectral range used in this work is between $900-4000 \,\mathrm{cm}^{-1}$. The most interesting spectral range lies between $1200-2400 \,\mathrm{cm}^{-1}$, where plasma-relevant molecules have strong absorption cross sections e.g., dinitrogen pentoxide (N_2O_5) , nitrous oxide (N_2O) , nitrogen dioxide (NO_2) , ozone (O_3) , hydrogen peroxide (H_2O_2) , and nitric acid (HNO_3) . This type of measurement gives us ample information on plasma reactivity.

Plasma jet is mounted on the entrance tube of a variable path length multipass cell (Pike Technologies, USA) operated at atmospheric pressure (Figure 3.11). An additional glass adaptor piece is added between the plasma jet and the measurement cell's entrance tube, to isolate the plasma plume and the added curtain from the ambient air. The cell has a total path length of 16m, and a volume of 3.5L. Since the feed gas flow is 3slm, it takes 3-5 minutes to fill the whole cell. After a stabilization time of 5 minutes, the gas exits through the exit tube and is extracted through the laboratory exhaust.

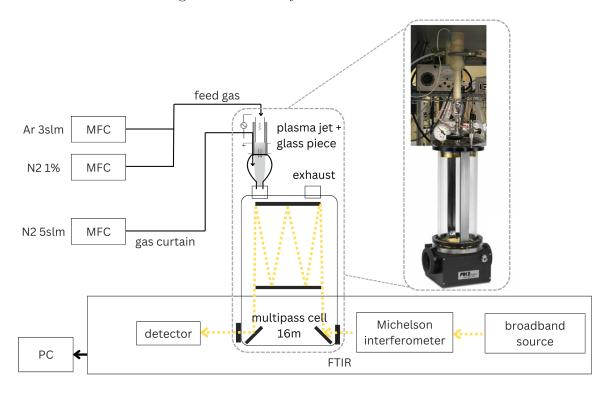


Figure 3.11 Schematics of FTIR setup

Since the multipass cell and the FTIR spectrometer are not from the same company, an adaptor piece was designed to align the cell's windows with the FTIR device's light path. A 3D model of the adaptor piece 3D-printed with Prusa MK4 printer (Prusa Research, Czech Republic) to achieve the alignment (Figure 3.12).

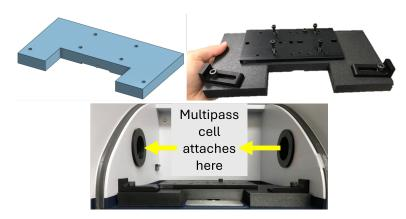


Figure 3.12 3D printed adapter plate for aligning multipass cell with FTIR spectrometer

The multipass cell is screwed on it's original plate which is fixed on the adaptor plate which then fits in the FTIR device. Broadband light source from the FTIR device enters the cell, reflects on all mirrors for a total path length of 16m and then exits the cell to be detected by the FTIR spectrometer.

The spectral resolution of the Vertex 80 can be up to 0.001cm^{-1} for a long integration time and a long mirror pathway [9]. Resolution used for the plasma measurement is set to 4cm^{-1} to have a reasonable integration time around 15 minutes.

A challenge in IR measurements is absorption by H_2O , since H_2O has a high absorption cross section around $1400\text{-}1800\text{cm}^{-1}$ and $3500\text{-}4000\text{cm}^{-1}$. This is also a difficulty in medical imaging where water from the body can completely overshadow all other interesting features. One solution, to still be able to identify other molecule peaks in these regions, is to have high enough resolution that all individual water absorption peaks can be distinguished from desired features. Another solution is to eliminate water content in the light path by purging the spectrometer. This is not the case in presented measurements, thus we concentrate on molecules outside water absorption regions, taking a closer look after 1800cm^{-1} .

Spectra of background signal and sample signal are measured to obtain absorbance spectrum of the plasma regime. RNS-plasma is turned on to fill the multipass cell for measuring the sample signal. Background signal is done with an empty measurement cell and the light on. Sample signal subtracted to the background signal gives the absorbance spectrum, same as OAS measurements.

Absorbance of the RNS-plasma is presented in Figure 3.13, alongside background and sample signals. Identified molecule absorption peaks are annotated.

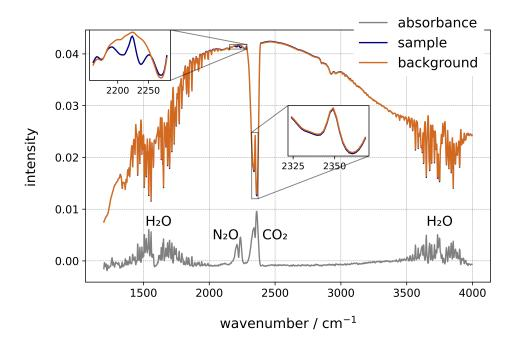


Figure 3.13 FTIR signals of RNS-plasma at $4 \,\mathrm{cm}^{-1}$ resolution

Densities of identifiable species can be calculated with their respective absorption cross section. Cross sections from relevant molecules are obtained through the HITRAN database. Cross sections retrieved from the database are plotted in Figure 3.14. These cross sections can be adapted to the experimental and environmental conditions by modifying multiple parameters. These parameters influence how much a molecule will absorb light and how much of this light intensity is detected by the spectrometer. Temperature and pressure parameters are set to setup environment. Instrument properties are also accounted for with resolution and apparatus function. Apparatus (or slit) function is convoluted with the theoretical high-resolution spectrum to mimic experimental results when light enters the spectrometer slit. Line profile accounts for different effects of line broadening. The parameters are used to increase the accuracy of the simulated spectra, and are listed in Table 3.1.

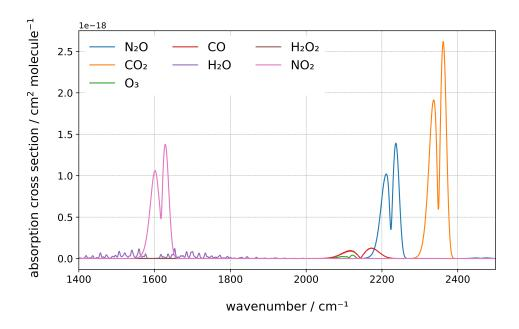


Figure 3.14 Absorption cross sections of relevant reactive species in the IR retrieved form HITRAN database

Table 3.1 Parameters used to retrieve cross sections

Parameter	Value
resolution	$4\mathrm{cm}^{-1}$
slit function	Gaussian
path length	16m
line profile	Voigt
temperature	$294.15\mathrm{K}$
pressure	1 atm

With adjusted cross sections and a known path length, Beer's law can be applied to simulate absorbance spectra of each molecule. Density value of a specific molecule is modified until simulation fits the experimental absorption peak of this molecule: the unknown densities of each molecule are used as the fitting parameters and this is how density values are determined. See Appendix B for the python code used to simulate absorbance spectra and calculate density values.

RNS-plasma FTIR measurement allowed to conclude on this plasma regime's composition and concentrations. As seen in Figure 3.15, O_3 is not present in the spectra (dotted line shows the absence of a peak where O_3 would absorb IR light). N_2O is detected with a high density of 2.5×10^{12} molecules/cm³, confirming nitrogen oxides are being produced in this regime. The detected carbon dioxide (CO_2) peak comes from the ambient air present in the light path of the spectrometer. As for the carbon monoxide (CO_2) peak, it comes from dissociated CO_2 from the air impurities in the plasma's interaction region.

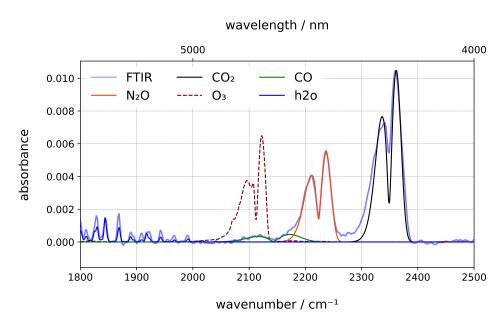


Figure 3.15 Fitting of molecule densities to FTIR absorbance signal of RNS-plasma

These results confirm that the chosen regimes are giving us the wanted plasma reactivity.

CHAPTER 4 Plasma Treatment of Fibroblasts

The work presented in this chapter is done at Montreal General Hospital, McGill University Health Centre (MUHC). It is a collaboration with Dr. Anie Philip's laboratory, as well as with Pr. Derek Rosenzweig.

4.1 Plasma Jet Setup in Biohood

The initial argon-plasma jet setup (installed by Jean-Baptiste Billeau and Laura Bouret) is placed in a laminar flow hood which provides an aseptic work area for manipulating cell cultures. The plasma jet is mounted on a CNC router with x, y, z movement. The well plates are placed on the CNC router plateau and secured in a bracket, 3D printed with Ultimaker printer S5 (Ultimaker, Netherlands). The bracket guarantees same position of well plate between treatments. The PVM power supply is placed under the CNC router which is elevated on a small rack. The argon gas bottle connection enters into the hood from the front, with the gas flow fixed at 2slm (Figure 4.1).

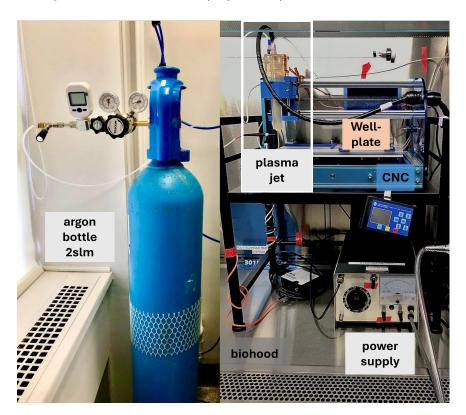


Figure 4.1 Plasma jet setup in laminar flow hood for cell culture treatments

To monitor plasma humidity in real time, a solarization-resistant fiber (Thorlabs, USA) and a USB2000+ spectrometer (OceanOptics, USA) are added to the setup. The fiber is fixed on the CNC router, and aligned with the plasma plume to detect its emission when the jet is placed on home position of the CNC router (Figure 4.2).



Figure 4.2 Fiber fixed on CNC router aligned with plasma plume emission

The spectrometer works with a USB cable and can be plugged to any laptop equipped with OceanView. Humidity is measured via OH emission peak at 309nm—water molecules inside the plasma are dissociated into H and OH molecules, thus OH informs us on H₂O presence. Plasma emission spectrum is measured every minute for up to 100 minutes. Intensity values of OH emission peak are plotted over time to visualize humidity evolution from the moment plasma jet is turned on. Argon emission intensity, at 696nm, is also plotted in time. We see an inverse trend in Ar emission compared to OH emission: humidity decreases in time and argon emission increases. Ar emission intensity is related to the electron properties in the plasma. The higher the electron density and energy, the higher the argon emission. As humidity decreases, water takes up less electrons making more available to excite Ar atoms in the plasma. The ratio of OH to Ar emission intensity reflects the changing plasma parameters and normalises the OH emission to the plasma parameters. The result is a more reliable signal for humidity concentration. These signals are plotted on Figure 4.3. A fit is performed on the normalized OH curve, with a exponential decay function.

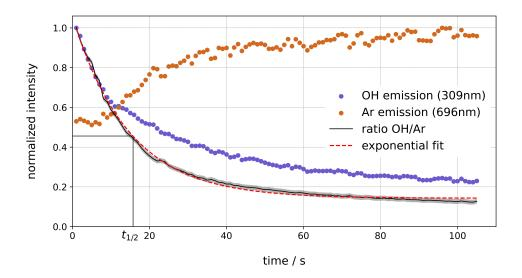


Figure 4.3 Evolution in time of OH emission from plasma jet plume

The half life of the exponential decay fit function is calculated: 15,73min is the time it takes for humidity to reach half of its initial value.

exponential decay fit function =
$$\mathbf{A_0}e^{bt} + \mathbf{c}$$

half life: $1/2A_0 = A_0e^{bt} + \mathbf{c}$
 $0.456 = 0.912e^{0.068 \, t} + 0.143$
 $\mathbf{t} = \frac{\ln(\frac{0.456 - 0.143}{0.912})}{0.068}$
 $\mathbf{t} = 15,73 \mathrm{min}$

Following this result, the plasma humidity stabilization time-frame is set to 60min. This is the time plasma needs to be turned on before using it for experiments. The aim is to control humidity variable and assure it is constant during plasma treatments. This eliminates a cause for variability in the biological results where repeatability is important for comparing treatment conditions. This add-in also allows reference spectra of plasma throughout treatment of well plate and from one treatment to the other.

4.1.1 Dual-Regime Plasma Jet Installation at MUHC

Before being able to install any plasma source in a hospital research laboratory context, an assessment of security risks concerning the use of a plasma device in this setting needed to be done, as well as solutions found to mitigate these risks. Such assessment is important since gas bottles are manipulated in small spaces, in a building shared with other people and because plasma produces potentially harmful species, especially when using admixtures in the feed

gas (species such as ozone and nitrogen oxides). This work was done in collaboration with Mihaela Cucu, Environmental Health and Safety Officer at MUHC. Security risks assessment and mitigation protocol is presented in Appendix A.

The assessment of produced toxic gas fumes by the plasma device is based on published empirical study done with the plasma jet kINPen MED (Plasma guidelines, AWMF Register No.: 007-107). The study took place in a non ventilated room and found that ozone concentration did not exceed 0.03 ppm at 40cm from the plasma plume over 5.5 hours. EU Directive 2002/3/EC recommends for a daily (8-hour) ozone exposure no more than 0.055ppm to avoid health risks. As for nitrogen oxides levels, the quantities produced were low enough that their concentrations around the plume couldn't be detected. Furthermore, in the case of our setup, the plasma is used in a laminar flow hood which should help diffuse the plasma species more efficiently.

Additional safety measures are proposed: to consider the use of ozone and nitric oxide sensors, placed on the plasma device users, as well as an alarm equipment unit for oxygen leak detection in the room. Oxygen safety data sheet (available of Air liquid website) specifies to avoid oxygen-rich atmospheres >23,5%. Commission des normes, de l'équité, de la santé et de la sécurité du travail (CNESST) advises that the percentage of oxygen by volume in the air must not be less than 19.5% at normal atmospheric pressure. The safety interval of O_2 percentage in the room is set between 19,5 and 23,5%.

Second is the question of compressed and inflammable gases stored in pressurized bottles. The gas bottles that are part of the setup are 1 argon, 1 nitrogen and 1 oxygen bottle. Oxygen is an inflammable gas. For this reason, a small oxygen bottle size 7 was chosen for the setup. This makes it easier to store and safer to manipulate. Fire Prevention Department of the MUHC, after inspecting the setup environment, ruled on guidelines for allowing the gas bottles in the laboratory: a) gas cylinders are to be firmly attached to the laboratory wall to assure physical stability; b) extra gas bottles are too be stored in a separate room designed for storage; c) an additional fire extinguisher ABC is to be made available in the laboratory.

The dual-regime plasma setup is designed to be compact and to fit in a narrow space between biohoods. It needs to comprise flow meters for argon gas, nitrogen admix, oxygen admix and nitrogen curtain. Since argon bottle was already installed in the laboratory, bottle and flow meter for argon did not need to be cared for. This leaves a nitrogen bottle size 50 (diameter 24cm, height 141cm) and an oxygen bottle size 7 (diameter 15cm, height 61cm), plus 3 flow meters connected to the bottles. The exit tubes from the flow meters deliver the gases to the plasma source inside the hood. The final setup is a metal rack, mounted with a panel

carrying all three flow meters on the front. The chosen flow meters are rotameters since they are independent units that do not take up much space. Gas connections are secured in the back of the panel. The dimensions are roughly 30x30cm wide. The oxygen bottle is placed on the floor, inserted inside the metal frame. The stated dimensions exclude the nitrogen bottle which is planned to be secured on the wall behind the metal frame, adding an extra 24cm to the total depth. The metal rack includes adjustable straps for securing bottle bottles. Valves are added to the gas connections too be able to switch from an RNS-plasma to an ROS-plasma easily or to an argon-plasma. A picture of the setup is shown on Figure 4.4.

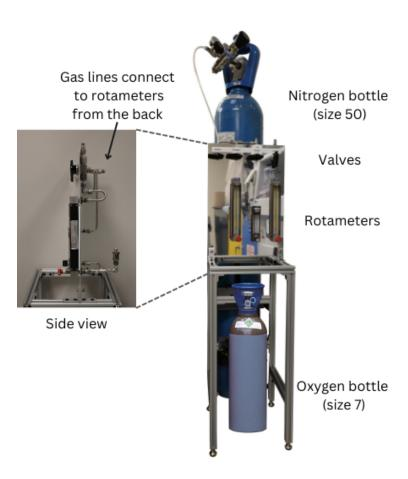


Figure 4.4 Dual-regime plasma device setup

4.2 Biological Model Used for Plasma Treatment

Many cell types can be used to study wound healing, e.g., epithelial cells, keratinocytes, and fibroblasts. Since this project focuses on fibrosis, fibroblasts are chosen for biological model.

It is common practice to start with a simple model, a monolayer cell culture, and to move towards more complex models as results are conclusive. Thus, the most simple model is used: adherent human telomerase reverse transcriptase (hTERT) fibroblast cells in a 2D monolayer culture. The next step would be a 3D cell model, such as spheroids or 3D printed cells, then tissue samples which could come from fibrotic lesions, or wounds of patients and eventually in vivo models with animals or humans as we head into clinical trials.

hTERT fibroblasts are an immortalized primary cell line with the ability to survive many passages and continuously multiply. The cells are cultured in dulbecco's modified eagle medium (DMEM). The medium is supplemented with foetal bovine serum (FBS), a mixture of biomolecules such as growth factors, proteins, vitamins and hormones, which are important for the survival and growth of cells. Antibiotics are added to prevent bacteria from colonizing the culture (penicillin for gram-negative and -positive bacteria, amphotericin for fungus, gentamicin for other bacterial infections). The cells are stored at 37 °C in 5% CO₂.

The methodology for seeding, and treating cells is as follows:

- 1. Cells are grown in increasingly large flasks (T25, T75, T125). Cells cultures like to grow in confined enough spaces, this is why we start in small flasks and as cells multiply we transfer them to bigger spaces. We repeat this until enough cells are available for seeding the well plates.
- 2. Cells are seeded on day 0 and are grown to reach confluence for 24 h. $7x10^4$ cells are diluted in 1mL of media, and seeded in 12 well plates;
- 3. Cells are treated with plasma 24h later, on day 1. The control for plasma treatment is defined as the neutral gas hence cells are treated with the same flow rate of argon, but with no applied voltage (plasma off);
- 4. Plasma's biological effects are analysed 24h after treatment, on day 2. All presented results are a mean of triplicate data.

When treating the cells, they should be confluent—confluence is defined as 80% of the well area being occupied by cells. The more cells there are, the stronger the results will show (more proteins, more activity, etc.). When the amount of cells is too low, this causes stress because cells do not thrive in isolated conditions. On the other hand, if cells grow too confluent they start to touch and contact inhibition occurs which is also not desirable. The number of cells seeded on day 0 is optimized to $7x10^4$ to have confluence on day 1.

In order to count the cells to be seeded, staining and microscope images are used. Cells grown in flasks are trypsinized to be detached and diluted in fresh media with a dye. A small

sample of the mixture is loaded on a microscope lamella equipped with a reference grid and placed under the microscope for counting. A dilution calculation tells how many cells are in the flasks. The desired amount of cells are pipetted and mixed with media for a total of 1mL inside each well of a 12 well plate. A 12 well plate is chosen as a compromise to have a good amount of cells for analysis after treatment/well, since the wells are bigger, as well as a satisfactory amount of wells to test many treatment conditions.

Plasma treatment conditions are also optimized. The plasma used for all first experiments is an argon-plasma. Argon-plasma produces more oxygen oxides and thus can be categorized as a ROS-plasma. The treatment of 12 well plates is coded to be a circle traced by the plasma plume (G-code for the CNC router presented in Appendix C). Since the well surface area is big compared to the plume diameter (26mm vs 1mm respectively), a stationary treatment was presumed to be less homogeneous than a circle which would distribute more evenly the reactive species around the diameter of the well. Each circle traced by the plasma takes 5 seconds—the number of circles is related to the treatment time (as a multiple of 5). Treatment distance needs to be optimized as well: too intense plasma treatment can cause cell necrosis or selective detachment of cells, leading to the formation of a clear zone, called plasma streak. The treatment distance is set as the minimal distance when such a streak is no longer present after plasma treatment (Figure 4.5). This way, the closest distance is selected to enhance plasma effect but without physically harming or detaching the cells with the plume. The treatment distance is set at 22.5mm from the plasma nozzle to the cells.

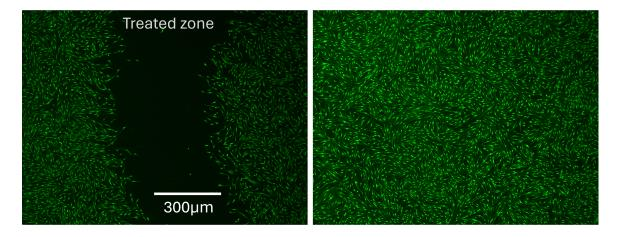


Figure 4.5 Plasma streak left by plasma on adherent cells (left) and no streak after plasma treatment (right)

4.3 Metabolic Activity Assay

The cells' metabolic activity following plasma treatment is the first bio-assay achieved with the biological model. This is a good assay to get a general portrait of plasma's effect on the cells: is plasma stimulating or inhibiting cells? To observe and quantify this effect, alamar-Blue reagent is used. This reagent contains resazurin which is an oxidized, non-fluorescent, blue colored compound. When put in contact with a reducing cellular environment, it is converted to resorufin which is fluorescent, and pink colored. This is using enzymatic activity as a marker for cell activity. The change in color and the increased fluorescence is detected using a plate reader that can read the compounds fluorescence (excitation at 560nm and emission at 590nm). The reducing power of the cells is proportionate to their metabolic activity and their viability. 24h post-plasma exposure, the cell culture medium, from each well, is replaced with a mixture of fresh medium and the resazurin solution. Cells are incubated for 4-6h with the resazurin, to give it time to be converted. After a few hours, the blue medium will start to turn pink. The fluorescence intensity of each plasma treated well is measured and normalized against the intensity of the control well. Each well corresponds to a treatment time at the fixed treatment distance. A large enough interval of treatment times are tested in order to observe a difference in metabolic activity. Interval choice is set to 5s-10min, and is based on many studies [5, 6, 12, 17, 35, 36, 42, 46, 48, 54, 55, 57–59, 73]. Metabolic activity of cells, as a percentage of the control, are presented in function of treatment times (Figure 4.6).

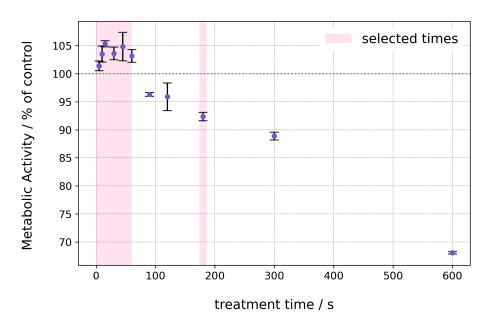


Figure 4.6 Metabolic activity of fibroblasts 24h after plasma treatment

These results inform us on the general effect of the argon-plasma on the cells. Short bursts of plasma treatment, between 5s and 60s, will increase cell activity and cell viability. We are in the oxidative eustress region where plasma can increase proliferation, migration, and general function of cells. When plasma treatment times surpass 60s, there is a linear relation to metabolic activity decrease. This is the oxidative distress region. These results are used to further narrow our treatment interval for future tests. The selected times are highlighted in pink in Figure 4.6. Short treatment times are favored since this is where plasma can be most beneficial. A long treatment time is also selected to compare how oxidative eustress vs distress can play out.

4.4 Western Blotting

Western blotting is a technique for quantifying specific proteins in a sample. It uses electrophoresis to separate the proteins based on their molecular weight (by applying a voltage). The proteins are transferred from the electrophoresis gel to a membrane. Target protein is marked with a primary antibody and then a secondary antibody which binds to the first and can be visualized by immunofluorescence. The higher the intensity of the fluorescence bands, the higher the expression of the protein. Housekeeping gene-coded proteins, presumed stable in all physiological conditions including plasma treated medium, are used as loading controls. -actin is used for this work. Ideally, the chosen protein has a different molecular weight than studied proteins to avoid overlaps in the bands. Protein ladders are also loaded on the electrophoresis gel: protein ladders are made up of protein compounds with proteins of varying molecular weights that will migrate at distinct distances on the gel, thus creating weight markers (colored bands) for identification of the target proteins.

Western blotting doesn't quantify protein concentration, but rather the ratio of this protein's concentration on the total protein concentration—it cannot tell how much of target protein there is, only how much there is relative to another sample. To achieve this, the same amount of proteins from each sample/condition needs to be loaded on the gel. If a protein band has more or less intensity compared to control this is because the ratio of expressed proteins has shifted, indicating a change in cell behavior. The protein concentration in samples need to be quantified in order to load a given quantity on the gel. The proteins are extracted from the cells with a lysis and are isolated by centrifuge. A Bradford assay is used to quantify the proteins. The Bradford reagent is added to the protein solution and binds to the proteins, changing color. The binded reagent has an absorption peak at 595nm, which can be quantified with a microplate reader. The absorption value is proportional to the amount of protein present in the sample. To convert the absorption measurements to protein

concentrations, a standard curve is done with a dilution series of bovine serum albumin (BSA) protein with standards of known concentrations.

The interest of western blot technique is to compare protein expression of cells under different plasma conditions. Proteins can give us a lot of information on cell function and cell activity. In the case of fibrosis, many proteins can serve as biomarkers to this pathology or its healing.

Collagen is an excellent biomarker for fibrosis since it is the dominant ECM component of fibrotic tissue and is deposited excessively when healing is malfunctioning. Fibronectin is another ECM component which precedes collagen deposition, it is also overexpressed in the case of fibrosis [74]. Another important protein in fibrotic wounds is α sma which is the main biomarker for myofibroblast differentiation [49]. Myofibroblasts use α sma to gain contractile properties and drive fibrotic development of the tissue.

The most important cytokine involved in fibrosis is TGF- β . This would be the ideal biomarker for monitoring fibrosis development. The difficulty with TGF- β is that our body contains a lot in latent form [3]. It is very hard to measure only activated TGF- β : in most cases we are simply measuring all TGF- β , which gives us no marker for a change in activation of the protein. Western blotting can be done for Smad proteins which are regulators of TGF- β signaling cascade. This can be used as an indirect way of measuring TGF- β .

In the end, α sma and coll 1 are chosen as the biomarkers for monitoring the biological effect of plasma treatment of fibroblasts. Expression of coll 1 represents the quantity of ECM proteins that are being synthesised. Expression of α sma represents differentiation of fibroblasts to myofibroblasts. Both proteins can be indicative of fibrotic development.

Fibroblasts are treated with selected treatment times and western blotting is performed in order to obtain a protein band for each treatment condition (Figure 4.7). This data can be used qualitatively to describe the effect of treatment on protein expression. By eye, it is easy to see in Figure 4.7 that the collagen bands vary in intensity compared to the α sma bands which look all the same, as the loading control β -actin bands. The individual band's intensity can be quantified as well, in order to measure relative changes between different treatment conditions. Common practice is to quantify bands using ImageJ, an open-source software developed for scientific image data [75]. This software performs a sum of the intensity of each framed band, calculated with the area under the curve. Each band's area is added in an excel sheet to calculate the relative densities. The areas are first normalized with the respective β -actin values. All normalized areas are divided by the control to get relative densities of protein expression in comparison to the control. These relative densities are written under each band in the figure below. The (value-1)x100 gives the percentage of change in the protein expression for the given treatment condition.

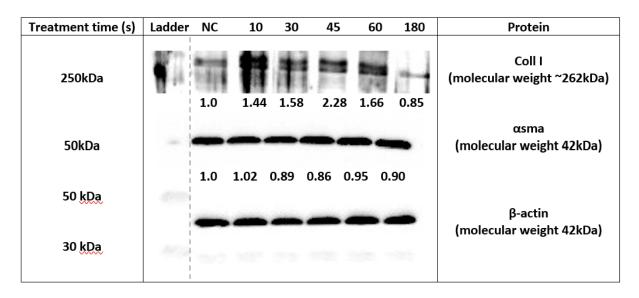


Figure 4.7 Protein bands

Western blot results are plotted for α sma and coll 1 proteins (Figure 4.8).

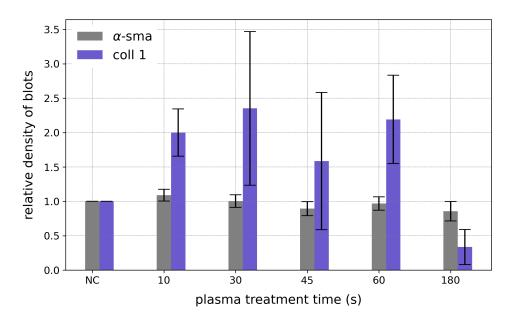


Figure 4.8 Western blot results: quantification of coll 1 and α sma expression

Plasma treatment times of 10, 30, 45, 60 and 180s are used as different treatment conditions. The results show us that α sma expression stays the same under control and all plasma treatment times. The expression coll 1 is induced for short plasma treatment times—10s, 30s, 60s—and decreases for longer treatment time 180s.

We can interpret from these results that plasma does not induce differentiation of fibroblasts into myofibroblasts in these conditions. Considering the context of cells cultured in a monolayer, the typical 3D forces acting on the cells are absent. This could explain in part why fibroblasts are not differentiating even after plasma treatment. Another hypothesis is that key signaling molecules might be missing for this process to take place.

As for coll 1 results, we can link these to metabolic activity results which tend the same way: an increased activity for low dosages and a diminished activity for high dosages. Collagen deposition is important in wound healing, and increased collagen expression can accelerate wound closure and tissue remodeling. More of it is good, too much of it becomes problematic. As presented in a study from Kang and al. [54], healthy fibroblasts reacted to plasma by expressing more collagen, but fibrotic fibroblasts reacted to plasma in the opposite way by reducing their collagen expression. The hypothesis is that we can have a stimulating effect with low plasma dosages in a healthy tissue, which is probably what is observed in the western blot results. But we can also have an anti-fibrotic effect with plasma treatments, where deregulated cells will react very differently to the burst of reactive species.

Plasma reactive species stimulate fibroblasts and this effect is marked by an increased collagen synthesis. What signaling pathways do reactive species trigger that lead to this stimulation? What links plasma to collagen? Augmented production of collagen is characteristic of fibroblasts stimulated by TGF- β , and TGF- β can be activated by plasma [2,3,48]. TGF- β could be the link between the observed biological effects in fibroblast cells and plasma.

It is hard to conclude further on these results since all hypotheses concern an isolated context of fibroblasts in a monolayer culture. Without the *in vivo* environment, many essential actors which modulate in turn plasma's effect are absent: the whole picture is missing. We can still confirm that reactive species from plasma treatment interacted with fibroblast cells and modulated their activity and their function by changes in metabolism and gene expression.

4.5 ROS- vs RNS-Regime

The aim of these biological experiments was to get plausible cause that our plasma jet can have biological effects on the studied cells. This bio-assay results confirm this and are in accordance with the theory of redox biology (oxidative eustress and distress) and plasma's ability to heal tissues. Now the real interest lies in doing all the biology assays for comparing different plasma regimes. This will give us insight on how specific reactive species may impact wound healing and the cells involved. It is also the foundation for going towards optimized plasma treatments and treatments that can be tailored to patients' needs, wound states, etc.

This is why RNS-plasma and ROS-plasma have been established, ready to be used for cell treatment in the hospital laboratory. Biological experiment protocols have been developed to treat cells with dual-regime plasma device.

4.6 Exploration of an Improved Fibrosis Model

In vitro models are practical since they are easy to cultivate and allow a better control of the experimental environment [76]. The limitation is that cell cultures are not comprehensive models of tissues. To push experiments further, the next logical step is a 3D cell culture model, adding the dimension of space. Cells are sensitive to their physical environment, even when cultivated in well plates. Allowing cells to agglomerate and interact with each other in three dimensions mimics *in vivo* conditions a little better. 3D models can be achieved with scaffolds, biomaterials or they can make use of cells natural tendency to agglomerate into a sphere [76].

The present work explored a 3D spheroid model as a future proposition for a fibrosis model. This spheroid model uses well plates prior coated with polyHEMA, a polymer that forms a hydrogel in liquids. This allows for non-adherent cell culture. Instead of adhering to the bottom of the well, cells tend to adhere to one another, forming a spheroid. From the moment cells are seeded, it takes about 2-3 days for spheroids to form and for the model to be ready. Figure 4.9 shows a microscope image of a fibroblast spheroid. Biology assays can then be performed on this model the same way as for 2D culture.

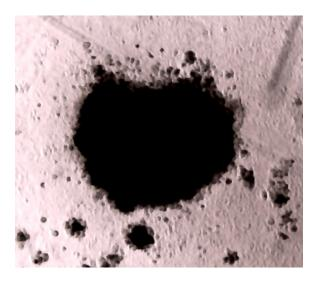


Figure 4.9 3D fibrosis model—fibroblasts in spheroid formation

CHAPTER 5 CONCLUSION

The achieved objectives of this work are as follows:

- 1. Characterization of plasma source reactivity with optical diagnostic tools that can quantify reactive species generated in the plasma;
- 2. Establishment of two plasma regimes with opposing reactivity—oxygen oxide species vs nitrogen oxide species production—by modulation of plasma source composition;
- 3. Development of a dual-regime plasma source and its installation in a hospital laminar flow hood;
- 4. Plasma treatment procedure for evaluating relation between plasma reactive species and a biological model.

5.1 Summary of Works

Optical UV-absorption spectroscopy is used to measure ozone densities in the plasma jet effluent. This diagnostic technique was the basis for choosing two plasma regimes with opposing species production—a RNS-plasma and a ROS-plasma. These regimes are then validated with two other optical diagnostic techniques: OES and FTIR spectroscopy. Optical emission spectroscopy measures the plasma plume emission through a spectrometer slit, revealing relevant differences between both chosen regimes. RNS-plasma has nitric oxide emission lines in the UV and ROS has atomic oxygen emission lines in the IR, confirming shifted reactivity towards nitrogen oxides in one case and oxygen oxides in the other. FTIR spectroscopy further confirmed (NON) for the RNS-plasma production of nitrogen oxide N_2O as well as the absence of an ozone peak. In the end, these diagnostic techniques allowed to establish and validate two opposing plasma regimes that can be used for biological experiments, achieving objective 1 and 2. RNS-plasma is achieved with an argon feed gas admixed with 1% N_2 and a N_2 curtain. ROS-plasma is achieved with an argon feed gas admixed with 1% O_2 .

The established dual-regime plasma device gives us a tool for studying biological effects of different plasma reactivities in the aim of understanding the specific role of single reactive species in wound healing. It also opens a door for tailoring plasma reactivity in response to the treated tissue depending on the state of healing, the pathology, the type of cells, etc. Dual-regime device was designed to optimize both reactivity but also compactness by

minimizing the amount of components needed, meeting objective 3. Only three bottles are needed to achieve both plasma regimes, one of which—the oxygen bottle— is small and can be stored under the rotameters panel. Rotameters are used to control gas flows, as a cluster free solution. One regime can be switched to the other simply by turning valves. In the end, the device fits in small spaces (e.g., between two hoods), is easy to install and is consistent with fire hazard and safety regulations. Dual-regime plasma setup has been transferred to a laminar flow hood at the Montreal General hospital. The plasma jet is mounted on a CNC router to automate treatment of biological models. This type of installation sets the stage for other research laboratories that would want to attempt similar work. The installation is now ready to be used for future work in fibrosis study, and also other fundamental research subjects linked to plasma such as cancer: Laura Bouret will be using this dual-regime in her PhD on plasma treatment for cancer.

The fourth objective is reached by laying the foundation to 2D model plasma treatment modalities, as well as exploring potential 3D fibrosis models. The biological model used is a 2D monolayer of fibroblast cells. The treatment distance is first optimized so the plume delivers a maximum of reactive species in the medium without detaching or killing adherent cells. Dosage interval is defined with metabolic activity assay realized for 5 seconds to 10 minutes treatment of cells. Results showed that short treatment times caused a burst in metabolic activity, indicative of a stimulation of cells which could translate to a stimulation of healing. Dosage interval is used to treat fibroblasts and western blotting is performed. Collagen type I and alpha smooth muscle actin protein expression are studied for each treatment time compared to a control. Fibroblasts expression of α sma stays unchanged under all plasma treatment times. Expression of coll 1 showed dependency of collagen to plasma. Increased collagen expression could mean faster closure of the wounds, thus faster healing. Over-expression of collagen is also a sign of fibrotic tissue. Now that the relation between plasma and collagen is made, in part explainable by cytokine TGF- β modulation, further tests can be done to elucidate reactive species' role in fibrosis. This objective set the basis for future projects with everything in place for starting more complex biology tests.

Other achievements of this work include: creating an interdisciplinary team with the help of scholarship funds TrandMedTech, best oral award of the plasma division at Canadian Association of Physicists (CAP) conference with the presented work, acceptance for a poster competition at the International Conference on Plasma Medicine (ICPM10) to present the work.

5.2 Limitations and Future Research

Plasma medicine in clinical research is largely missing distinct plasma regimes that can be used to study plasma-tissue redox-based interaction. Certified plasma devices operate with either argon or helium feed gas, but without admixtures or gas curtain that can shift plasma reactivity towards wanted regime. A key advantage of plasma is that it can be adapted quickly by turning a few knobs and potentially have drastically different interactions with biological tissues. There are different reasons why so few studies are using this type of plasma device in a clinical context. There are technical reasons for this, since adding layers to plasma composition requires more components like gas bottles, flow controllers, etc. and space is scarce in hospitals. There are also safety concerns that come with added admixtures since more reactive species are produced and end up in the working environment. Both these aspects have been dealt with in the frame of this work.

Combining plasma devices with spectroscopic imaging technologies for real-time monitoring of both plasma characteristics and target features during treatments will allow for tailored plasma treatments. Characterizing plasma was achieved within the scope of this work. Characterizing (2 fois) target tissue features is explored as a proposed solution for future works now that dual-regime plasma device is installed in a fundamental research hospital setting. The proposition is to use optical coherence tomography and hyperspectral imaging spectroscopy input of the tissue and use this input to adapt plasma dosage of reactive species and get desired biological effect(s). These technologies can be used to diagnose wound healing phases and pathologies, to highlight structures, biomarkers specific to each. Fibrosis state can be modified by plasma, one of the key actors responsible for this is TGF- β . Literature is convincing in this sense. The motivation is to have $ex\ vivo$ and eventually $in\ vivo$ fibrosis models treated with the established dual-regime plasma device to compare the outcomes: Giving us insights on both pathological processes and optimization of plasma treatments.

REFERENCES

- [1] A. V. Van Huizen, S. J. Hack, J. M. Greene, L. J. Kinsey, and W. S. Beane, "Reactive oxygen species signaling differentially controls wound healing and regeneration," bioRxiv, p. 2022.04.05.487111, 2022. [Online]. Available: http://biorxiv.org/content/early/2022/04/08/2022.04.05.487111.abstract
- [2] T. A. Wynn, "Common and unique mechanisms regulate fibrosis in various fibroproliferative diseases," *J Clin Invest*, vol. 117, no. 3, pp. 524–9, 2007.
- [3] K. K. Kim, D. Sheppard, and H. A. Chapman, "Tgf-beta1 signaling and tissue fibrosis," *Cold Spring Harb Perspect Biol*, vol. 10, no. 4, 2018. [Online]. Available: https://www.ncbi.nlm.nih.gov/pubmed/28432134
- [4] D. B. Graves, "Mechanisms of plasma medicine: Coupling plasma physics, biochemistry, and biology," *IEEE Transactions on Radiation and Plasma Medical Sciences*, vol. 1, no. 4, pp. 281–292, 2017.
- [5] B.-S. Lou, J.-H. Hsieh, C.-M. Chen, C.-W. Hou, H.-Y. Wu, P.-Y. Chou, C.-H. Lai, and J.-W. Lee, "Helium/argon-generated cold atmospheric plasma facilitates cutaneous wound healing," *Frontiers in Bioengineering and Biotechnology*, vol. 8, 2020. [Online]. Available: http://dx.doi.org/10.3389/fbioe.2020.00683
- [6] J.-P. Zhang, L. Guo, Q.-L. Chen, K.-Y. Zhang, T. Wang, G.-Z. An, X.-F. Zhang, H.-P. Li, and G.-R. Ding, "Effects and mechanisms of cold atmospheric plasma on skin wound healing of rats," *Contributions to Plasma Physics*, vol. 59, no. 1, pp. 92–101, 2019. [Online]. Available: https://doi.org/10.1002/ctpp.201800025
- [7] S. Arndt, P. Unger, A. K. Bosserhoff, M. Berneburg, and S. Karrer, "The anti-fibrotic effect of cold atmospheric plasma on localized scleroderma in vitro and in vivo," *Biomedicines*, vol. 9, no. 11, 2021.
- [8] R. Guay-Lord, X. Attendu, K. L. Lurie, L. Majeau, N. Godbout, A. K. Bowden, M. Strupler, and C. Boudoux, "Combined optical coherence tomography and hyperspectral imaging using a double-clad fiber coupler," *J Biomed Opt*, vol. 21, no. 11, p. 116008, 2016.
- [9] S. Reuter, J. S. Sousa, G. D. Stancu, and J.-P. Hubertus van Helden, "Review on vuv to mir absorption spectroscopy of atmospheric pressure plasma jets," *Plasma*

- Sources Science and Technology, vol. 24, no. 5, p. 054001, 2015. [Online]. Available: https://dx.doi.org/10.1088/0963-0252/24/5/054001
- [10] A. Schmidt-Bleker, R. Bansemer, S. Reuter, and K.-D. Weltmann, "How to produce an nox- instead of ox-based chemistry with a cold atmospheric plasma jet," *Plasma Processes and Polymers*, vol. 13, no. 11, pp. 1120–1127, 2016. [Online]. Available: https://onlinelibrary.wiley.com/doi/abs/10.1002/ppap.201600062
- [11] J.-B. Billeau, J. Thomas, R. Kashyap1, D. Rosenzweig, and S. Reuter, "A comparative study of fibre bragg grating for spatially and temporally resolved gas temperat ure measurements in cold atmospheric pressure plasma jets," *Plasma Source Science and Technology*, 2024. [Online]. Available: underreview
- [12] Y. Ge, J. Wang, D. Gu, W. Cao, Y. Feng, Y. Wu, H. Liu, Z. Xu, Z. Zhang, J. Xie, S. Geng, J. Cong, and Y. Liu, "Low-temperature plasma jet suppresses bacterial colonisation and affects wound healing through reactive species," Wound Repair and Regeneration, vol. n/a, no. n/a, 2024. [Online]. Available: https://doi.org/10.1111/wrr.13178
- [13] T. V. Woedtke, A. Schmidt, S. Bekeschus, K. Wende, and K.-D. Weltmann, "Plasma medicine: A field of applied redox biology," In Vivo, vol. 33, no. 4, pp. 1011–1026, 2019.
- [14] D. B. Graves, "The emerging role of reactive oxygen and nitrogen species in redox biology and some implications for plasma applications to medicine and biology," *Journal of Physics D: Applied Physics*, vol. 45, no. 26, p. 263001, 2012. [Online]. Available: https://dx.doi.org/10.1088/0022-3727/45/26/263001
- [15] J. Moszczyńska, K. Roszek, and M. Wiśniewski, "Non-thermal plasma application in medicine—focus on reactive species involvement," *International Journal of Molecular Sciences*, vol. 24, no. 16, p. 12667, 2023. [Online]. Available: https://www.mdpi.com/1422-0067/24/16/12667
- [16] H. Jablonowski, J. Santos Sousa, K. D. Weltmann, K. Wende, and S. Reuter, "Quantification of the ozone and singlet delta oxygen produced in gas and liquid phases by a non-thermal atmospheric plasma with relevance for medical treatment," Sci Rep, vol. 8, no. 1, p. 12195, 2018.
- [17] R. Clemen, D. Singer, H. Skowski, and S. Bekeschus, "Argon humidification exacerbates antimicrobial and anti-mrsa kinpen plasma activity," *Life*, vol. 13, no. 2, p. 257, 2023. [Online]. Available: https://www.mdpi.com/2075-1729/13/2/257

- [18] A. G. Volkov, J. S. Hairston, G. Taengwa, J. Roberts, L. Liburd, and D. Patel, "Redox reactions of biologically active molecules upon cold atmospheric pressure plasma treatment of aqueous solutions," *Molecules*, vol. 27, no. 20, p. 7051, 2022. [Online]. Available: https://www.mdpi.com/1420-3049/27/20/7051
- [19] S. Bekeschus, "Medical gas plasma technology: Roadmap on cancer treatment and immunotherapy," *Redox Biology*, vol. 65, p. 102798, 2023. [Online]. Available: https://www.sciencedirect.com/science/article/pii/S2213231723001994
- [20] G. Isbary, G. Morfill, H. Schmidt, M. Georgi, K. Ramrath, J. Heinlin, S. Karrer, M. Landthaler, T. Shimizu, B. Steffes, W. Bunk, R. Monetti, J. Zimmermann, R. Pompl, and W. Stolz, "A first prospective randomized controlled trial to decrease bacterial load using cold atmospheric argon plasma on chronic wounds in patients," British Journal of Dermatology, vol. 163, no. 1, pp. 78–82, 2010. [Online]. Available: https://doi.org/10.1111/j.1365-2133.2010.09744.x
- [21] B. Haertel, T. v. Woedtke, K.-D. Weltmann, and U. Lindequist, "Non-thermal atmospheric-pressure plasma possible application in wound healing," *Biomolecules Therapeutics*, vol. 22, no. 6, pp. 477–490, 2014. [Online]. Available: http://www.biomolther.org/journal/view.html?doi=10.4062/biomolther.2014.105
- [22] I. Adamovich, S. Agarwal, E. Ahedo, L. L. Alves, S. Baalrud, N. Babaeva, A. Bogaerts, A. Bourdon, P. J. Bruggeman, C. Canal, E. H. Choi, S. Coulombe, Z. Donkó, D. B. Graves, S. Hamaguchi, D. Hegemann, M. Hori, H.-H. Kim, G. M. W. Kroesen, M. J. Kushner, A. Laricchiuta, X. Li, T. E. Magin, S. M. Thagard, V. Miller, A. B. Murphy, G. S. Oehrlein, N. Puac, R. M. Sankaran, S. Samukawa, M. Shiratani, M. Šimek, N. Tarasenko, K. Terashima, E. T. Jr, J. Trieschmann, S. Tsikata, M. M. Turner, I. J. v. d. Walt, M. C. M. v. d. Sanden, and T. v. Woedtke, "The 2022 plasma roadmap: low temperature plasma science and technology," Journal of Physics D: Applied Physics, vol. 55, no. 37, p. 373001, 2022.
- [23] J. E. Thomas and K. Stapelmann, "Plasma control: A review of developments and applications of plasma medicine control mechanisms," *Plasma*, vol. 7, no. 2, pp. 386–426, 2024. [Online]. Available: https://www.mdpi.com/2571-6182/7/2/22
- [24] A. Schmidt, G. Liebelt, F. Nießner, T. von Woedtke, and S. Bekeschus, "Gas plasma-spurred wound healing is accompanied by regulation of focal adhesion, matrix remodeling, and tissue oxygenation," *Redox Biology*, vol. 38, p. 101809, 2021. [Online]. Available: https://www.sciencedirect.com/science/article/pii/S2213231720310144

- [25] S. Di Meo, T. T. Reed, P. Venditti, and V. M. Victor, "Role of ros and rns sources in physiological and pathological conditions," Oxid Med Cell Longev, vol. 2016, p. 1245049, 2016.
- [26] S. Galadari, A. Rahman, S. Pallichankandy, and F. Thayyullathil, "Reactive oxygen species and cancer paradox: To promote or to suppress?" Free Radical Biology and Medicine, vol. 104, pp. 144–164, 2017. [Online]. Available: https://www.sciencedirect.com/science/article/pii/S0891584917300035
- [27] A. Bloodsworth, V. B. O'Donnell, and B. A. Freeman, "Nitric oxide regulation of free radical— and enzyme-mediated lipid and lipoprotein oxidation," Arteriosclerosis, Thrombosis, and Vascular Biology, vol. 20, no. 7, pp. 1707–1715, 2000. [Online]. Available: https://www.ahajournals.org/doi/abs/10.1161/01.ATV.20.7.1707
- [28] B. Groitl and U. Jakob, "Thiol-based redox switches," *Biochimica et Biophysica Acta* (BBA) Proteins and Proteomics, vol. 1844, no. 8, pp. 1335–1343, 2014. [Online]. Available: https://www.sciencedirect.com/science/article/pii/S1570963914000570
- [29] A. Schmidt, S. Bekeschus, H. Jablonowski, A. Barton, K. D. Weltmann, and K. Wende, "Role of ambient gas composition on cold physical plasma-elicited cell signaling in keratinocytes," *Biophysical Journal*, vol. 112, no. 11, pp. 2397–407, 2017. [Online]. Available: http://dx.doi.org/10.1016/j.bpj.2017.04.030
- [30] P. D. Ray, B. W. Huang, and Y. Tsuji, "Reactive oxygen species (ros) homeostasis and redox regulation in cellular signaling," *Cell Signal*, vol. 24, no. 5, pp. 981–90, 2012.
- [31] P. González, P. Lozano, G. Ros, and F. Solano, "Hyperglycemia and oxidative stress: An integral, updated and critical overview of their metabolic interconnections," Int J Mol Sci, vol. 24, no. 11, 2023.
- [32] G. Pizzino, N. Irrera, M. Cucinotta, G. Pallio, F. Mannino, V. Arcoraci, F. Squadrito, D. Altavilla, and A. Bitto, "Oxidative stress: Harms and benefits for human health," Oxid Med Cell Longev, vol. 2017, p. 8416763, 2017.
- [33] E. Rendra, V. Riabov, D. M. Mossel, T. Sevastyanova, M. C. Harmsen, and J. Kzhyshkowska, "Reactive oxygen species (ros) in macrophage activation and function in diabetes," *Immunobiology*, vol. 224, no. 2, pp. 242–253, 2019. [Online]. Available: https://www.sciencedirect.com/science/article/pii/S0171298518302134
- [34] C. Dunnill, T. Patton, J. Brennan, J. Barrett, M. Dryden, J. Cooke, D. Leaper, and N. T. Georgopoulos, "Reactive oxygen species (ros) and wound healing: the functional

- role of ros and emerging ros-modulating technologies for augmentation of the healing process," *International Wound Journal*, vol. 14, no. 1, pp. 89–96, 2017.
- [35] E. J. Szili, F. J. Harding, S.-H. Hong, F. Herrmann, N. H. Voelcker, and R. D. Short, "The hormesis effect of plasma-elevated intracellular ros on hacat cells," *Journal of Physics D: Applied Physics*, vol. 48, no. 49, p. 495401, 2015. [Online]. Available: https://dx.doi.org/10.1088/0022-3727/48/49/495401
- [36] A. Iswara, K. Tanaka, T. Ishijima, Y. Nakajima, K. Mukai, Y. Tanaka, Y. Nakano, J. Sugama, M. Oe, M. Okuwa, and T. Nakatani, "Wound healing in db/db mice with type 2 diabetes using non-contact exposure with an argon non-thermal atmospheric pressure plasma jet device," *PLOS ONE*, vol. 17, no. 10, p. e0275602, 2022. [Online]. Available: https://doi.org/10.1371/journal.pone.0275602
- [37] A. Jakovija and T. Chtanova, "Skin immunity in wound healing and cancer," Frontiers in Immunology, vol. 14, 2023. [Online]. Available: https://www.frontiersin.org/journals/immunology/articles/10.3389/fimmu.2023.1060258
- [38] J. Li, J. Chen, and R. Kirsner, "Pathophysiology of acute wound healing," *Clinics in Dermatology*, vol. 25, no. 1, pp. 9–18, 2007. [Online]. Available: https://www.sciencedirect.com/science/article/pii/S0738081X06001386
- [39] B. Yue, "Biology of the extracellular matrix: an overview," *J Glaucoma*, vol. 23, no. 8 Suppl 1, pp. S20–3, 2014.
- [40] A. J. Singer and R. A. Clark, "Cutaneous wound healing," N Engl J Med, vol. 341, no. 10, pp. 738–46, 1999.
- [41] T. J. Shaw and P. Martin, "Wound repair at a glance," Journal of Cell Science, vol. 122, no. 18, pp. 3209–3213, 2009. [Online]. Available: https://doi.org/10.1242/jcs.031187
- [42] L. Melotti, T. Martinello, A. Perazzi, E. Martines, M. Zuin, D. Modenese, L. Cordaro, S. Ferro, L. Maccatrozzo, I. Iacopetti, and M. Patruno, "Could cold plasma act synergistically with allogeneic mesenchymal stem cells to improve wound skin regeneration in a large size animal model?" Research in Veterinary Science, vol. 136, pp. 97–110, 2021. [Online]. Available: https://www.sciencedirect.com/science/article/pii/S003452882100031X
- [43] B. Rybinski, J. Franco-Barraza, and E. Cukierman, "The wound healing, chronic fibrosis, and cancer progression triad," *Physiol Genomics*, vol. 46, no. 7, pp. 223–44, 2014.

- [44] C. Nathan and A. Ding, "Nonresolving inflammation," *Cell*, vol. 140, no. 6, pp. 871–882, 2010. [Online]. Available: https://www.sciencedirect.com/science/article/pii/S0092867410001820
- [45] P. Rousselle, F. Braye, and G. Dayan, "Re-epithelialization of adult skin wounds: Cellular mechanisms and therapeutic strategies," *Advanced Drug Delivery Reviews*, vol. 146, pp. 344–365, 2019. [Online]. Available: https://www.sciencedirect.com/science/article/pii/S0169409X18301583
- [46] G. Isbary, J. L. Zimmermann, T. Shimizu, Y. F. Li, G. E. Morfill, H. M. Thomas, B. Steffes, J. Heinlin, S. Karrer, and W. Stolz, "Non-thermal plasma—more than five years of clinical experience," *Clinical Plasma Medicine*, vol. 1, no. 1, pp. 19–23, 2013. [Online]. Available: https://www.sciencedirect.com/science/article/pii/S2212816612000030
- [47] S. Chawla and S. Ghosh, "Regulation of fibrotic changes by the synergistic effects of cytokines, dimensionality and matrix: Towards the development of an in vitro human dermal hypertrophic scar model," *Acta Biomaterialia*, vol. 69, pp. 131–145, 2018. [Online]. Available: https://www.sciencedirect.com/science/article/pii/S1742706118300047
- [48] S. Fathollah, S. Mirpour, P. Mansouri, A. R. Dehpour, M. Ghoranneviss, N. Rahimi, Z. Safaie Naraghi, R. Chalangari, and K. M. Chalangari, "Investigation on the effects of the atmospheric pressure plasma on wound healing in diabetic rats," *Scientific Reports*, vol. 6, no. 1, p. 19144, 2016. [Online]. Available: https://doi.org/10.1038/srep19144
- [49] R. J. Ruthenborg, J. J. Ban, A. Wazir, N. Takeda, and J. W. Kim, "Regulation of wound healing and fibrosis by hypoxia and hypoxia-inducible factor-1," *Mol Cells*, vol. 37, no. 9, pp. 637–43, 2014.
- [50] C. K. Sen and S. Roy, "Redox signals in wound healing," Biochimica et Biophysica Acta (BBA) - General Subjects, vol. 1780, no. 11, pp. 1348–1361, 2008. [Online]. Available: https://www.sciencedirect.com/science/article/pii/S030441650800007X
- [51] B. Kunkemoeller and Т. R. Kyriakides, "Redox signaling diabetic in extracellular wound healing regulates matrix deposition," Antioxidants12. signaling, vol. 27,823–838, 2017. amp; redox no. pp. Online. Available: http://europepmc.org/abstract/MED/28699352https://europepmc. org/articles/pmc5647483?pdf=renderhttps://doi.org/10.1089/ars.2017.7263https: //europepmc.org/articles/PMC5647483

- [52] Y. Mori, K. Oguri, N. Iwata, T. Murata, M. Hori, and M. Ito, "Plasma-generated nitric oxide radical (no•) promotes the proliferation of fibroblast cells in liquid," *Japanese Journal of Applied Physics*, vol. 62, no. SL, p. SL1016, 2023. [Online]. Available: https://dx.doi.org/10.35848/1347-4065/acd9b6
- [53] A. V. Butenko, A. B. Shekhter, A. V. Pekshev, A. B. Vagapov, A. L. Fayzullin, N. B. Serejnikova, N. A. Sharapov, V. A. Zaborova, and V. N. Vasilets, "Review of clinical applications of nitric oxide-containing air-plasma gas flow generated by plason device," *Clinical Plasma Medicine*, vol. 19-20, p. 100112, 2020. [Online]. Available: https://www.sciencedirect.com/science/article/pii/S2212816620300196
- [54] S. U. Kang, Y. S. Kim, Y. E. Kim, J. K. Park, Y. S. Lee, H. Y. Kang, J. W. Jang, J. B. Ryeo, Y. Lee, Y. S. Shin, and C. H. Kim, "Opposite effects of non-thermal plasma on cell migration and collagen production in keloid and normal fibroblasts," *PLoS One*, vol. 12, no. 11, p. e0187978, 2017.
- [55] H. Y. Kim, S. K. Kang, S. M. Park, H. Y. Jung, B. H. Choi, J. Y. Sim, and J. K. Lee, "Characterization and effects of ar/air microwave plasma on wound healing," *Plasma Processes and Polymers*, vol. 12, no. 12, pp. 1423–1434, 2015. [Online]. Available: https://onlinelibrary.wiley.com/doi/abs/10.1002/ppap.201500017
- [56] Y.-W. Hung, L.-T. Lee, Y.-C. Peng, C.-T. Chang, Y.-K. Wong, and K.-C. Tung, "Effect of a nonthermal-atmospheric pressure plasma jet on wound healing: An animal study," *Journal of the Chinese Medical Association*, vol. 79, no. 6, pp. 320–328, 2016. [Online]. Available: https://journals.lww.com/jcma/fulltext/2016/06000/effect_of_a_nonthermal_atmospheric_pressure_plasma.6.aspx
- [57] G. Li, D. Li, J. Li, Y.-N. Jia, C. Zhu, Y. Zhang, and H.-P. Li, "Promotion of the wound healing of in vivo rabbit wound infected with methicillin-resistant staphylococcus aureus treated by a cold atmospheric plasma jet," *IEEE Transactions on Plasma Science*, vol. 49, no. 8, pp. 2329–2339, 2021. [Online]. Available: http://dx.doi.org/10.1109/TPS.2021.3092946
- [58] D. Li, G. Li, J. Li, Z.-Q. Liu, X. Zhang, Y. Zhang, and H.-P. Li, "Promotion of wound healing of genetic diabetic mice treated by a cold atmospheric plasma jet," IEEE Transactions on Plasma Science, vol. 47, no. 11, pp. 4848–4860, 2019. [Online]. Available: http://dx.doi.org/10.1109/TPS.2019.2928320
- [59] B. Eggers, M. B. Stope, J. Marciniak, A. Mustea, S. Eick, J. Deschner,M. Nokhbehsaim, and F.-J. Kramer, "Non-invasive physical plasma reduces the

- inflammatory response in microbially prestimulated human gingival fibroblasts," *International Journal of Molecular Sciences*, vol. 24, no. 22, p. 16156, 2023. [Online]. Available: https://www.mdpi.com/1422-0067/24/22/16156
- [60] X. Xu, J. Geng, G. Liu, and Z. Chen, "Evaluation of optical coherence tomography for the measurement of the effects of activators and anticoagulants on the blood coagulation in vitro," *IEEE Trans Biomed Eng*, vol. 60, no. 8, pp. 2100–6, 2013.
- [61] A. Fadlelmoula, D. Pinho, V. H. Carvalho, S. O. Catarino, and G. Minas, "Fourier transform infrared (ftir) spectroscopy to analyse human blood over the last 20 years: A review towards lab-on-a-chip devices," *Micromachines (Basel)*, vol. 13, no. 2, 2022.
- [62] R. Rutkowski, M. Schuster, J. Unger, C. Seebauer, H. R. Metelmann, T. v. Woedtke, K. D. Weltmann, and G. Daeschlein, "Hyperspectral imaging for in vivo monitoring of cold atmospheric plasma effects on microcirculation in treatment of head and neck cancer and wound healing," Clinical Plasma Medicine, vol. 7-8, pp. 52–57, 2017. [Online]. Available: https://www.sciencedirect.com/science/article/pii/S2212816617300100
- [63] U. Fantz, "Basics of plasma spectroscopy," Plasma Sources Science and Technology, vol. 15, no. 4, p. S137, 2006. [Online]. Available: https://dx.doi.org/10.1088/0963-0252/ 15/4/S01
- [64] J.-B. Billeau, P. Cusson, A. Dogariu, A. Morozov, D. V. Seletskiy, and S. Reuter, "Coherent homodyne detection for amplified cross-beam electric-field induced second harmonic," *Applied Optics*, vol. 63, no. 19, pp. 5203–5207, 2024. [Online]. Available: https://opg.optica.org/ao/abstract.cfm?URI=ao-63-19-5203
- [65] J. Winter, K. Wende, K. Masur, S. Iséni, M. Dünnbier, U. Hammer, Malte, H. Tresp, K.-D. Weltmann, and S. Reuter, "Feed gas humidity: a vital parameter affecting a cold atmospheric-pressure plasma jet and plasma-treated human skin cells," *Journal of Physics D: Applied Physics*, vol. 46, no. 29, pp. 295401–295401, 2013. [Online]. Available: https://hal.science/hal-03271692
- [66] S. Bekeschus, T. von Woedtke, S. Emmert, and A. Schmidt, "Medical gas plasmastimulated wound healing: Evidence and mechanisms," *Redox Biol*, vol. 46, p. 102116, 2021.
- [67] S. S. A. R. G. K. N. J. F. A. G. V. S.-v. d. G. D. O. A Wijaikhum, D Schröder and T. Gans, "Absolute ozone densities in a radio-frequency driven atmospheric pressure plasma using two-beam uv-led absorption spectroscopy and numerical simulations," *Plasma Sources Science and Technology*, vol. 26, no. 11, 2017.

- [68] J. D. McClurkin, D. E. Maier, and K. E. Ileleji, "Half-life time of ozone as a function of air movement and conditions in a sealed container," *Journal of Stored Products Research*, vol. 55, pp. 41–47, 2013. [Online]. Available: https://www.sciencedirect.com/science/article/pii/S0022474X13000659
- [69] L. T. Molina and M. J. Molina, "Absolute absorption cross sections of ozone in the 185- to 350-nm wavelength range," *Journal of Geophysical Research: Atmospheres*, vol. 91, no. D13, pp. 14501–14508, 1986. [Online]. Available: https://agupubs.onlinelibrary.wiley.com/doi/abs/10.1029/JD091iD13p14501
- [70] S. B. Bayram and M. V. Freamat, "Vibrational spectra of n2: An advanced undergraduate laboratory in atomic and molecular spectroscopy," American Journal of Physics, vol. 80, no. 8, pp. 664–669, 2012. [Online]. Available: https://doi.org/10.1119/1.4722793
- [71] S. Iséni, S. Reuter, and K.-D. Weltmann, "No2 dynamics of an ar/air plasma jet investigated by in situ quantum cascade laser spectroscopy at atmospheric pressure," *Journal of Physics D: Applied Physics*, vol. 47, no. 7, p. 075203, 2014. [Online]. Available: https://dx.doi.org/10.1088/0022-3727/47/7/075203
- [72] Y. Fu, D. Kong, X. Gu, Y. Wang, Y. Wu, and R. Zhang, "Quantitative evaluation of the low-temperature pulsed plasma-wound interaction based on splint model," *Applied Physics Letters*, vol. 123, no. 19, 2023. [Online]. Available: https://doi.org/10.1063/5.0176678
- [73] M. Weiss, J. Barz, M. Ackermann, R. Utz, A. Ghoul, K. D. Weltmann, M. B. Stope, D. Wallwiener, K. Schenke-Layland, C. Oehr, S. Brucker, and P. Loskill, "Dose-dependent tissue-level characterization of a medical atmospheric pressure argon plasma jet," ACS Applied Materials amp; Interfaces, vol. 11, no. 22, pp. 19841–53, 2019. [Online]. Available: http://dx.doi.org/10.1021/acsami.9b04803
- [74] W. S. To and K. S. Midwood, "Plasma and cellular fibronectin: distinct and independent functions during tissue repair," Fibrogenesis Tissue Repair, vol. 4, no. 1, p. 21, 2011. [Online]. Available: https://doi.org/10.1186/1755-1536-4-21
- [75] J. Schindelin, I. Arganda-Carreras, E. Frise, V. Kaynig, M. Longair, T. Pietzsch, S. Preibisch, C. Rueden, S. Saalfeld, B. Schmid, J.-Y. Tinevez, D. J. White, V. Hartenstein, K. Eliceiri, P. Tomancak, and A. Cardona, "Fiji: an open-source platform for biological-image analysis," *Nature Methods*, vol. 9, no. 7, pp. 676–682, 2012. [Online]. Available: https://doi.org/10.1038/nmeth.2019

[76] S. Chawla, A. Mainardi, N. Majumder, L. Dönges, B. Kumar, P. Occhetta, I. Martin, C. Egloff, S. Ghosh, A. Bandyopadhyay, and A. Barbero, "Chondrocyte hypertrophy in osteoarthritis: Mechanistic studies and models for the identification of new therapeutic strategies," Cells, vol. 11, no. 24, 2022.

APPENDIX A SECURITY RISKS ASSESSMENT AND MITIGATION PROTOCOL

Appendix A presents the security risks assessment and mitigation protocol prepared for approving dual-regime plasma source setup and usage in a hospital setting.

Protocol PDF attached below:

Plasma source—MGH Security Risks Assessment

This document serves as an assessment of security risks concerning the use of a plasma jet in a hospital research laboratory context. And how to mitigate these issues. The plasma jet is to be used in a biohood to treat sterile cell cultures.

Plasma source uses gas (argon, nitrogen, oxygen, air) to produce mainly reactive species such as ozone, nitrogen oxides, hydrogen peroxide in small quantities in liquids and in air. We can measure these species with sensitive optical equipment since the concentrations are very low.

The security risks when using the plasma jet at MGH are the following:

- High electrical voltage
- Gases
- Hospital context

1- High electrical voltage

This risk is controlled with simple handling directives of the high-power source and its connections. The directives are stated later in section 1 of this document.

2- Gases

The gases which represent a risk when using the plasma jet are mainly ozone, NOx and if in the case of them being present in large quantities—e.g. in case of a leak—asphyxiating gases. The norms that regulate these gas are available on CNSST website.

For ozone, the secure exposure level has a ceiling value of 0.1ppm.

Exposure limit Canada:

OSHA Permissible Exposure Limit: 8 hour Time Weighted Average **0.1 ppm**ANSI/ASTM: 8 hour TWA **0.1 ppm**, Short Term Exposure Limit **0.3 ppm**ACGIH: 8 hour TWA **0.1 ppm**; STEL **0.3 ppm**NIOSH: Exposure Limit Ceiling Value **0.1 ppm** light; **0.08 ppm** moderate; **0.05 ppm**, heavy;

Figure 1: Exposure limit Canada (Chrystal Air Canada – Safety Data Sheet)

<u>Nitrogen</u>, <u>oxygen</u> and <u>argon</u> are asphyxiants—Category 1, and the norm states their concentration in the room should be the same percentage as in the air at normal atmospheric pressure.

Oxygen is also an oxidizing gas—Category 1, meaning it can feed a fire.

The admixture of oxygen to the gas does not exceed the content of oxygen in the room (i.e. 1% admixture to argon feed gas and 20% admixture to curtain in certain conditions)

Admixture of oxygen or nitrogen can increase the ozone concentration by a factor of 10 locally. Dilution with inflow of air and room ventilation reduces ozone below threshold.

An empirical study in a 39.1 m³ unventilated test room found that an ozone concentration of 0.03 ppm was not exceeded at a distance of 40 cm from the plasma effluent over a period of 5.5 hours (see below) Dilution of ozone in hood by an inflow of 100 FPM, which is 100l/s for an opening of 100 cm x 20 cm of the biohood at 3 liter per minute gas flow in the plasma jet at 100 times concentration of plasma jet without oxygen admixture (0.03 ppm @ 40 cm distance in an unventilated room) is calculated at 1 ppb ozone concentration at 40 cm distance to the plasma jet. Concentrations of NOx is 10 to 100 times lower at any given conditions.

A measure which will assure security in the laboratory: sensors able to detect if there is a leak in the lab environment, or detect unsafe level of gases

- Ozone and/or NOx sensors placed on the plasma jet user
- Oxygen sensor for the room to make sure there are no leaks from the bottles

Plasma jets are used in a hospital context and in biological hoods. The flow of the hood dilutes the ozone concentration.

3- Hospital context

Plasma jets are clinically certified medical devices (https://neoplas-med.eu/) and are used to treat patients and in research laboratories. E.g. of plasma jet being used in biohood for biological experiments presented in section 2 of this document.

See <u>section 3</u> for current security measures taken in the optics lab at Polytechnique Montréal where the plasma is used in free space for optics diagnostics measurements.

Section 1: Plasma Operation Protocol

Basic safety rules (<u>high electrical voltage security</u>):

- 1) Always make sure that you work in **group of two** (or at least check on you frequently) in case of electrical tetanization
- 2) In case of someone being tetanized, do not touch the person with your hand (use an insulated material to make the person let go)
- 3) **Never put a ring, watch or any other metallic object** on your hand that can conduct electricity when using the plasma source
- 4) Always double/triple check the electrical connections (GROUND +++)
- 5) A rule of thumb: **electrical discharge in air happens at around 15 kV/cm**, so keep a safe distance between you and the high voltage wires
- 6) Never let the plasma run without any surveillance
- 7) Even if the source is made for biological interaction, you are prohibited from touching it

Opening plasma source:

1) Opening the gas bottle

- 1. Make sure that the flow valve (small one) is closed, the regulating valve is opened (unscrewed) and the flow meter is on
- 2. To open/close a gas bottle, always start from the safety lever (red) to the other valves
- 3. Increase slowly the pressure of the regulating valve (small steps)
- 4. Open slowly the flow valve
- 5. Verify the flow with the flow meter
- 6. If the desired flow is not attained, repeat steps 3 to 5
- 7. Connect the gas tube to the plasma jet

2) Ignite the plasma source

- 1. Make sure that the switch is off
- 2. Make sure that everything is connected and secured (the ground should be connected to a power outlet)
- 3. Connect the high voltage to the plasma source
- 4. Make sure that the gas is on
- 5. Plug the power source to the power bar and double check your connections
- **6.** Turn the **switch on**
- 7. Turn the plasma on with an amplitude of max 10% (get an estimate of the resonance frequency)
- 8. Increase amplitude to wanted %
- 9. Fine tune the frequency until getting a nice plasma plume

Closing plasma source

1) Closing the plasma jet

- 1. Turn the switch off
- 2. Turn the power source off (frequency to 0 when hearing a click sound) and reduce the amplitude to 0% (at that point, no red light should be on)
- 3. Get rid of residual charges by carefully making sure that the exposed part of the high voltage wire touches the ground

2) Closing the gas bottle

- 1. Close the safety valve first (red lever) and verify the gas amount left in the bottle
- 2. Wait for the pressure to reduce to zero at the regulator
- 3. Open the regulating valve to decrease the pressure output
- 4. Close the flow valve

Contact number:

Jean-Baptiste Billeau — 438-868-4798 or <u>jean-baptiste.billeau@polymtl.ca</u> Juliette Letellier-Bao — 514-557-9290 or <u>juliette.letellier-bao@polytmtl.ca</u> Laura Bouret — 438-500-3658 or laura-melanie.bouret@polymtl.ca

Section 2: Plasma Chemistry and Biological Usage

Gases used and potential toxic species

Pure gases used from bottles: oxygen, argon, nitrogen

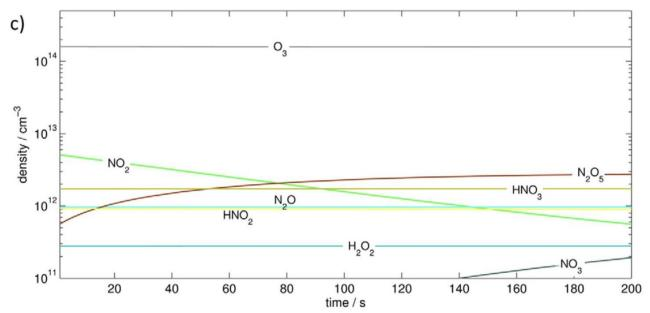


Figure 2: species which can be produced by plasma jet in a collection multipass absorption cell

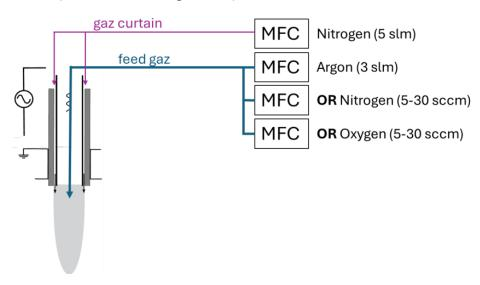
Schmidt-Bleker, A., J. Winter, A. Bösel, S. Reuter, and K.-D. Weltmann, *On the plasma chemistry of a cold atmospheric argon plasma jet with shielding gas device.* Plasma Sources Science and Technology, 2016. **25**: p. 015005.

Gas flows

- Argon flow: 2-3 SLM

- N2 flow: 0.03 SLM (1% mixed with Argon flow) + 5 SLM as a gas curtain

- O2 flow: 0.03 SLM (1% mixed with Argon flow)



Species concentrations

For concentrations released in the lab environment refer to document:

German Society for Oral, Maxillofacial and Facial Surgery (DGMKG). *Rational therapeutic use of cold physical plasma*. AWMF register number: 007 – 107. S2k guidelines. February 23, 2022. https://neoplasmed.eu/wp-content/uploads/2022/04/007-107l Rationaler-therapeutischer-Einsatz-von-kaltem-physikalischem-Plasma 2022-02 web.pdf

See page 14 of document for assessment and mitigation of gas fume dangers (this applies for non-ventilated environment, in the case of the plasma being in biological hood we have a flow diffusing the plasma species more efficiently):

"The application of cold plasma in the oral cavity and at a tracheostoma raises the question of whether the gas may be inhaled: The detection of potentially toxic gas emissions (especially ozone and nitrogen oxides) that can arise during the operation of cold atmospheric pressure plasma sources is part of the recommendations "General requirements for medical plasma sources" in DIN SPEC 91315:2014-06 [141]. With regard to cold atmospheric pressure plasma sources currently in clinical use, investigations have been published for the cold atmospheric pressure plasma jet kINPen MED. In the immediate vicinity of the visible plasma effluent, relatively high ozone concentrations around 0.2 ppm were measured. The odor threshold for ozone is reported in the literature as 0.02 ppm or 40 μg/m3. According to EU Directive 2002/3/EC, daily (8-hour) ozone exposure should not exceed 0.055 ppm or 120 mg/m3 to avoid health risks. Nitrogen dioxide (NO2) could not be measured in the vicinity of the plasma effluent [142, 143]. An empirical study in a 39.1 m³ unventilated test room found that an ozone concentration of 0.03 ppm was not exceeded at a distance of 40 cm from the plasma effluent over a period of 5.5 hours [144, 145]"

As for **NOx levels**, the quantities produced are so low we are not able to detect their concentration in close vicinity of the plasma jet plume, even with highly sensible optics.

Protocol for experiments with biological material

- Spray workstation with ethanol 70% concentration
- Make sur the cells are confluent in the wells for best results (cells used are human fibroblasts)
- Discard media in well plates and add fresh media—1mL
- Place well plate inside the biological hood on the CNC and take cover off
- Turn all gases needed ON
 - a) For Ar plasma only need argon bottle ON with a flow of 2-3 SLM
 - b) For oxygen-based plasma need argon bottle and oxygen bottles ON
 - c) For nitrogen-based plasma need argon bottle and nitrogen bottles ON
- Turn plasma ON—begin cell treatment with wanted treatments times and treatment distances
- Once treatment is finished turn plasma OFF, turn all gas bottles OFF
- Cover well plate before removing it from biological hood and place back in incubator for 24h

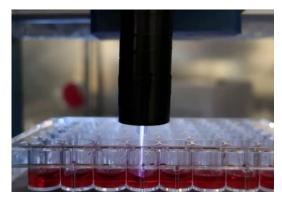
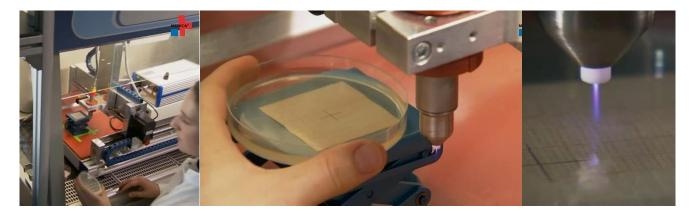


Figure 4: plasma jet ON in the biohood treating a well plate with cell culture

Plasma being used as medical device:

Plasma jet certified medical devices: https://neoplas-med.eu/

Video of plasma jet being used to treat human / in biohood (see pictures below for example): https://www.youtube.com/watch?v=39CbO27SYtk



Section 3: Setup at Polytechnique Optics Laboratory

The plasma jet at Polytechnique laboratory is used in free space (no cabinet or hood) in a ventilated room of volume 250 m³ with 3-6 air changes/hour. There is no accumulation of gases within normal usage of plasma jet. We use the jet for plasma diagnostics like measuring species concentrations. In the case where the plasma accumulates in e.g. a glass cell, we use ventilation to have some air changes locally close to the jet. The ventilation capacity of such nozzle is between 75-100L/min. No additional security measure is used concerning gas security.

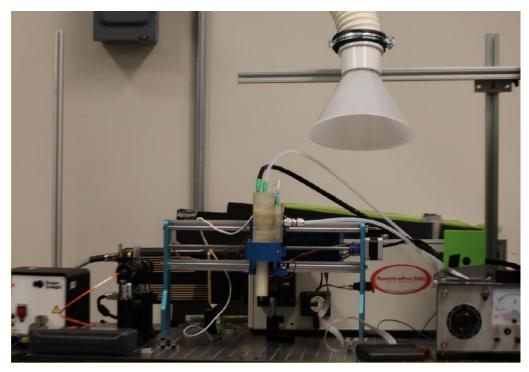


Figure 5: setup with plasma jet and ventilation is physics lab at Polytechnique Montreal

APPENDIX B FTIR PYTHON CODE

Appendix B presents written python code for simulating absorbance with HITRAN cross sections, for plotting experimental FTIR signals, and for performing fitting to determine species densities.

```
import matplotlib.pyplot as plt
import numpy as np
import pandas as pd
import os
# Parent path
parent dir = 'results/FTIR/2024-05-09 FTIR 16m/'
fig path = os.path.join(parent dir, 'graphs/')
if not os.path.isdir(fig_path):
   os.makedirs(fig path)
#%% Experimental data load and plot
path = 'results/FTIR/2024-05-09 FTIR 16m/'
df = pd.read_excel(path + 'Ar-3slm n2-admix n2 curtain-5slm' + '.xlsx')
x ftir = df['wavelength']
absorb ftir =df['absorb']
ref ftir = df['ref']
sample_ftir = df['sample']
fig, ax = plt.subplots(figsize=(8,5))
ax.plot(x_ftir, absorb_ftir, color='grey', label='absorbance')
ax.plot(x ftir, sample ftir, color='navy', label='sample')
ax.plot(x_ftir, ref_ftir, color='chocolate', label='background')
#z.oom1
zm = ax.inset axes([0.01, 0.8, 0.2, 0.2])
zm.plot(x ftir[498:561], sample ftir[498:561], color='navy')
```

```
zm.plot(x ftir[498:561], ref ftir[498:561], color='chocolate')
# zm.xaxis.set_visible(False)
zm.yaxis.set_visible(False)
ax.indicate_inset_zoom(zm, edgecolor='black')
#zoom2
zm2 = ax.inset axes([0.5, 0.5, 0.2, 0.2])
zm2.plot(x ftir[583:607], sample ftir[583:607], color='navy')
zm2.plot(x_ftir[583:607], ref_ftir[583:607], color='chocolate')
# zm.xaxis.set visible(False)
zm2.yaxis.set visible(False)
ax.indicate_inset_zoom(zm2, edgecolor='black')
ax.set_ylabel('intensity', fontsize=15, labelpad=20)
ax.set_xlabel('wavenumber / $\mathrm{cm^{-1}}$', fontsize=15,
              labelpad=20)
plt.tick params(axis='both', labelsize=12)
color= 'black'
plt.text(1615, 0.0075, 'H\u20820', va='center', ha='center', color=color,
          fontsize=15)
plt.text(3750, 0.0075, 'H\u20820', va='center', ha='center', color=color,
          fontsize=15)
plt.text(2125, 0.0049, 'N\u20820', va='center', ha='center', color=color,
          fontsize=15)
plt.text(2500, 0.0049, 'CO\u2082', va='center', ha='center', color=color,
          fontsize=15)
plt.legend(loc='upper right', facecolor='white',
            framealpha=1, frameon=True, edgecolor='white',
            fontsize=15, bbox to anchor=(1, 1.1))
plt.grid(color = 'gray', linestyle = '--', linewidth = 0.4)
plt.savefig(fig path+'all-signals', dpi=800, bbox inches='tight')
#%% cross sections
fig, ax = plt.subplots(figsize=(8, 5), constrained_layout=True)
wavenum_min=1400
```

```
wavenum max=2500
res = 4
path_xs = 'results/FTIR/cross sections/'
list = ['n2o', 'co2', 'o3', 'co', 'h2o', 'h2o2', 'no2']
names = ['N\u20820', 'CO\u2082', 'O\u2083', 'CO', 'H\u20820',
         'H\u20820\u2082', 'NO\u2082']
dict = \{\}
dict_wavenum = {}
for molecule, name in zip(list, names):
    f=open(path_xs + molecule + '_' + str(res) +'.txt',"r")
    lines=f.readlines()
    header = lines[5]
    X = []
    xs=[]
    for line in lines[7:]:
        line = line.split()
        line = [float(i) for i in line] # Convert strings to ints
        x.append(line[0])
        xs.append(line[1])
    f.close()
    dict[molecule] = xs
    dict_wavenum[molecule] = x
    ax.plot(x, xs, linewidth=1.3, label='{}'.format(name))
    print(name)
ax.set_ylabel(' absorption cross section / cm$^2$ molecule$^{-1}$',
              fontsize=15, labelpad=20)
ax.set_xlabel('wavenumber / cm\u207b\u00B9', fontsize=15, labelpad=20)
ax.tick_params(axis='both', labelsize=12)
ax.legend(loc='upper left', facecolor='white',
          framealpha=1, frameon=True, edgecolor='white',
          ncol=3, fontsize=15)
```

```
ax.set xlim(wavenum min, wavenum max)
ax.grid(color = 'gray', linestyle = '--', linewidth = 0.4)
plt.savefig(path + 'graphs/' + 'cross-sections', dpi=800,
            bbox_inches='tight')
#%% PLOT ABSORBANCE
wavenum min=1800
wavenum max=2500
path xs = 'results/FTIR/cross sections/'
list = ['n2o', 'co2', 'o3', 'co', 'h2o']
names = ['N\u20820', 'CO\u2082', 'O\u2083', 'CO', 'h2o']
concentrations = [2.5e12, 2.5e12, 1e14, 2.3e12, 4e13] # mol/cm<sup>3</sup>
colors = ['orangered', 'black', 'maroon', 'green', 'blue']
res = 4 \# /cm^1
Lexp = 1600 \# cm
fig, ax = plt.subplots(figsize=(8, 5), constrained layout=True)
ax.plot(x_ftir, absorb_ftir+0.0009, color='blue', alpha=0.3,
          linewidth=1.8, label='FTIR')
ax2 = ax.twiny()
ax2.set xticks(ax.get xticks())
ax2.set_xbound((wavenum_min, wavenum_max))
ax2.set_xticklabels([round((1/x)*1e7) for x in ax.get_xticks()])
ax3 = ax.twinx()
ax3.set axis off()
ax3.plot(x ftir, absorb ftir+0.0009, color='blue', alpha=0.3,
          linewidth=1.8, label='FTIR')
dict = {}
dict wavenum = {}
for molecule, c, color, name in zip(list, concentrations, colors, names):
    f=open(path_xs + molecule + '_' + str(res) +'.txt', "r")
```

```
lines=f.readlines()
    header = lines[5]
   X = []
    xs=[]
    for line in lines[7:]:
        line = line.split()
        line = [float(i) for i in line] # Convert strings to ints
        x.append(line[0])
        xs.append(line[1])
    f.close()
    dict[molecule] = xs
    dict wavenum[molecule] = x
    absorbance = (np.array(xs)*c*Lexp) # SIMULATION FIT PARAM = c
    if molecule == 'o3': # molecule absent
        ax3.plot(x, absorbance, '--', color=color, linewidth=1.3,
                 label='{}'.format(name))
    else: # molecule fit known concentration
        ax3.plot(x, absorbance, color=color, linewidth=1.3,
                 label='{}'.format(name)) #[{:.1e}molecules/cm\u00b3] c
ax.set_ylabel('absorbance', fontsize=15, labelpad=20)
ax.set_xlabel('wavenumber / cm\u207b\u00B9', fontsize=15, labelpad=20)
ax2.set_xlabel('wavelength / nm', fontsize=15, labelpad=20)
ax.tick params(axis='both', labelsize=12)
ax2.tick params(axis='x', labelsize=12)
ax3.legend(loc='upper left', facecolor='white',
            framealpha=1, frameon=True, edgecolor='white',
            ncol=3, fontsize=15)
ax.set_xlim(wavenum_min, wavenum_max)
ax.grid(color = 'gray', linestyle = '--', linewidth = 0.4)
plt.savefig(path + 'graphs/' + 'fit all molecules', dpi=1200, bbox_inches='tight')
```

APPENDIX C AUTOMATED PLASMA TREATMENT OF 12-WELL PLATE

Appendix C presents the python code written to generate G-code for treating cells cultured in a 12-well plate with plasma jet mounted on CNC router along with an example of a G-code.

```
import dataframe image as dfi
import numpy as np
import pandas as pd
from string import ascii_uppercase as abc
## DEFINE WELL PLATE PARAMETERS
class well plate:
## DEFINE OFFSET FROM HOME TO WELL LOWER LEFT CORNER in mm
## NEEDS TO BE CALIBRATED WHEN CHANGING WORK STATION
    data = {'type':['CELLSTAR'],
                'x_offset':[169.9],
                'y_offset': [52.6],
                'z_offset':[-36], # for nozzel to touch bottom of well -34 1mL
                'well distance': [26], # distance entre puits
                'diameter': [22.7],
                'n plates':[12]}
plate = well plate()
index = 0
# for reference only z treatement based on distance from bottom of plate
volume = 1000 # in uL
h_media = volume / (np.pi * (plate.data['diameter'][index]/2)**2)
print('hight media: ' + str(h_media) + 'mm')
## CREATE WELLPLATE MAP
def n rows ncols(n plates):
    a, b, i = 1, n_{plates}, 0
    while a < b:
        i += 1
```

```
if n plates \% i == 0:
            a = i
            b = n_plates//a
    return b, a
rows, cols = n rows ncols(plate.data['n plates'][index])
row_names = [i for i in abc[0:rows]]
col names = [i for i in range(0, cols)]
class Well(object):
    def __init__(self):
        self.time = None
        self.distance = None
        self.label = 'sample'
wells = {}
list wells = []
for i in row names:
    for j in col_names:
        id = i+str(j)
        wells[id] = Well()
        list_wells.append(id)
## ASSIGN TREATMENT TIMES TO WELLS
times = [10, 10, 30, 30, 45, 45, 60, 60, 180, 180, 60, 60]
# times = [5, 5, 10, 10, 15, 15, 30, 30, 45, 45, 60, 60]
# times = [90, 90, 120, 120, 180, 180, 300, 300, 600, 600, 60, 60]
sum time = 0
for i in times:
    sum time += i
print('total treatment time/plate: ' + str(sum_time/60))
for key, time in zip(wells, times):
    wells[key].time = time # in seconds
```

ASSIGN TREATMENT DTSANCES TO WELLS

```
# treatment distances
for id in ['AO', 'A1', 'A2', 'A3',
           'BO', 'B1', 'B2', 'B3',
           'CO', 'C1', 'C2', 'C3']:
    wells[id].distance = 22.5 # in mm
# no treatment
for id in \Pi:
    wells[id].distance = None # in mm
## DEFINE WELL TYPE IF NOT SAMPLE
# Plasma flow control
for id in ['C2', 'C3']:
    wells[id].label = 'control'
# No treatment
for id in []:
    wells[id].label = 'nothing'
## EXPORT TO PNG
df = pd.DataFrame()
df = (df.T)
for key in wells:
    df.loc[key, 'time (s)'] = wells[key].time
    df.loc[key, 'distance from media (mm)'] = wells[key].distance
    df.loc[key, 'type'] = wells[key].label
df.to_excel('cnc_plasma_treatments/' +
           str(plate.data['n_plates'][index])+'wells_'+
           plate.data['type'][index]+'_'+
           'plasma-treatment.png''.xlsx')
def style(styler):
    styler.set_caption("plasma treatment of " +
                       str(plate.data['n_plates'][index]) +
                       ' well plates '+
                       plate.data['type'][index]
    styler.set_precision(0)
```

```
return styler
df = df.style.pipe(style)
dfi.export(df, 'cnc_plasma_treatments/' +
           str(plate.data['n plates'][index])+'wells '+
           plate.data['type'][index]+' '+
           'plasma-treatment.png')
## WRITE
n = plate.data['n plates'][index]
path = 'cnc plasma treatments/'
with open(path + 'Fb_wb' + '.gcode', 'w') as f:
    f.write('; GCODE file for printing in ' + str(n) + 'wellplate\n\n' +
            'G21 ; set units to millimeters\n' +
            'G90 ; use absolute coordinates\n\n')
    f.write('; Go to reference position bottom left well\n' +
            'GO X{} Y{} M3 S10000\n\n'.format(plate.data['x offset'][index],
                                               plate.data['y_offset'][index]))
    count=0
    r = 5.73
    speed = 432 \text{ } \text{mm/min} for circle of R5.73 C36 36mm/5s
    for i in range(1, rows+1):
        y = plate.data['y offset'][index] + plate.data['well distance']
            [index] * (rows-i)
        for j in range(0, cols):
            x = plate.data['x offset'][index] + plate.data['well distance']
                [index] * j
            f.write('; '+ list wells[count]+ '\n')
            if wells[list_wells[count]].distance == None:
                # no plasma treatement
                print(list wells[count] + ' no plasma treatment')
            else:
```

```
f.write('GO X{} Y{} M3 S10000 ; Displacement and plasma
            OFF\n'.format(x, y))
if wells[list_wells[count]].distance == None:
    # no plasma treatement
   z = None
else:
   z = plate.data['z offset'][index] +
   wells[list wells[count]].distance # + h media
   f.write('GO Z{} ; distance of treatment\n'.format(round(z, 1)))
time = wells[list_wells[count]].time
num_circles = round(time/5) # number of seconds for 1 circle =
5s this can be redefined
if wells[list wells[count]].label == 'sample': # plasma ON SO
    # f.write('G4 P {} M3 S{} ; Treatment time in seconds\n'.format(
                      time, 0))
   y_{down} = round(y - r, 1)
   f.write('GO X{} Y{} ; go down r\n'.format(x, y down))
   for circle in range(0, num circles):
        f.write('G2 X{} Y{} IOJ{} F{} M3 S{}; treat in several
        circles\n'.format(x, y_down, r, speed, 0))
    f.write('GO X{} Y{} ; go back center of well\n'.format(x, y))
    f.write('GO Z-1 M3 S10000; Z reset position and plasma OFF\n\n')
if wells[list wells[count]].label == 'control': # plasma OFF S10000
    # f.write('G4 P {} M3 S{} ; Treatment time in seconds\n'.format(
                      time, 10000))
   y down = round(y - r, 2)
   f.write('GO X{} Y{} ; go down r\n'.format(x, y down))
   for circle in range(0, num circles):
        f.write('G2 X{} Y{} IOJ{} F{} M3 S{} ; Plasma flow control
                \n'.format(x, y down, r, speed, 10000))
    f.write('GO X{} Y{} ; go back center of well\n'.format(x, y))
    f.write('GO Z-1 M3 S10000; Z reset position and plasma OFF\n\n')
if wells[list_wells[count]].label == 'nothing':
```

None

```
print("{} position (x,y): ({}, {}, {})".format(list_wells[count],
                                                           x, y, z))
            count += 1
    f.write('GO XO YO ZO M3 S10000; Homing to initial position plasma OFF')
Below is a snippet of an output g-code
    ; GCODE file for printing in 12wellplate
G21; set units to millimeters
G90; use absolute coordinates
; Go to reference position bottom left well
GO X168.1 Y51.3 M3 S10000
; AO
GO X168.1 Y103.3 M3 S10000; Displacement and plasma OFF
GO Z-14.3; distance of treatment
G4 P 0 M3 S0; Treatment time in seconds
GO X168.1 Y97.57; go down r
GO Z-1 M3 S10000; Z reset position
; A1
GO X220.1 Y103.3 M3 S10000 ; Displacement and plasma OFF
GO Z-14.3; distance of treatment
GO X220.1 Y97.57; go down r
G0 X220.1 Y97.57 I0J5.73 F432 M3 S0 ; treat in several circles
GO X220.1 Y97.57 IOJ5.73 F432 M3 SO; treat in several circles
GO Z-1 M3 S10000; Z reset position
; A2
GO X246.1 Y103.3 M3 S10000; Displacement and plasma OFF
GO Z-14.3; distance of treatment
```

```
GO X246.1 Y97.57; go down r
G0 X246.1 Y97.57 I0J5.73 F432 M3 S0 ; treat in several circles
GO X246.1 Y97.57 IOJ5.73 F432 M3 SO; treat in several circles
GO X246.1 Y97.57 IOJ5.73 F432 M3 SO; treat in several circles
GO X246.1 Y97.57 IOJ5.73 F432 M3 SO; treat in several circles
GO X246.1 Y97.57 IOJ5.73 F432 M3 SO; treat in several circles
GO X246.1 Y97.57 IOJ5.73 F432 M3 SO; treat in several circles
GO Z-1 M3 S10000; Z reset position
; B0
GO X168.1 Y77.3 M3 S10000; Displacement and plasma OFF
GO Z-14.3; distance of treatment
GO X168.1 Y71.57; go down r
GO X168.1 Y71.57 IOJ5.73 F432 M3 SO; treat in several circles
GO X168.1 Y71.57 IOJ5.73 F432 M3 SO; treat in several circles
GO X168.1 Y71.57 IOJ5.73 F432 M3 SO; treat in several circles
GO X168.1 Y71.57 IOJ5.73 F432 M3 SO; treat in several circles
GO X168.1 Y71.57 IOJ5.73 F432 M3 SO; treat in several circles
GO X168.1 Y71.57 IOJ5.73 F432 M3 SO; treat in several circles
GO X168.1 Y71.57 IOJ5.73 F432 M3 SO; treat in several circles
GO X168.1 Y71.57 IOJ5.73 F432 M3 SO; treat in several circles
GO X168.1 Y71.57 IOJ5.73 F432 M3 SO; treat in several circles
GO X168.1 Y71.57 IOJ5.73 F432 M3 SO; treat in several circles
GO X168.1 Y71.57 IOJ5.73 F432 M3 SO; treat in several circles
GO X168.1 Y71.57 IOJ5.73 F432 M3 SO; treat in several circles
GO Z-1 M3 S10000; Z reset position
```

. . .